

Facility-specific greenhouse gas footprints of renewable electricity sources

Louise Christine Dammeier

Dit onderzoek is het resultaat van project nummer 016.Vici.170.190, gefinanciëerd door de Nederlandse Organisaie voor Wetenschappelijk Onderzoek (NWO).

Facility-specific greenhouse gas footprints of renewable electricity sources
Louise Christine Dammeier

Radboud Dissertation Series

ISSN: 2950-2772 (Online); 2950-2780 (Print)

Published by RADBOUD UNIVERSITY PRESS Postbus 9100, 6500 HA Nijmegen, The Netherlands www.radbouduniversitypress.nl

Design: Proefschrift AIO | Annelies Lips Cover: Louise Christine Dammeier Printing: DPN Rikken/Pumbo

ISBN: 9789465151762

DOI: 10.54195/9789465151762

Free download at: https://doi.org/10.54195/9789465151762

© 2025 Dammeier, L.C.

RADBOUD UNIVERSITY PRESS

This is an Open Access book published under the terms of Creative Commons Attribution-Noncommercial-NoDerivatives International license (CC BY-NC-ND 4.0). This license allows reusers to copy and distribute the material in any medium or format in unadapted form only, for noncommercial purposes only, and only so long as attribution is given to the creator, see http://creativecommons.org/licenses/by-nc-nd/4.0/.

Facility-specific greenhouse gas footprints of renewable electricity sources

Proefschrift ter verkrijging van de graad van doctor
aan de Radboud Universiteit Nijmegen
op gezag van de rector magnificus prof. dr. J.M. Sanders,
volgens besluit van het college voor promoties
in het openbaar te verdedigen op

maandag 24 november 2025 om 10.30 uur precies

door

Louise Christine Dammeier

geboren op 15 september 1989 te Minden, Duitsland

Promotor:

Prof. dr. M.A.J. Huijbregts

Copromotor:

Dr. J.H.C. Bosmans (Milieu Centraal)

Manuscriptcommissie:

Dr. R. van Zelm

Prof. dr. S. Pfister (Eidgenössische Technische Hochschule Zürich, CH)

Dr. M. Hauck (Technische Universiteit Eindhoven)

Facility-specific greenhouse gas footprints of renewable electricity sources

Dissertation to obtain the degree of doctor
from Radboud University Nijmegen
on the authority of the Rector Magnificus prof. dr. J.M. Sanders,
according to the decision of the Doctorate Board
to be defended in public on

Monday, November 24, 2025 at 10:30 am

by

Louise Christine Dammeier born on September 15, 1989

in Minden, Germany

PhD supervisor:

Prof. dr. M.A.J. Huijbregts

PhD co-supervisor:

Dr. J.H.C. Bosmans (Milieu Centraal)

Manuscript Committee:

Dr. R. van Zelm

Prof. dr. S. Pfister (Swiss Federal Institute of Technology, CH)

Dr. M. Hauck (Eindhoven University of Technology)

Table of contents

1. Introduction	11
1.1 Renewable Electricity	11
1.1.1 Energy sources	11
1.1.2 Wind power	11
1.1.3 Solar power	13
1.1.4 Hydropower	13
1.2 Life cycle greenhouse gas emissions of renewable electricity	14
1.2.1 Life Cycle Assessment	14
1.2.2 Life cycle GHG emissions of renewable electricity	15
1.3 Scientific challenges	17
1.4 Goal and outline	18
2. Space, Time and Size Dependencies of Greenhouse Gas Payback Times	
of Wind Turbines in Northwestern Europe	21
2.1 Introduction	23
2.2 Materials and Methods	25
2.3 Results	29
2.4 Discussion	33
3. Variability in Greenhouse Gas Footprints of the Global Wind Farm Fleet	39
3.1 Introduction	41
3.2 Materials and methods	42
3.2.1 GHG emissions of wind turbine construction	42
3.2.2 Electricity generation	43
3.2.3 Metamodel	45
3.3 Results	46
3.3.1 Greenhouse gas footprint	46
3.3.2 Metamodel	47
3.4 Discussion	49
3.4.1 GHG emissions of wind turbines	49
3.4.2 Electricity generation	50
3.5 Conclusions	52
4. Greenhouse Gas Footprints of Utility-scale Photovoltaic Facilities	
at the Global Scale	
at the Global Scale	55
4.1 Introduction	55

4.2.1 GHG footprint	58
4.2.2 Facility-specific technology and location data	60
4.2.3 Climate data	62
4.2.4 GHG emission—supply curves	62
4.2.5 Regression analyses	63
4.3 Results	63
4.3.1 GHG footprints	63
4.3.2 GHG emission – supply curves	65
4.3.3 Regression analyses	66
4.4 Discussion	67
4.4.1 Interpretation	67
4.4.2 Production location	69
4.4.3 Limitations	69
4.4.4 Outlook	71
4.5 Conclusion	72
4.6 Data availability statement	72
5. Greenhouse Gas Footprints of Individual Hydropower Facilities in	
the United States of America	75
5.1 Introduction	77
5.2 Materials and methods	78
5.2.1 Greenhouse gas footprint	78
5.2.2 GHG emissions of hydropower	79
5.2.3 Electricity generation	81
5.3 Results	83
5.3.1 Yearly GHG emissions during operation	83
5.3.2 Electricity generation	83
5.3.3 GHG footprints	83
5.4 Discussion	86
5.4.1 GHG emissions	86
5.4.2 Electricity generation	88
5.5 Conclusions and outlook	89
6. Synthesis	93
6.1 Introduction	94
6.2 Technological variability	94
6.3 Spatial variability	96
6.4 Temporal variability	98
6.5 Conclusions and Recommendations	99

References		103
Appendices		123
Appendix A	Appendix for chapter 3	124
Appendix B	Appendix for chapter 4	144
Appendix C	Appendix for chapter 5	164
End matter		179
Summary		180
Samenvatting		183
Research Data M	Management	186
Acknowledgem	ents	187
Curriculum vitae	e	188
Publications		189



1. Introduction

1.1 Renewable Electricity

1.1.1 Energy sources

Fossil fuels – coal, oil and natural gas – are still the dominant energy sources in our world today [1]. We depend on fossil fuels for electricity and heat generation, to fuel vehicles, and as feedstock for the production of a variety of products, such as plastics and paints. The use of fossil fuels causes emissions of greenhouse gasses (GHGs), such as carbon dioxide (CO_2) and methane (CH_4), which are widely accepted to cause global warming through radiative forcing. The IPCC estimated that in 2019 64% of the global net anthropogenic GHG emissions came from CO_2 from fossil fuel and industry [2], indicating that in order to limit global warming and climate change, fossil fuels should be replaced by cleaner energy sources. The energy system accounted for 32% of the direct GHG emissions in 2019 and therefore is a major consumer of fossil fuels [3].

Alternatively, renewable energy sources can be used, such as wind and solar power, to reduce the GHG emissions of the energy system. Wind, water and the sun have been used as energy sources for generations. Wind has first been used for sailing, more than 5,000 years ago [4] and the first windmills to grind grain and pump water are believed to have been developed as early as the 9th century [5]. The United Nations [6] describe renewable energy as "energy derived from natural sources that are replenished at a higher rate than they are consumed." There are several types of renewable energy, with biomass currently making the largest contribution, mainly to transport and as traditional biomass to heat [7]. The three most important non-biomass renewables are hydropower, wind, and solar, generating respectively 16%, 5.5%, and 2.5% of the global electricity in 2019 [2]. The development of these non-biomass renewables shares since 2000 with a projection beyond 2025 is shown in Figure 1-1. In my thesis, the focus will be on utility-scale non-biomass renewable energy sources, i.e. wind power, solar power and hydropower.

1.1.2 Wind power

Electricity from wind has first been generated in the 19th century [8] and utility scale wind turbines were developed in the middle of the 20th century [9]. Wind turbines installed today usually have a rated capacity of at least 1 MW and the largest wind

turbine has a capacity of 26 MW [10]. The principle by which wind turbines generate electricity is straightforward: The blades of a wind turbine are moved by differences in pressure created when wind flows around them – similar to the way lift is created around airplane wings [11]. The rotational energy of the blades is then converted to electricity through a generator connected to the rotor.

Currently, wind power is becoming increasingly competitive with other forms of electricity generation as costs are continuing to decline [12]. Wind power can be developed both onshore and offshore, with the wind speeds on average being higher and less variable offshore than onshore. This variability of the wind resource is one of the biggest drawbacks of wind power and requires flexible grid integration and can be offset by amongst others storage, possibly in a combination with solar PV [13]. Wind turbines can also have an impact on local ecology, for instance on bats and birds [14 - 17]. Social impacts can include shadow flicker and noise emissions [18, 19]. However, these impacts can be mitigated by implementing curtailment measures during certain times of day or migrating seasons, or employing algorithms to determine shut-down times [20]. Advantages of wind turbines are that their impact on land area is generally low as the area between turbines can continue to be used. Furthermore, GHG emissions from wind turbines occur mainly during manufacturing, construction and demolition and are relatively low compared to fossil electricity sources [21, 22].

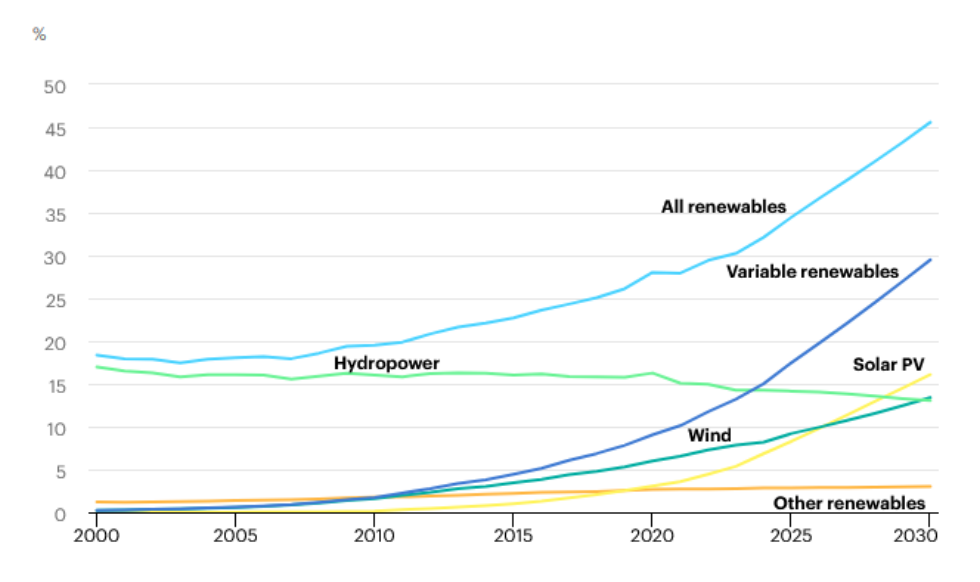


Figure 1-1 Share of renewable electricity generation by technology in %, 2000-2030 [23]. Biomass is not included here because its mainly used for transportation and heat and not electricity generation. "Variable renewables" combines the shares of wind and solar PV.

1.1.3 Solar power

Solar PV panels can be installed virtually everywhere, from being integrated into roof slates and building panels to solar cells integrated in fabric [24, 25]. The first practical PV cell was built in the mid-20th century [26] and their first application was in the Vanguard satellite in 1958 [27]. PV cells generate electricity because the energy from the sun that hits the solar panel is absorbed by the material [28]. A PV cell consists of different materials with different electronic properties and the photons hitting it are creating an electric field, creating the current which is needed to generate electricity [28].

Prices started to drop in the 1970s and currently, utility-scale solar PV is becoming increasingly competitive with other forms of electricity generation [12] and several PV parks already exceed an installed capacity of 1 GW [29]. Different types of PV panels exist, the most common one being mono-crystalline silicon, followed by multi-crystalline silicon and thin film panels, examples of the latter being cadmium telluride (CdTe) and copper indium gallium selenide (Cl(G)S) [30]. They differ in the types of materials used, cost and efficiency. Utility-scale solar PV is usually ground-mounted, often on fixed racks, but the mounting systems can also track the sun along one or two axes [30]. In addition to the intermittent nature of the solar resource, which varies greatly with location – locations closer to the equator having a higher solar resource than those closer to the poles – another possible disadvantage of solar PV is the use of land necessary to build utility-scale PV, which can potentially compete with alternative uses such as agriculture [31]. However, solar PV can be integrated with other uses, such as combining it with agriculture using shade-tolerant crops or sheep herding [32]. Competition with other uses can also be minimized by installing PV on closed landfills [33] or as floating PV on reservoirs, which also can reduce water evaporation [34]. Solar PV can also create barriers to species movement, although mitigation measures, such as wildlifefriendly fences or travel corridors, are available and can be implemented [32]. As with wind power, GHG emissions occur mainly during manufacturing, construction and end-of-life, but during the use phase emissions are negligible [30].

1.1.4 Hydropower

Hydropower has been used to produce electricity since the 19th century [35]. Therefore, it is a mature and proven technology to provide renewable electricity worldwide. Different types of hydropower technologies exist, the most common ones being reservoir and run-of-river facilities, which can range in capacity from a few kilowatts (kWs) to several gigawatts (GWs) [36]. Hydroelectricity is generated by water flowing through a turbine, causing it to rotate, which in turn spins a generator producing the electricity [37].

One of the advantages of hydropower in an energy system with growing amounts of intermittent renewable energy sources is that it can provide flexibility and therefore balance the electricity supply, as water can be stored in the reservoirs and released when necessary [38]. Furthermore, dams generally have long lifetimes, some being more than 100 years old, and they can provide additional services to the community, such as recreation, irrigation and flood control, and municipal water supply [36]. However, hydropower also has drawbacks, as it is susceptible to climate change, where droughts may lead to an insufficient amount of water being available [39]. Another disadvantage of hydropower is that it can have negative social and environmental impacts. Dam construction can lead to loss of land and fragmentation of ecosystems [40]. While hydropower is generally perceived to be a clean source of electricity, emissions are caused throughout the life cycle of a project, through material used during construction and operation, as well as through biogenic GHG emissions from a mad-made reservoir through decaying biomass after land has been flooded [40].

1.2 Life cycle greenhouse gas emissions of renewable electricity

1.2.1 Life Cycle Assessment

A life cycle assessment (LCA) is a standardized methodology to assess the environmental impact of a product, process or service covering its entire life cycle, from cradle to grave, thus covering the extraction of raw materials, the use phase and the end-of-life phase (see Figure 1-2). An LCA consists of four distinctive phases, which are described in International Organization for Standardization (ISO) standards 14040 and 14044 [41, 42]:

- 1. Goal and scope definition: First phase of an LCA stating the intended application and rationale behind the study, as well as the functional unit, product system and its boundaries, assumptions and limitations, and the allocation procedure.
- 2. Inventory analysis: In the inventory analysis, raw materials, energy requirements and resource uses are quantified as are emissions to land, water and air and other discharges to the environment.
- 3. Impact assessment: In this phase, the impacts on the environment and human health are evaluated.
- 4. Interpretation: In this final phase, the significant issues of the LCA are identified and the study is evaluated on its completeness and consistency, resulting in conclusions, limitations and recommendations.

If applied in practice, a life cycle assessment can be an iterative process, whereby the results of the assessment and interpretation inform decisions to for instance adjust the production process, which in turn alters the inputs for the inventory analysis etc.

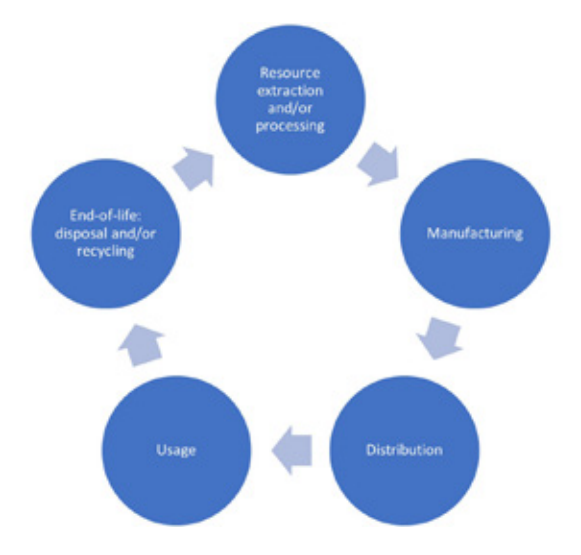


Figure 1-2 Schematic representation of the life cycle of a product, process or service [43].

1.2.2 Life cycle GHG emissions of renewable electricity

GHG footprint

LCAs are used to quantify the life cycle impacts of the generation of electricity using renewable energy technologies, such as wind power, solar power and hydropower.

Often, the focus is on life cycle greenhouse gas emissions, presented as so-called greenhouse gas (GHG) footprints F_{GHG} (in g CO₂eq/kWh), which is the life cycle GHG emissions (I) in g CO₂eq per facility divided by the lifetime electricity production (E) in kWh per facility:

$$F_{GHG} = \frac{I}{E} \tag{1-1}$$

Wind power

The greenhouse gas (GHG) emissions associated with wind power reported in literature range from 2 to 156 g CO₂eq/kWh (see Table A-3), typically based on mean wind speeds at hub height [44 - 51]. It is important to note, however, that electricity production can vary significantly with minor changes in wind speed, because electricity generation depends on the wind speed cubed. Generally, larger wind turbines tend to produce lower life cycle GHG emissions per kWh. Caduff et al. [45] have estimated emissions by developing a metamodel based on rotor diameter and hub height. However, their study was limited by its focus on onshore turbines only and not accounting for the variability of climatological data. A recent Danish study [52, 53] employed spatiotemporal wind speed data with a resolution of approximately 50 by 50 km to model life cycle emissions, underscoring the necessity of accounting for the spatial and temporal variability in wind speed.

Solar power

Much research has been conducted on life cycle greenhouse gas emissions of photovoltaic (PV) systems. A common approach involves performing a metaanalysis by consolidating case studies reported in the literature and harmonizing their findings to establish standardized system boundaries regarding irradiation, lifetime, performance ratio, and/or module efficiency [54 - 57]. These studies show that the GHG footprints of PV systems range from approximately 14 to 82 g CO₂eg/kWh under harmonized conditions. The fact that the footprints of thin-film panels can be about 40% lower than those of crystalline silicon panels shows that the type of panel is the most significant source of variation [58 - 61]. While metaanalyses offer insights into the sources of life cycle GHG emissions related to PV systems, the harmonization process may obscure real-world variations in footprints.

On the one hand, it has been shown that locations with higher irradiation lead to increases in electricity production. Therefore, higher irradiation leads to a reduction in GHG footprints [54, 60, 62-66]. On the other hand, the manufacturing location affects GHG emissions during production [60, 62, 63, 64, 67]. Other important factors which can explain differences in PV GHG footprints are variations in module efficiency, mounting system types, lifespan, degradation rates, and capacity between different types of PV panels [54, 65, 66, 68 - 71]. A study that has investigated spatial differences in environmental footprints of PV systems has been conducted by Louwen et al. [72] for rooftop PV in Eurasia and Africa, showing that installing a PV facility in a high-irradiation area can reduce the GHG footprint by up to 75%. Ito et al. [73] have investigated GHG footprints for two sites in France and Morocco. Pérez-López et al. ([74] and [75]) for utility-scale PV globally, who showed that even within one country, selecting a location with higher irradiation can reduce the footprint by about 25%. These studies highlight the significant variance in PV GHG footprints based on location.

Hydropower

Greenhouse gas footprints from hydropower have been shown to vary greatly, ranging from 2.0·10⁻⁴ to 6.6 kg CO₂eq/kWh [76 - 93]. The reported range of 4.5 orders of magnitude in GHG footprint of hydropower facilities can be caused by differences in various environmental and technological factors. Emissions from the reservoirs themselves heavily depend on the reservoir lifetime and the climate zone in which the reservoir is located, as well as pre-impoundment land cover type [94]. Earlier studies have shown that the ratio of GHG emissions from the dam itself compared to those of the reservoir lies anywhere between 100% for diversion dams to 0.01% for tropical reservoirs [91]. Little research has been done on quantifying facilityspecific GHG footprints of hydropower at large geographical scales. Most studies focus on one or a few plants, focusing on a specific type of dam and associated technology. Wang et al. [95] assessed carbon emission and water consumption of hydropower plants in China, but they did not relate the impacts to the facilities' electricity generation. A study by Harrison et al. [96] used the G-res tool to calculate GHG emissions from reservoirs on a global scale but neglected dam construction and also does not relate the emissions to electricity production. Scherer and Pfister [97] modelled the biogenic carbon footprint of hydropower reservoirs and reported an average GHG footprint of 0.273 kg CO₂eg/kWh, again focussing solely on the reservoir and not accounting for dam construction. Gemechu and Kumar [98] assessed LCA studies of hydropower and found that the wide range of emission intensities reported (1.5·10⁻³ - 3.7 kg CO₃ eq/kWh) is caused by inconsistency in how LCA is used, high variability in key reservoir characteristics and data limitations.

1.3 Scientific challenges

While conducting an LCA is a standardized process, various sources of variability can cause large differences in the life cycle GHG emissions of renewable electricity sources. Possible sources of variability can be spatial, temporal and/or technical in nature.

- Spatial variability arises because resources (wind speed, solar irradiation and water flows) are not distributed evenly across the globe, influencing electricity production.
- Temporal variability is introduced by changes in the same renewable resources over time, which also influences electricity production.
- Technical variability is caused by the choice of technology to be deployed at a certain location. Changing the type of wind turbine, solar PV module or hydropower plant influences the type and amount of resources used and thus the life cycle GHG emissions as well as the electricity production.

Typically, LCA studies use only one variant of a given technology at a certain point in time and space or a small set of variants of either of the three sources of variability. The main reason that most LCA studies include only a limited amount of variability is that conducting an LCA is a time-consuming process because a lot of information needs to be collected, processed and analysed. Therefore, in order to capture information on the location, time and technology for a specific project, each time a new LCA has to be carried out.

Up to now, integrating spatial, temporal and technical variation into one assessment of GHG footprints of renewable electricity sources has not been done on larger spatial scales. Moreover, it is not known what the main contributors are to the variability in GHG footprints observed between different studies of the same technology. Such an assessment adds value because it enables policy makers and developers to easily assess differences in GHG performance between either different technologies in the same location or the same technology in multiple locations. Furthermore, the comparison to other (non-)renewable electricity sources offers the possibility to determine how much can be gained in terms of GHG emission mitigation at each location. Such an assessment may be feasible by developing models that allow for straightforward calculation of the GHG footprints of the most important non-biomass renewable energy sources on a global scale identifying and using a key set of technological and meteorological variables.

1.4 Goal and outline

The main goal of my thesis is to quantify facility-specific GHG footprints of wind power, solar power and hydropower at large spatial scales. Understanding how differences in technology and meteorology influence GHG footprints of renewable electricity sources will allow for the identification of the most suitable technology to deploy in any given location from a life cycle perspective.

Apart from the introduction, this PhD thesis consists of four individual chapters and a synthesis (see Table 1-1 for the sources of variability considered in each chapter).

Chapter 2 describes the space, time and size dependencies of greenhouse gas payback times of wind turbines in Northwestern Europe.

Chapter 3 quantifies the variability in GHG footprints between individual wind farms at the global scale.

Chapter 4 assesses the GHG footprints of utility-scale PV facilities on a global scale.

Chapter 5 investigates the variability of GHG footprints of hydropower facilities in the United States of America.

Finally, in **chapter 6** the results of the previous chapters are synthesized.

Table 1-1 Sources of variability in GHG footprints for electricity from wind, solar and hydropower considered in the chapters of my thesis.

	Chapter 2 (wind)	Chapter 3 (wind)	Chapter 4 (solar PV)	Chapter 5 (hydropower)
Geographic Scale	Northwestern Europe	Global	Global	US
Technological variability	Rotor diameter Hub height Onshore/ offshore	Rotor diameter Hub height Onshore/offshore Rated power Power curve Wind farm size	Panel type Capacity Construction year	Natural lakes vs. man-made reservoirs Capacity Reservoir area Height
Temporal meteorologic variability	Wind speed	Wind speed Temperature Pressure	Irradiation Temperature Wind speed	Water flow CO ₂ and CH ₄ emission factors
Spatial meteorologic variability	Wind speed	Wind speed Temperature Pressure	Irradiation Temperature Wind speed	Water flow Chlorophyll-a CO ₂ and CH ₄ emission factors

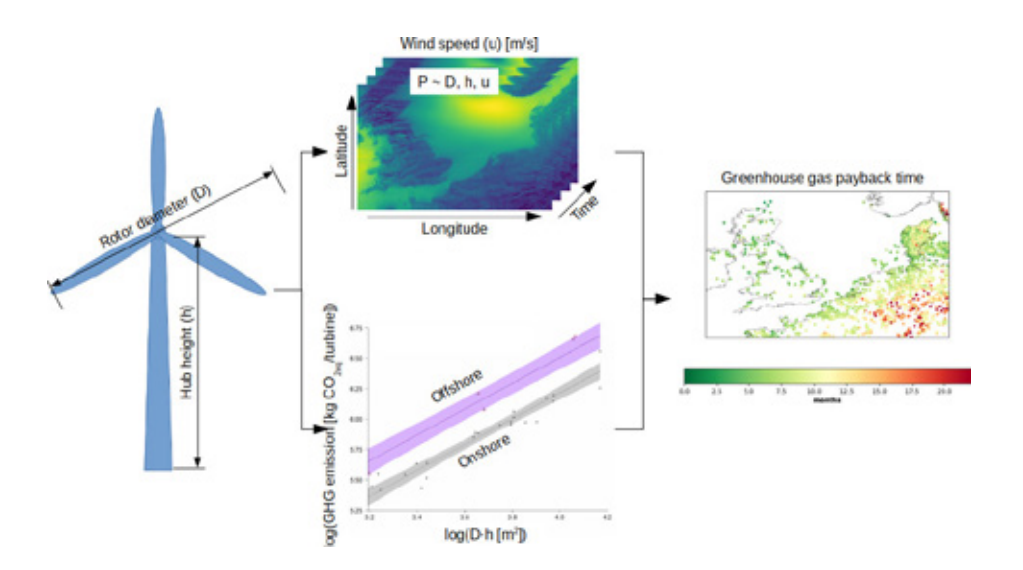


2. Space, Time and Size Dependencies of Greenhouse Gas Payback Times of Wind Turbines in Northwestern Europe

L.C. Dammeier, J.M. Loriaux, Z.J.N. Steinmann, D.A. Smits, I.L. Wijnant, B. van den Hurk, M.A.J. Huijbregts (2019). *Environmental Science & Technology 53: 9289-9297*

Abstract

The net greenhouse gas benefits of wind turbines compared to their fossil energy counterparts depend on location-specific wind climatology and the turbines' technological characteristics. Assessing the environmental impact of individual wind parks requires a universal but location-dependent method. Here, the greenhouse gas pay-back time for 4,161 wind turbine locations in northwestern Europe was determined as a function of (i) turbine size and (ii) spatial and temporal variability in wind speed. A high-resolution wind atlas (hourly wind speed data between 1979 and 2013 on a 2.5 by 2.5 km grid) was combined with a regression model predicting the wind turbines' life cycle greenhouse gas emissions from turbine size. The greenhouse gas payback time of wind turbines in northwestern Europe varied between 1.8 and 22.5 months, averaging 5.3 months. The spatiotemporal variability in wind climatology has a particularly large influence on the payback time, while the variability in turbine size is of lesser importance. Applying lower-resolution wind speed data (daily on a 30 by 30 km grid) approximated the high-resolution results. These findings imply that forecasting location-specific greenhouse gas payback times of wind turbines globally is well within reach with the availability of a high-resolution wind climatology in combination with technological information.



2.1 Introduction

Wind energy is becoming increasingly important in the world's electricity supply as it becomes cost competitive and the demand for sustainable energy is rising [99]. By the end of 2017, the cumulative capacity of all wind turbines installed globally reached over 539 GW, meeting approximately 5% of the world's electricity demand [100]. It is projected that wind could contribute 18% to 36% of the world's electricity production in 2050 [101, 102].

The environmental performance of wind electricity is typically determined by means of a life cycle assessment (LCA) [103], which is a systematic approach to determine the environmental impact of a technology considering all the resources required and related emissions during the different stages of its life cycle [41]. For wind, the environmental impact per unit of electricity produced depends on the amount and type of materials used to build and maintain the wind turbine as well as the electricity produced over its life cycle [44]. Because it is virtually impossible to perform specific LCAs for all individual wind turbines worldwide, Caduff et al. [45] developed a regression model estimating the life cycle greenhouse gas (GHG) emission of onshore wind turbines as a function of rotor diameter and hub height. They found that the bigger the wind turbine, the lower the GHG emissions per unit of electricity produced. However, their analysis was focused on onshore turbines and did not take climatological variations of wind speed into account.

LCAs of wind turbines are typically based on the mean wind speed at hub height [44 - 51]. More recently, a comprehensive LCA study for wind electricity in Denmark built a model to estimate a wind turbine's life cycle GHG emissions based on technological scaling relationships and spatiotemporal information on wind speed data with approximately a 50 by 50 km grid resolution [52, 53]. Their study emphasized the importance of including spatiotemporal variation of wind speed in the power calculations. The required spatiotemporal resolution of wind speed data to obtain reliable LCA results was, however, not analysed in their study. To our knowledge, a comparison of the site-specific environmental performance of wind electricity on larger spatial scales that takes into account detailed spatiotemporal variability in the local wind resource is currently lacking. Moreover, it is not known which spatiotemporal resolution actually is sufficient to capture the variability in the wind resource in such an assessment.

Here, the greenhouse gas payback time (GPBT) of 4,161 wind turbine locations in northwestern Europe was quantified, accounting for variability in both wind climatology and turbine technology. The GPBT is a commonly used metric to identify the environmental performance of wind energy compared with a fossil energy benchmark, which equals the time it takes until the total GHG savings due to the replacement of fossil energy by wind energy equals the GHG emissions during a turbine's life cycle [104].

To simulate the yearly average power output of the individual wind turbines highresolution wind data for 35 years on a 2.5 by 2.5 km grid [105] was combined with technical information for individual wind turbines [106]. The life cycle GHG emissions for onshore and offshore wind turbines were derived from the turbine size with an updated regression model based on the work by Caduff et al. [45]. The importance of using a high-resolution wind climatology data set and turbinespecific data was assessed by analysing the sensitivity of wind turbine GPBTs to (i) differences in spatiotemporal detail of wind speed and (ii) including or excluding differences in turbine size.

2.2 Materials and Methods

Overview. The influence of time and space dependencies in wind speed and size variations of wind turbine characteristics on the environmental impacts was analysed according to the steps shown in Figure 2-1. These steps are further explained below.

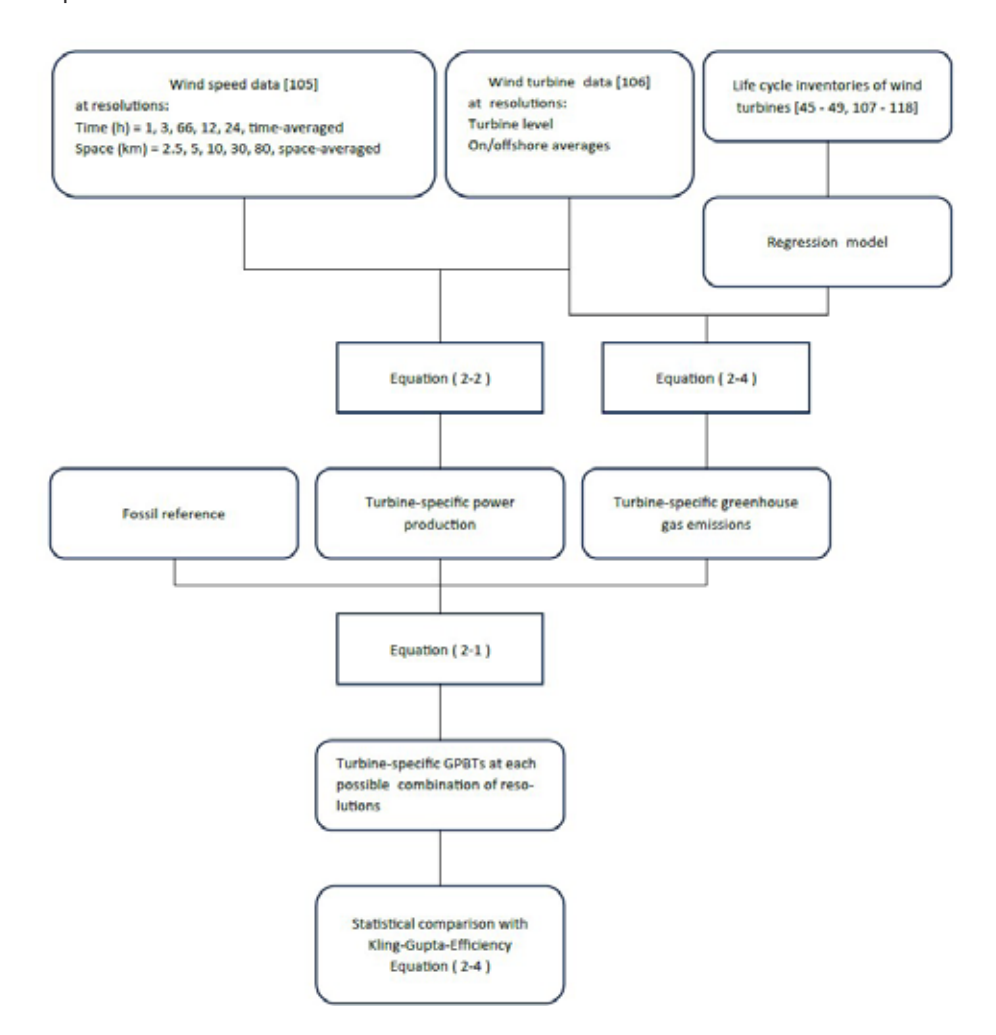


Figure 2-1 Schematic representation of the calculation of the turbine-specific greenhouse gas payback time (GPBT).

Greenhouse Gas Payback Time. The GPBT depends on the total emissions during the lifetime of the wind turbine and its power output, as well as the greenhouse gas emissions of the fossil energy reference. The GPBT (in months) of a wind turbine is calculated as

$$GPBT_{turbine} = \frac{GHG_{turbine}}{P_{turbine} \cdot GHG_{fossil}}$$
 (2-1)

where $\mathrm{GHG}_{\mathrm{turbine}}$ is the cumulative GHG emission resulting from the production and installation of the wind turbine (kg CO₂eq/turbine), P_{turbine} the lifetime average electricity production of the wind turbine (kWh/month), and GHG_{fossil} the GHG emission of the fossil energy benchmark (kg CO₃eq/kWh). The average emission of natural gas-fired power plants of 0.5 kg CO₂eg/kWh was chosen as reference for the whole study area [59].

GHG Emissions of Wind Turbine Production. To calculate the GHG emissions, a regression model was developed that expresses GHG emissions of a turbine during its lifetime (GHG_{turbine}) as a function of rotor diameter (D) and hub height (h). For this, the model from Caduff et al. [45]. was modified by expanding the underlying empirical data set [46 - 49, 107 - 118] and including systematic differences in GHG emissions between onshore and offshore turbine production [119]. A Gaussian generalized linear model was applied using RStudio (RStudio Team, 2015), based on 28 wind turbine LCA studies of 22 on- and 6 offshore locations. Cross-validation was performed using a leave-one-out method [120]. The best model was chosen based on the Akaike information criterion (AIC).

Power Output. The turbine's power output $P_{\text{turbine},i}$ at time i depends on the timevarying wind speed at hub height u_i (m/s) and the rotor diameter (m) through

$$P_{turbine,i} = 0.5 \cdot \mu \cdot \mu_{Betz} \cdot \rho \cdot A_{turbine} \cdot u_i^3 \qquad (2-2)$$

where $\mu = 0.85$ is the overall efficiency (including grid losses and machine downtime, among others) [121], $\mu_{\mbox{\tiny Retz}}$ the theoretical maximum power that a wind turbine can produce (16/27 , Betz's law) [122], ρ the air density (1.225 kg/m²), and $A_{turbine}$ the swept area (m²) given by $0.25 \cdot \pi \cdot D^2$. A wind turbine operates in a limited wind speed range (between cut-in and cut-out wind speeds), below and above which no electricity is produced. Above the rated wind speed the turbine is programmed to operate at its rated power output until it reaches the cut-out wind speed.

Data. Wind Turbines. Wind turbines in Northwestern Europe within the domain of 48°N to 60°N and -8°E to +12°E were included in this study. Their location and technical specifications were taken from The WindPower database [106], which provides information on the turbines' hub heights and rotor diameters. This information is used in the calculation of the turbines' life cycle GHG emissions (equation (2-4)) as well as their power output (equation (2-2)). Data was available for 4,161 wind power locations within the selected domain, of which 80 are offshore and 4,081 are onshore. The included technological turbine characteristics are given in Figure 2-1.

Wind Speed. Wind speed data was derived from the KNMI North Sea Wind Atlas (KNW-Atlas) [105]. This data set contains hourly wind speed data on a 2.5 by 2.5 km grid for all years between 1979 and 2013. The KNW-Atlas is based on ERA-Interim reanalysis data [123] downscaled with the high-resolution, nonhydrostatic weather forecasting model HARMONIE CY37h1.1 [124, 125]. It contains wind speeds at heights of 10, 20, 40, 60, 80, 100, 150, and 200 m. The KNW-Atlas has been validated [126, 127] and produces accurate wind climatology up to 200 m above sea level. For the wind turbine locations, wind speed data at the nearest KNWgrid point were used. The wind speed at hub height was calculated by a linear interpolation of KNW-levels to the hub height. This wind speed was then used to calculate the average yearly power output for each wind turbine location over the full period of 35 years.

Statistical Analysis. Technology versus Climatology. In the reference situation, the turbines' GPBTs were calculated using the high-resolution data from the KNW-Atlas (2.5 by 2.5 km grid, hourly data). To assess the importance of knowing the locationspecific turbine size and wind climatology, this reference was compared to the turbines' GPBTs for four scenarios in which variability characteristics were modified:

- 1. The importance of spatial variability in the GPBT calculations was assessed by using a **spatial average** of the wind data.
- 2. The importance of temporal variability was assessed by using a temporal average of the wind data.
- 3. The importance of spatial and temporal variability was assessed using a spatial and temporal average of the wind data.
- 4. The importance of technological variation was assessed using average turbine **sizes** for on- and offshore turbines.

Spatial average means that for every hour in the 35-year study period, the wind data of each grid point were averaged and used as wind speed value at that hour for every grid point in the domain prior to calculating the power output for that hour. Similarly, a temporal average means that all hourly wind speed values at a certain grid point were averaged and used for every time slot at that location. Using both the spatial and the temporal average, only one wind speed value was used for all turbines for the whole study period, resulting in only the technological variability of the wind turbines (e.g., hub height, diameter, and cut-in and cut-out wind speeds) remaining. Lastly, technological averages were created by using average onshore and offshore turbine characteristics based on the turbines in the study area, which are shown in Figure 2-2.

The Kling–Gupta efficiency (KGE) was used to calculate the effect of neglecting spatial, temporal, or technological variability. The KGE is a combination of correlation, bias, and variability between scenario n (constant wind in space, time, or both or constant turbine type) and the reference scenario and is defined as [128]

$$KGE_n = 1 - \sqrt{(\beta_n - 1)^2 + (\gamma_n - 1)^2 + (r_n - 1)^2}$$
 (2-3)

with r_n the Pearson correlation coefficient between the GPBT, γ_n the variability ratio $((\sigma_n/\mu_n) \cdot (\mu_r/\sigma_r))$, and β_n the bias ratio (μ_n/μ_r) , with σ the standard deviation and μ the mean of the GPBT results, of scenario n (see above) compared to the reference scenario with a 2.5 by 2.5 km grid, hourly wind speed data, and turbine-specific data. The KGE ranges from $-\infty$ to 1 (1 being a perfect fit).

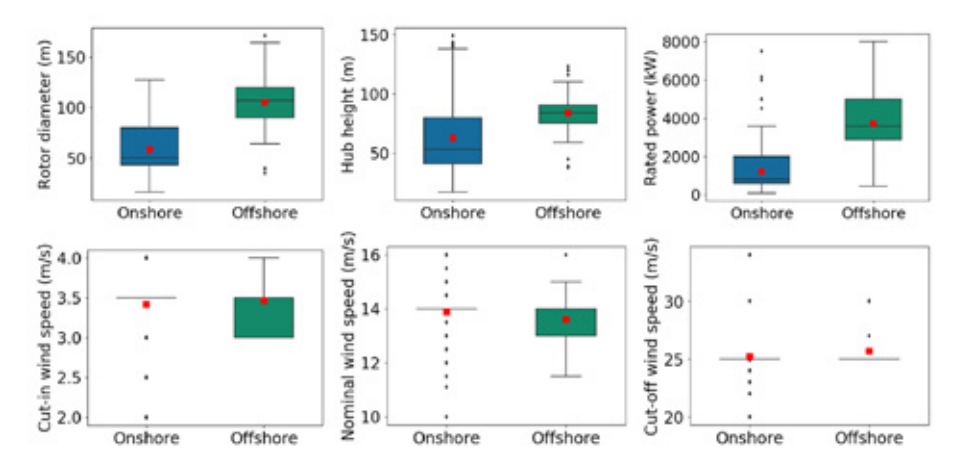


Figure 2-2 Boxplots show the distribution of important technological wind turbine characteristics for the turbines in the data set. Blue bars are onshore turbines (n = 4,061), and green bars are offshore turbines (n = 80). The plots show the three quartile values of the distribution, the 1.5 interquartile range represented by the whiskers, and the data points outside this range as individual values. The red dots represent the mean used for average turbine sizes.

Importance of Spatial and Temporal Resolution. The importance of using a high spatial and temporal resolution in the GPBT calculations was investigated as well, because wind data on large spatial scales are usually available at coarser resolutions than used in this study [129, 130]. For this, 25 data sets were created from the KNW-Atlas data by aggregating temporal and spatial resolutions to a coarser scale, based on typical resolutions of regional and global climate archives [131]:

- temporal resolution: 1 h (default), 3 h, 6 h, 12 h, and 24 h
- spatial resolution: 2.5 by 2.5 km (default), 5 by 5 km, 10 by 10 km, 30 by 30 km, and 80 by 80 km

Reduction of temporal and spatial resolutions was obtained by subsampling the default data at indicated space and time intervals. Daily wind speed data were constructed by sampling data at noon (12:00 UTC). GPBTs of the 4,161 wind power locations were recalculated for the 25 additional data sets, and the results of each data set were evaluated against the reference data set using the KGE (see equation (2-3)). All spatiotemporal analyses were carried out using NCL [132].

2.3 Results

Regression Model. The optimal AIC model fit to describe turbine life cycle GHG emission as a function of its diameter (D), hub height (h), and onshore/offshore technology indicator (T) was

$$log(GHG_{turbine}) = c_0 + c_1 \cdot log(D) + c_2 \cdot log(h) + c_3 \cdot T \qquad (2-4)$$

where $c_0 = 2.00 \ [\pm 0.45]$ is the intercept, $c_1 = 1.27 \ [\pm 0.50]$, $c_2 = 0.84 \ [\pm 0.56]$, and $c_3 = 0.29$ [±0.10]. Figure 2-3 shows the regression lines for offshore and onshore wind turbines based on 28 LCA studies found in the literature [45 - 49, 107 - 118].

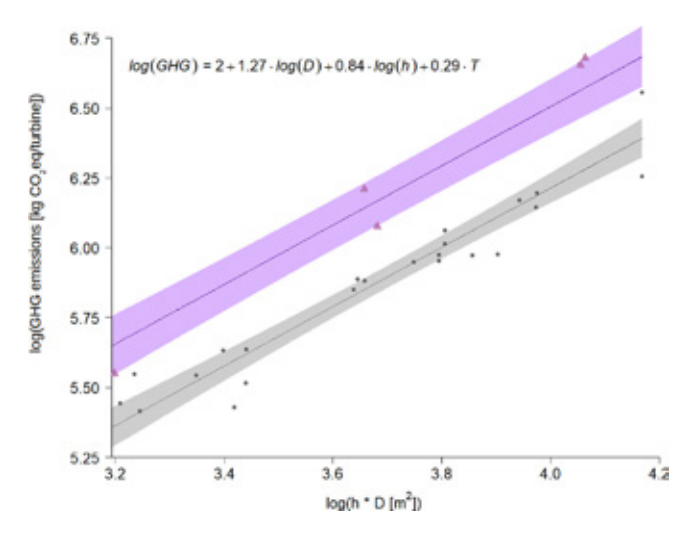


Figure 2-3 GHG emissions of onshore turbines (T = 0, grey line shading) and offshore turbines (T = 1, purple line shading) as a function of log (D \cdot h). The shading represents the 95% confidence interval. The markers are the harmonized LCA results from the literature (circles are onshore and triangles offshore wind turbines).

Reference Situation. Using the turbine-specific GHG emissions and wind data from the KNW-Atlas at the highest spatiotemporal resolution, GPBTs show a pronounced spatial pattern (Figure 2-4). The lowest values are located offshore and close to the coast (1.8 months as lowest GPBT), where wind speeds tend to be higher. Inland, where lower wind speeds prevail, the GPBT is typically higher (up to 22.5 months). The average GPBT for wind turbines in northwestern Europe is 5.25 months.

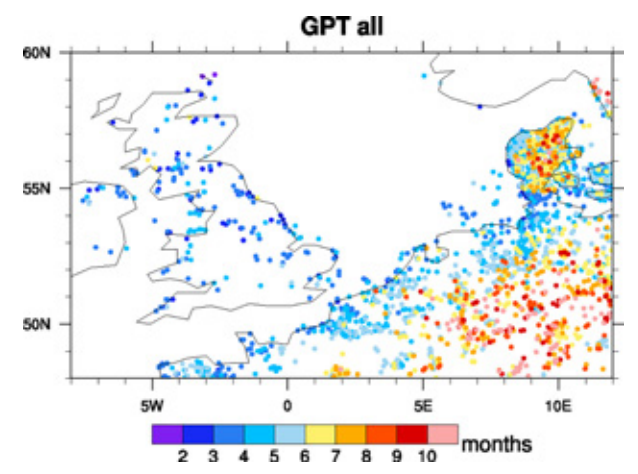


Figure 2-4 Greenhouse gas payback time (in months) for the reference situation (wind data at 2.5 by 2.5 km and hourly resolution and turbine-specific size characteristics) [132].

Ignoring Variability in Wind Speed and Turbine Size. Spatially averaging wind speed while maintaining the hourly temporal resolution and the variation in turbine technology results in a poor match with the reference data (KGE = -0.27) (Figure 2-5a). This is due to a 2-fold underestimation of the GPBT ($\beta = 1.93$), while the spread in the GPBT is smaller than in the reference situation (y = 0.27). The correlation between GPBTs of the spatially averaged wind speed and the reference situation is also relatively low (r = 0.53).

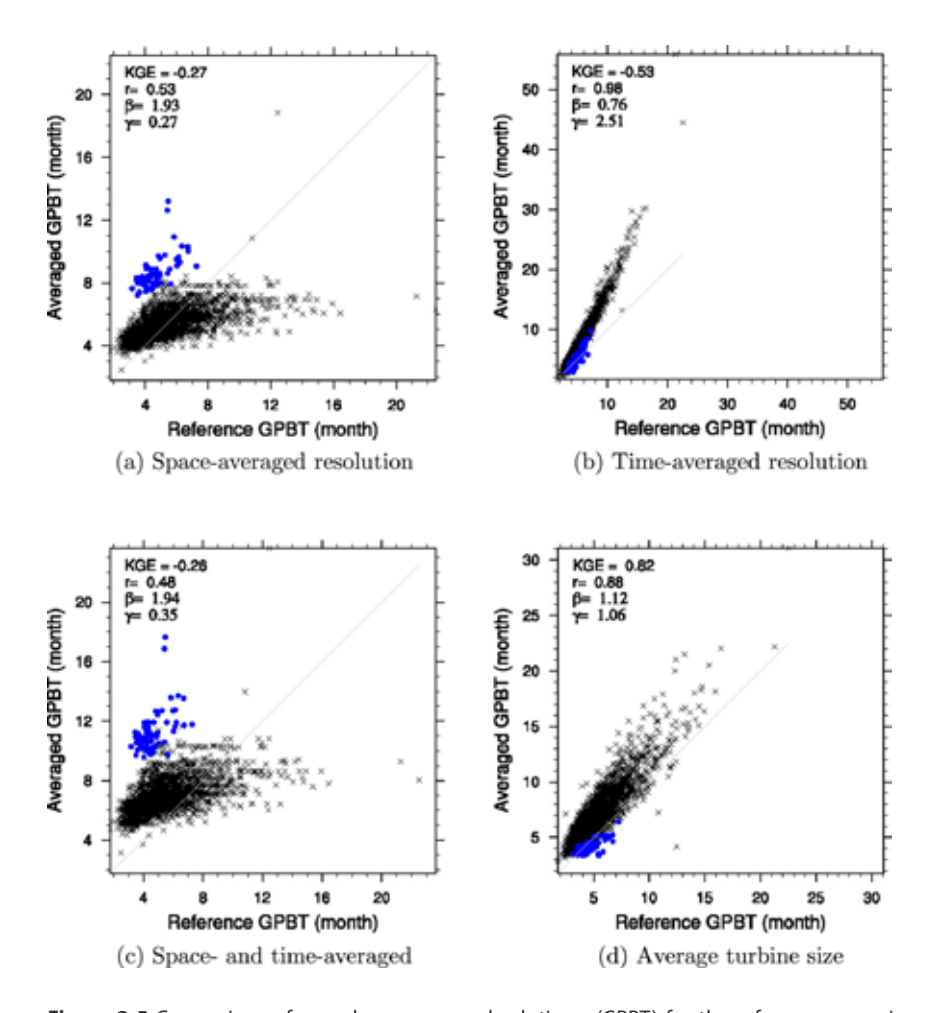


Figure 2-5 Comparison of greenhouse gas payback times (GPBT) for the reference scenario vs the scenarios with spatially averaged wind speed (a), time-averaged wind speed (b), wind speed averaged over space and time (c), and average turbine size for onshore and offshore wind farms (d). Offshore wind locations are represented by the blue dots, and onshore wind locations are represented by the black crosses. KGE is the Kling-Gupta efficiency, r the Pearson correlation coefficient, γ the variability ratio, and β the bias ratio [132].

Using a time-averaged wind speed at a 2.5 by 2.5 km spatial resolution results in an even poorer match with the reference data with a KGE of -0.53 (Figure 2-5b). This low KGE value is mainly due to a large overestimation of the spread in GPBT (y = 2.51). Averaging wind speed both spatially and temporally also gives a negative KGE of -0.26 (Figure 2-5c). Similar to the spatially homogeneous wind field, the average GPBT is strongly overestimated ($\beta = 1.94$).

Using an average turbine size for on- and offshore wind turbines results in a much higher KGE of 0.82 (Figure 2-5d), compared to neglecting climatological variability. The correlation coefficient is relatively high (r = 0.88), and systematic deviations of the mean and spread are relatively small ($\beta = 1.12$; y = 1.06).

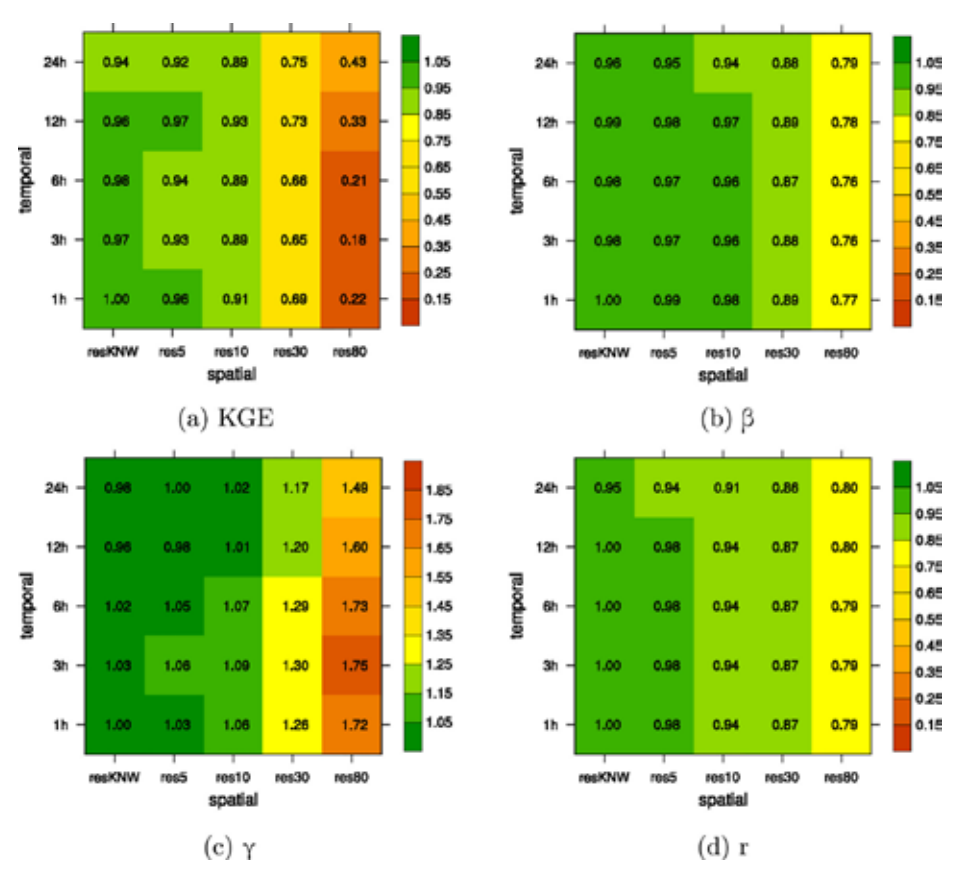


Figure 2-6 Kling-Gupta efficiency (a), Pearson correlation coefficient (b), variability ratio (c), and bias ratio (d) of the GPBT at various coarser spatial (5 by 5, 10 by 10, 30 by 30, and 80 by 80 km) and temporal resolutions (3, 6, 12, 24 hly) relative to the most detailed reference resolution (resKNW, hourly and 2.5 by 2.5 km) [132].

Spatial and Temporal Resolution. Figure 2-6 summarizes the influence of the spatial and temporal resolution on the KGE performance metric and its components. Figure 2-6a shows that decreasing the spatial resolution is the dominant factor for lowering the KGE, while temporal resolution (hourly vs daily wind speed estimations) has only a limited influence on the KGE. The lowest KGE is found for the spatial resolution of 80 by 80 km (KGE = 0.18-0.43). The 30 by 30 km resolution provides intermediate KGEs (0.65-0.75), while a 10 by 10 km resolution or higher always results in a KGE greater than 0.89. The relatively low KGE for the 80 by 80 km resolution is caused by an overestimation of the spread in GPBT ($\gamma = 1.48-1.75$; Figure 2-6c) in combination with a decrease in the correlation coefficient (r = 0.79-0.81; Figure 2-6d). The y coefficient shows two interesting trends: it decreases with a decrease in temporal resolution, and it increases with a decrease in spatial resolution. These two trends counteract one another resulting in a higher KGE for the 80 by 80 km resolution with the lowest temporal resolution (24 hly).

2.4 Discussion

Interpretation. The analysis showed that the spatial and temporal wind information are of particular importance when assessing the wind turbine greenhouse gas payback time, a fact that is often neglected in LCAs, while the variation in turbine size appears to be of relatively lower importance. The analysis further indicated that daily wind speed data on a 30 by 30 km grid provide results that still match the reference high-resolution data (KGE = 0.75), although a spatial resolution of 10 by 10 km would further improve model performance (KGE = 0.89).

When time-averaged wind speeds over 35 years were used as an extreme scenario, GPBTs were severely overestimated. Wind speed shows a non-normal temporal frequency distribution, with lower wind speeds occurring more frequently than higher values [121]. Combined with the nonlinear dependence of the power output on the wind speed, the long-term average wind speed causes a strong underestimation of the power output and hence an overestimation of the GPBT. Using one daily wind speed value measured at noon performed equally well compared to the use of hourly data. In Europe, the average wind speed at noon is slightly higher than the daily mean for vertical levels up to 80 m [133]. Because more than 75% of the wind turbines included here have hub heights lower than 80 m, this leads to slightly higher power yields and consequently a 10% underestimation of GPBT compared to using the daily averaged wind data.

Completely neglecting spatial variability in the wind speed led to large over- and underestimations of GPBT of individual wind turbines. Although offshore wind turbines require more building materials (and hence have higher GHG emissions) than onshore installations, offshore GPBT are typically lower because of the higher wind speeds over sea. The results reflect, however, only a relatively small sample of only 80 offshore wind turbine locations; more offshore locations should be included to consolidate this conclusion.

Uncertainties. This study showed that it is highly relevant to account for spatiotemporal and technological variation when calculating the GPBT of wind electricity. A number of uncertainties may, however, influence the results, which are further discussed below.

First, wind farms were treated as a single geographical location, while in reality wind farms may occupy large surface areas. The largest farm in the data set (175 turbines with a diameter of 107 m) covers an area of approximately 56 km², thus covering multiple grid cells in the KNW-Atlas, which could each have a distinct wind climatology. However, less than 2% of the wind turbine locations in the data set span more than one grid cell and less than 0.6% more than two grid cells. Additionally, large wind farms are predominantly located offshore, where wind climatology is more stable because of low surface roughness [121]. Therefore, the effect of ignoring the spatial extent of wind farms is considered limited in the context of this study.

The power performance of wind turbines can also be influenced by wake effects. In a wind farm, downstream turbines are affected by a decrease in wind speed due to momentum loss caused by upstream turbines [134]. Several studies [121, 135] report that power output in wind farms are typically 5 to 10% lower because of these wake effects, but losses could be as high as 50% in large farms with narrow turbine spacing [136]. Here, more than 75% of the locations consisted of fewer than 4 turbines and only 0.1% of the locations had array sizes exceeding 10×10 turbines. Wake effects therefore are unlikely to influence the GPBT calculations. Still, wake effects may become important for other locations in the world and as more large wind farms are built in the future.

Another source of uncertainty is that a resolution of 2.5 km is most likely not sufficient to capture the local properties of wind speed at the top of mountain ranges. The energy yield of a wind turbine at mountain tops is therefore most likely underestimated in this analysis. However, with increasing height the air density decreases, which also influences power performance. A recent study by Jung and Schindler [137] showed that at a height of 800 m, the highest elevation with wind turbines in the study area, annual energy yields are overestimated by 6% when changes in air density are not considered. The same error in GPBTs is achieved when taking one daily wind speed measure instead of hourly data or changing from a 2.5 by 2.5 km to a 5 by 5 km grid. While the uncertainty from this simplification is not negligible, the 6% error in GPBT from neglecting air density changes is relatively small compared to the error introduced by using average wind speeds, as shown in the analysis. In areas with even higher elevations, spatiotemporal variance in air density should be accounted for because errors in energy yield can otherwise amount to up to 25%.

Incorporating more turbine-specific losses can further improve the GPBT calculations. Examples are performance decline due to aging, which has been reported to lie around 0.6% per year [138], and losses due to rotor blade soiling and/or icing, which are generally assumed to account for 2%, but can in rare cases exceed 20% [139].

Finally, a gas-fired power plant was chosen as the background energy system to focus the investigation on the effect of changes in wind climatology and turbine technology. More advanced reference systems that more precisely reflect what is replaced by the produced wind electricity can also be considered, but that would require a substantial amount of extra information about the electricity system as a whole [140]. Another possibility to evaluate the environmental trade-offs of wind electricity is to integrate the location-specific long-term power output and material requirements for wind turbines into integrated assessment models [141].

Outlook. The method presented here can be used to derive the environmental performance of current and future individual wind turbines worldwide even when limited information on turbine technology is available. Following the developments in the wind energy market to build larger wind farms, wake effects should be included in the future, and when areas with higher elevation are considered, the spatiotemporal variability in air density has to be considered.

Recent studies specifically focused on the energy production potential of wind turbines but did not consider environmental impacts such as GPBT [129, 142, 143] or use wind climatology that is either not globally available or at coarser resolutions. This study indicates that the use of current spatial resolution for global climate data archives (e.g., ERA-Interim [123]) of 80 by 80 km introduces a relatively large uncertainty in the power predictions (KGE = 0.18-0.43). A new ERA-suite, ERA5 [144], is under development with global climatological data at an hourly and 30 by 30 km resolution at which the KGE exceeds 0.7.

Therefore, using this method with the new ERA-suite would provide a good opportunity for location-specific predictions of the environmental impacts for wind turbines at the global scale. The method may also be used to identify optimal locations for wind turbines taking into account environmental impacts. The results could be incorporated as an extra factor in wind energy potential studies for various regions worldwide. In addition to the GPBT, this method can also be used to calculate payback times for other environmental impacts, such as water and mineral resource scarcity [145, 146], giving a more complete picture of wind turbines' environmental performances.

This study showed that the GPBT of wind turbines in northwestern Europe varies between 1.8 and 22.5 months. Detailed spatiotemporal (at least daily wind speed on a 30 by 30 km grid) wind climatology as well as hub height and rotor diameter of the wind turbines are required to assess the greenhouse gas payback times of wind electricity with sufficient accuracy. The findings imply that a location-specific assessment of wind turbines' GPBTs at the global scale is well within reach with the availability of high-resolution reanalysis data sets and wind turbine databases.

Acknowledgments

This work is part of project number 016. Vici. 170. 190, which is financed by The Netherlands Organisation for Scientific Research (NWO). The TOC art graphic was created in part using matplotlib, hosted at https://github.com/matplotlib/matplotlib.



3. Variability in Greenhouse Gas Footprints of the Global Wind Farm Fleet

L.C. Dammeier, J.H.C. Bosmans, M.A.J. Huijbregts (2023). *Journal of Industrial Ecology* 27(1): 272-282

Abstract

While technological characteristics largely determine the greenhouse gas (GHG) emissions during the construction of a wind farm and meteorological circumstances the actual electricity production, a thorough analysis to quantify the GHG footprint variability (in g CO₂eg/kWh electricity produced) between wind farms is still lacking at the global scale. Here, we quantified the GHG footprint of 26,821 wind farms located across the globe, combining turbine-specific technological parameters, life cycle inventory data, and location- and temporal-specific meteorological information. These wind farms represent 79% of the 651 GW global wind capacity installed in 2019. Our results indicate a median GHG footprint for global wind electricity of 10 g CO₂eg/kWh, ranging from 4 to 56 g CO₂eg/kWh (2.5th and 97.5th percentiles). Differences in the GHG footprint of wind farms are mainly explained by spatial variability in wind speed, followed by whether the wind farm is located onshore or offshore, the turbine diameter, and the number of turbines in a wind farm. We also provided a metamodel based on these four predictors for users to be able to easily obtain a first indication of GHG footprints of new wind farms considered. Our results can be used to compare the GHG footprint of wind farms to one another and to other sources of electricity in a location-specific manner.

3.1 Introduction

In order to limit global warming to 1.5 °C by 2100, a drastic reduction of greenhouse gas (GHG) emissions is needed [147]. While there are multiple pathways to achieve such a reduction, renewable energy technologies, such as wind energy, are an essential part in mitigation GHG emissions. Wind energy is often considered to be related to low emissions of air since its operation does not involve the emission of large quantities of GHGs and therefore wind energy operates at much lower GHG emissions than fossil fuel-based electricity generation technologies [148]. In recent years, wind energy has played an increasingly important role in supplying renewable energy, with more than 20% added installed capacity for onshore farms and more than 35% added installed capacity offshore between 2000 and 2018 and expected annual growth rates exceeding 7% and 11% until 2050 [149]. In 2019, the cumulative installed capacity worldwide was 651 GW [150] generating more than 1,400 TWh - roughly 5% of all electricity produced [151] - and the installed capacity could exceed 6,000 GW in 2050 [149].

However, GHG emissions from electricity production with wind turbines are not zero, as GHGs are emitted during other life cycle stages, mainly manufacturing of wind turbines [59, 152]. To assess the life cycle emissions of electricity production with wind turbines, all direct and indirect emissions need to be assessed. Expressing the life cycle GHG emissions per unit of electricity production provides the so-called GHG footprint (in g CO₂eg/kWh) [45], a metric enabling comparing life cycle GHG emissions of, among others, various technologies at different locations. Several studies report the GHG footprint of wind turbines, often by studying only one or a few wind turbines (see Table A-3 in Appendix A for references) or by harmonizing the conditions of multiple studies to cover a greater range of locations [58, 153]. These meta-analyses provide excellent insights into the main causes of GHG emissions of wind farms but do not show the variation in footprints between facilities at the global scale. A number of studies have looked at the GHG footprints of wind turbines on a larger scale, however often limited to one or a few countries [53, 152] or have not yet taken into account the effect of variation in climatology and technology [59].

Here, we quantified the GHG footprint of 26,821 wind farms worldwide, combining turbine-specific technological parameters, life cycle inventory data, and locationand temporal-specific meteorological information. To this end, we first applied a model to predict GHG life cycle emissions of wind turbines, excluding the end-of-life phase [21], using turbine-specific technological information from thewindpower. net database [106]. Electricity production of the wind turbines was estimated by combining turbine-specific power curves with meteorological information from the ERA5 reanalysis data set [154] at a 0.25° by 0.25° grid and hourly temporal resolution over a standard turbine lifetime of 30 years [155]. Based on our GHG footprint calculations for wind farms at the global scale, we further developed a metamodel for users to straightforwardly quantify the GHG footprint of a new wind farm, based on a limited number of technological and climatological key variables.

3.2 Materials and methods

We first describe the calculation of GHG emissions of wind turbine construction (section 3.2.1). Section 3.2.2 provides insight into the calculation of the lifetime electricity generation of the wind farm. Section 3.2.3 explains the development of the metamodel on the basis of the GHG footprints of the individual wind farms.

3.2.1 GHG emissions of wind turbine construction

The prediction of GHG emission related to wind turbine construction and maintenance are based on Dammeier et al. [21], in which a regression model was developed relating GHG emissions per turbine (in kg CO₃eq/turbine) to the wind turbine's rotor diameter (D; in m), hub height (H; in m) and on- or offshore location (O; 0 for onshore, 1 for offshore):

$$log_{10}(GHG_{turbine}) = 1.99 + 1.31 \cdot log_{10}(D) + 0.79 \cdot log_{10}(H) + 0.29 \cdot O$$
 (3-1)

based on information from 28 wind turbine LCA studies, which were standardized by Dammeier et al. [21], using the same LCI database (EcoInvent version 3.2) for the materials and energy required for the construction of the wind turbines as reported in these LCA studies. Maintenance cycles were also standardized in Dammeier et al. [21]. The model excludes the emissions related to the end-of life and grid connection of a turbine. Differences in materials used and construction are included implicitly through the use of different LCA studies. In order to calculate GHG emissions for a wind farm, GHG_{turbine} is multiplied by the number of turbines in a wind farm.

Data on the wind turbine's rotor diameter, hub height, and on- or offshore location were derived from thewindpower.net database [106], which provides data on wind farm location and technological turbine characteristics for 31,298 wind farms worldwide, consisting of 266,074 wind turbines. For 132 offshore wind farms, information on location was supplemented with updated information from [106] and [156]. Data on both diameter and hub height were complete for 15,684 of the wind farms (50%). The 4,609 wind farms were excluded because information on location was unavailable. For the other wind farms, information on rotor diameter D (n = 5,132) or hub height H (n = 10,336) were lacking. In these cases, other turbine-specific parameters, such as nameplate capacity, were used to predict rotor diameter and/or hub height (see Appendix A, section A.1). We were able to include 26,821 (85.7%) wind farms with a total capacity of 523.3 GW in our GHG footprint calculations. This is 80% of the 651 GW installed in 2019 [150]. In the supporting information (section A.2) we provide per country the installed capacity we were able to include in our calculations versus the total installed capacity reported by Ritchie and Roser [151] and IRENA [157].

3.2.2 Electricity generation

Power curves were used to predict net electricity generation of wind turbines (P_{turbine} in kW), which can be described by a logistic function chosen to stay as close as possible to the information provided by the manufacturers and which is of the form [158]:

$$P_{turbine} = \frac{P_{rated}}{1 + e^{\left(-k \cdot (v_H - b)\right)}}$$
(3-2)

where P_{rated} is the turbine's nameplate capacity [MW], v_H is the instantaneous wind speed at hub height [m/s], k the logistic growth rate, and b the sigmoid's midpoint wind speed. The power curves were fitted to the data provided by the manufacturers through the wind farm database using SciPy's curve fit routine [159]. The average R² of the fit for each wind farm with power curve data is 99.6% (ranging from 98.6 to 99.9 as the 2.5th and 97.5th percentiles). For the 7,771 wind farms for which data on the power curve were not available, the average k of 0.74 (0.58-0.77; 95% confidence interval) and an average b of 8.58 (7.20-8.82; 95% CI) of the wind farms with power curves were used.

Note that below the cut-in wind speed, a wind turbine is not operational. If the actual wind speed is higher than the rated wind speed, the wind turbine produces at its nameplate capacity up to the cut-off wind speed. Under circumstances that the wind speed is above the cut-off wind speed, the turbine is turned off. If this type of data were not available for an individual wind farm, the cut-in wind speed was set to 3 m/s, the rated wind speed to 13 m/s, and the cut-off wind speed to 25 m/s, which are the typical cut-in, rated, and cut-off wind speeds of wind farms in the data set (see Appendix A, section A.1 for more information on gap filling). All instantaneous power calculations were added to calculate the total power produced by a turbine during its lifetime.

The wind speed at hub height v_u [m/s] is calculated from wind speed at 10 m [m/s] according to the power law

 $v_H = v_{10} \cdot \left(\frac{H}{10}\right)^{\alpha} \cdot \left(\frac{\rho_H}{1225}\right)^{\frac{1}{3}}$ (3-3)

with H the hub height in m, air density ρ_H at hub height in kg/m³, and the wind shear exponent a being given through

$$\alpha = log_{10}\left(\frac{v_{100}}{v_{10}}\right) \tag{3-4}$$

with v_{100} the wind speed at 100 m and v_{10} the wind speed at 10 m. In order to be consistent throughout the calculations, the same spatial and temporal resolution applied in the other calculations is used here as well.

Often, a standard air density of 1.225 kg/m³ is used when estimating annual energy production of wind turbines [160]. However, air density decreases with decreasing temperature and increasing altitude and neglecting air density in power production can lead to over- and underestimations of power production of more than 20%. Differences increase with increasing wind speed (up until the rated wind speed) [160]. Therefore, air density p was corrected for temperature and altitude to give air density at hub height (ρ_H [kg/m³]) through

$$\rho_H = \frac{p_H}{(R \cdot T_H)} \tag{3-5}$$

with p_H air pressure at hub height [Pa], T_H temperature at hub height [K], and R the ideal gas constant of 8.31447 J/mol/K [137]. Pressure and temperature also vary with height, which is further explained in section A.3 of Appendix A.

The location-specific climate data required for the calculations of the wind speed, including the wind shear exponent and the air density, has been downloaded from ERA5, the most recent and highest-resolution reanalysis data set [144]. Here, hourly data over a period of 30 years was used (years 1988 until 2017) for v, T, and p on a 0.25° by 0.25° grid, which has recently been shown to provide sufficient spatial and temporal details [21], because a lower temporal resolution can lead to overand underestimations of GHG footprint calculations. For each of these hourly data points, the power output is calculated using equation (3-2) and subsequently aggregated over the 30 years to give the lifetime power production of the wind

farms. We used a typical 30-year life span of a wind turbine, as reported in a recent survey carried out in the United States [155].

The so-called wake effects can decrease the net electricity generation P_{net} of wind farms, because the wind speed downstream of a wind turbine is lower than upstream. We included the wake effect in our calculations via:

$$P_{net} = P_{turbine} \cdot N_{turbine} \cdot f_w \tag{3-6}$$

The relative reduction in net electricity generation due to wake effects (f_w is dimensionless between 0 and 1) depends on a wind farm's size according to:

$$f_w = 1 - 0.033 \cdot ln(N_{turbines}) \tag{3-7}$$

with N_{turbines} the number of turbines in the wind farm. The relationship in equation (3-7) was derived by extrapolating information on the power loss in different wind farm settings given in [136] (see Appendix A, section A.4 for more information). Here, we assume an average turbine spacing of nine rotor diameters, as we do not have location-specific information on turbine spacing. The number of turbines is given in the windpower.net database [106].

3.2.3 Metamodel

A metamodel was developed to be able to directly approximate the GHG footprint of a specific wind farm with a limited number of technological and climatological variables. The metamodel was derived with a generalized linear modelling (GLM) approach, linking the log-transformed GHG footprints we derived with our detailed calculations for the individual wind farms to hub height, rated power, on-/offshore location, number of turbines in farm, and the 30-year average 100 m wind speed at farm location. Rotor diameter was excluded from the GLM fitting due to high covariance with other wind turbine characteristics, that is, a variation inflation factor of higher than five. The metamodel was built with data from the 15,684 wind farms for which all relevant turbine-specific data were reported. The best model was chosen based on the Akaike information criterion (AIC). Variable importance in the metamodel was assessed by predictor randomization. Every predictor was randomized in turn and the model was rebuilt, after which the R² of the rebuilt models are compared. The bigger the drop in R², the more important a predictor. For the best model, partial dependency plots were created, which show how each predictor affects the GHG footprint. More information on the metamodel can be found in Appendix A, section A.5.

3.3 Results

We show the GHG footprint of the global wind farm fleet (section 3.3.1) and the results of the metamodel development (section 3.3.2).

3.3.1 Greenhouse gas footprint

Figure 3-1 maps the individual GHG footprints of the global wind farm fleet, with a median of 10 g CO₂eg/kWh and a range of 4-56 g CO₂eg/kWh [2.5-97.5% interval]. Maps of the GHG footprints per continent can be found in Appendix A, section A.6. We found relatively low GHG footprints along the coast and offshore, while higher footprints are typically found further inland. While the GHG footprint ranges can vary, with Africa and Asia showing larger ranges than America, Europe, and Oceania, the median does not vary greatly between continents (Figure 3-2).

The wind farms included here have an average calculated capacity factor of 24% ranging from 2% to 70% (2.5th to 97.5th percentiles), with more detail provided in section A.7 of Appendix A.

The results from our study are in line with what previous studies on individual turbines have found, in which footprints range from 3.6 to 46 g CO₂eq/kWh (see Table A-3 in Appendix A for reference) (Figure 3-3).

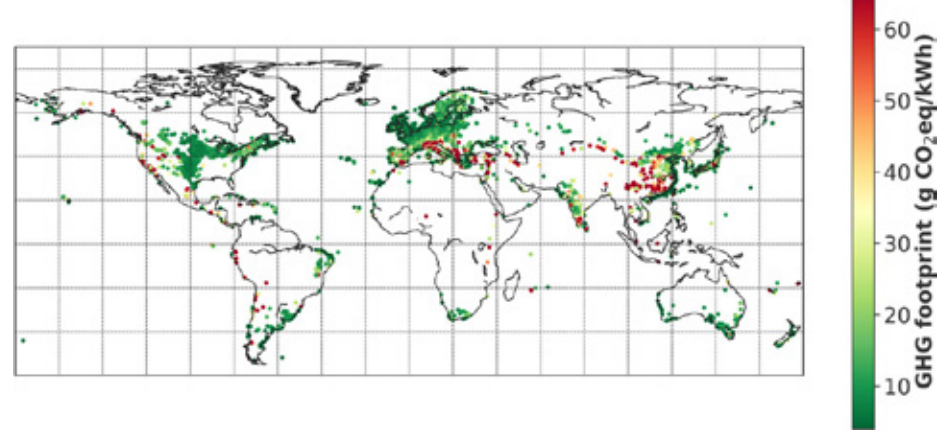


Figure 3-1 Greenhouse gas footprints of the individual wind farms in CO,eq/kWh of the global wind farm fleet. Underlying data for Figure 3-1 can be found in Supporting Information S2.

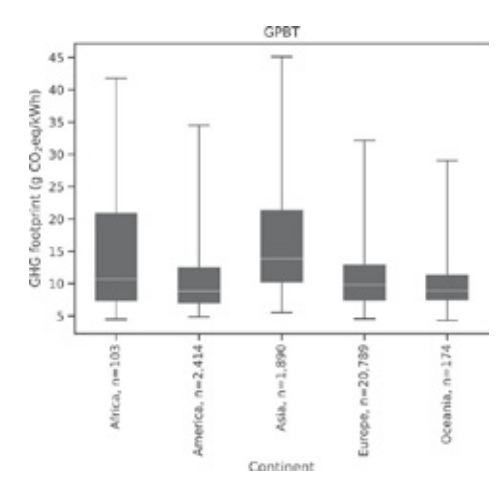


Figure 3-2 Greenhouse gas footprints grouped by continent. The white line is the median, the box the 25th to 75th percentile, and the whisker the 2.5th to 97.5th percentile. Underlying data for Figure 3-2 can be found in Supporting Information S2.

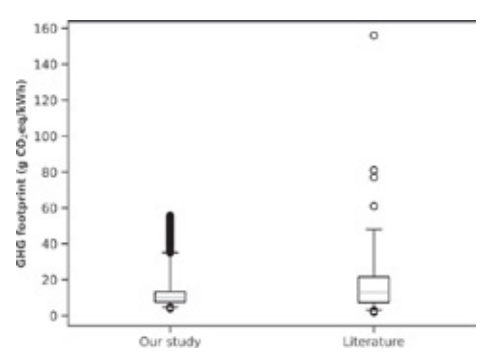


Figure 3-3 Greenhouse gas footprint ranges of our study compared to values found in literature (see Table A-3 of Appendix A for details). The orange line is the median, the box the 25th to 75th percentile, and the whisker the 2.5th to 97.5th percentile. Underlying data for the results from this study in Figure 3-3 can be found in Supporting Information S2. Data from the literature can be found in Table A-3 of Appendix A.

3.3.2 Metamodel

The best model based on the AIC is

$$log_{10}(GHG) = 2.41 - 0.20 \cdot v_{avg} - 5.9 \cdot 10^{-4} \cdot P_{rated} - 8.3 \cdot 10^{-5} \cdot H + 5.3 \cdot 10^{-3} \cdot N_t + 0.33 \cdot O$$

$$(3-8)$$

 v_{avq} is the 30-year average wind speed at 100 m [m/s], P_{rated} the turbine's rated farm, and O is a categorical variable denoting either onshore (0) or offshore (1) wind farms. This means that GHG footprints decrease with increasing average wind speed, capacity, and hub height and increase with increasing number of turbines and offshore location. The model's R2 is 0.85 with a residual standard error (RSE) of 0.10. The RSE of 0.1 implies that 95% of the GHG footprint estimates of the metamodel fall within a factor of ±1.6 of the more detailed GHG footprint calculations with hourly time steps.

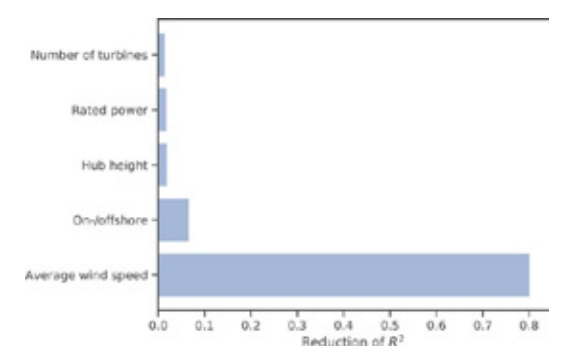


Figure 3-4 Importance of predictors of greenhouse gas footprints after rebuilding the model with randomized variables. A bigger reduction of R2 means that the variable is more important. R2 reductions are 0.015 for the number of turbines, 0.018 for the rated power, 0.020 for the hub height. 0.067 for on-/offshore, and 0.802 for average wind speed.

Figure 3-4 shows the effect of randomization on the R². Randomizing the average wind speed leads to the biggest reduction in R², which means that it is the most important predictor of wind farms' GHG footprints, followed by whether a farm is located on- or offshore. Hence, an increase of the average wind speed of 1 m/s would lead to a factor 1.6 decrease in the log of the GHG footprint, while changing from on- to offshore would lead to a factor 2.1 decrease in the log of the GHG footprint. Similarly, Figure 3-5 shows the effect of each variable on the GHG footprint of wind farms. The effect is shown for on- and offshore wind farms separately. A bigger change means that the variable is more important, and the figure also shows the direction of change in GHG footprint related to a variable. Higher wind speeds result in lower footprints while more turbines lead to higher GHG footprints.

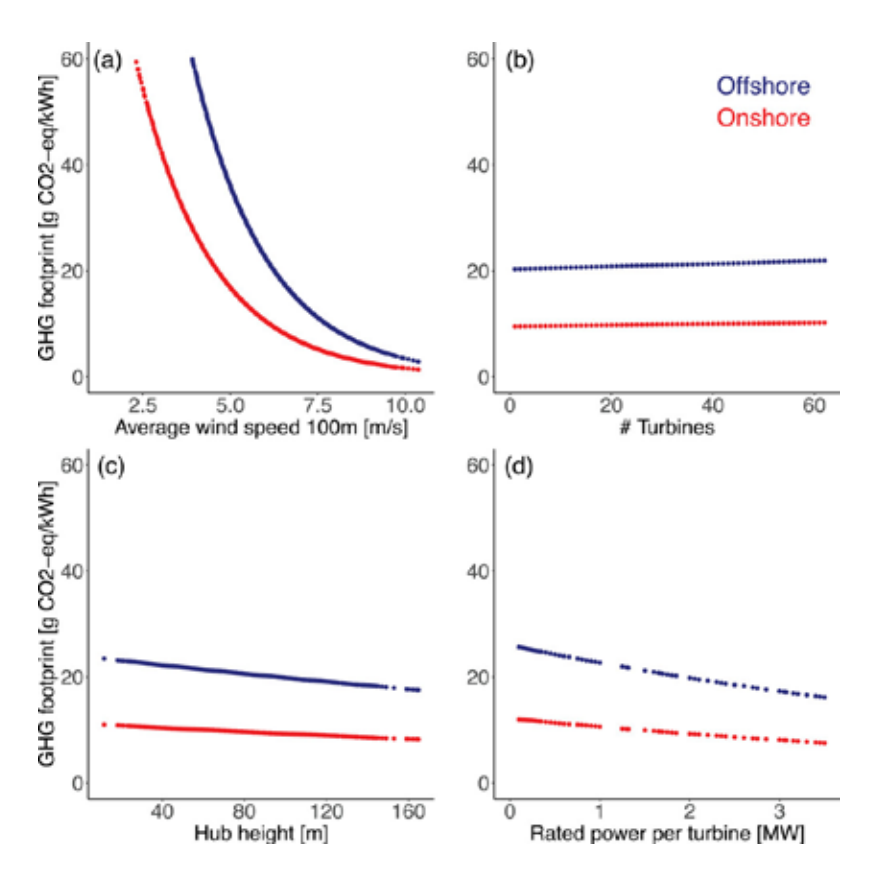


Figure 3-5 Partial dependency plots showing the effect of each variable on the greenhouse gas (GHG) footprint of wind farms. A bigger change in GHG footprint means that the variable is more important. (a) Average wind speed at 100 m in m/s. (b) Number of turbines. (c) Hub height in m. (d) Rated power per turbine in MW. Underlying data for Figure 3-5 can be found in Supporting Information S2.

3.4 Discussion

We first discuss the GHG emissions of wind turbines (section 3.4.1) and section 3.4.2 discusses the factors influencing the electricity generation calculations.

3.4.1 GHG emissions of wind turbines

The model to predict the life cycle GHG emissions of the production of a wind turbine, based on a limited number of technological characteristics, has been developed in an earlier study [21]. While 78% of the wind farms evaluated in our study have a hub height and rotor diameter that fall within the limits of the turbines used to build the regression model (see Appendix A, section A.9), further improvements in the model can be considered by expanding the LCA data set with smaller and bigger turbines to further increase the applicability domain. With a larger data set, other predictor variables, such as more detailed information on wind turbine type, can be considered as well in the regression model development. Furthermore, our model includes major life cycle stages of wind turbines but does not take into account emissions that occur during a wind turbine's end-of-life. While most materials can be recycled, the end-of-life of turbine blades is a pending point of discussion as no common recycling method is available yet [161]. Also, the grid connection is not included in the analysis, which can be especially important in offshore wind farms [52]. Future studies could incorporate these aspects as well, to make the model more complete. Furthermore, it would be interesting to see the effect of energy storage, which will likely be needed as the share of wind energy in the electricity mix increases, on the GHG footprint of wind farms [162].

To understand possible consequences of gap filling, we compared the GHG footprint ranges of the group of wind farms for which all information was complete to the group for which at least one variable was estimated. The results can be seen in Figure A-9 of Appendix A, which shows that there are no systematic differences between the GHG footprints of wind farms for which all information was available and those for which information had to be derived via gap filling.

3.4.2 Electricity generation

An important factor in GHG footprint calculations is the amount of electricity generated by a wind turbine. To verify electricity production estimates, we compare our results with empirical electricity production data at the level of individual wind farms for the United States of America and Denmark (see Figure 3-6). These two countries provide long-term electricity production data for which comparison on a wind farm by wind farm basis was possible. We obtained empirical electricity production data from wind farms in the United States for the period 2001 through 2017 [163]. We included empirical data from 657 wind farms in the United States that could be matched to wind farms in our database, based on specific name and state. On average, electricity production reported by the EIA was 1.15 higher than the yearly average electricity production we calculated over the 17 years time period, with extremes ranging from 0.64 times our calculated yearly average electricity production to 4.80 times that [2.5th and 97.5th percentile range]. This relatively large range could in part be caused because matching is solely done on name and state, but additional information on capacity and technology was unavailable. We also compared our yearly average electricity production estimates of 1,724 wind farms with empirical data for the Danish wind farm fleet [164], using data from 1988 to 2017. The reported electricity production was, on average, 0.78 times our estimated

electricity production for the Danish farms over a period of 30 years (with 0.45 and 1.17 the 2.5th-97.5th percentiles) (see section 3.3 for more details).

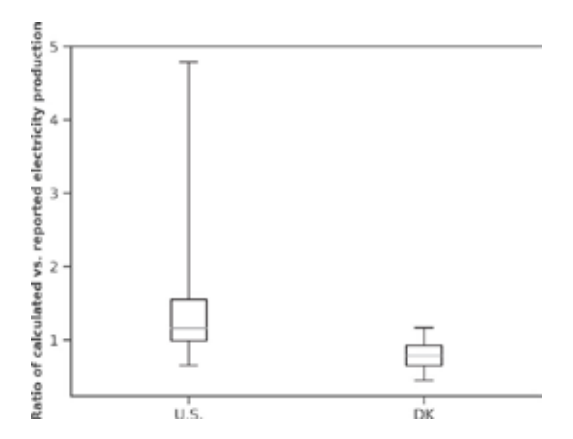


Figure 3-6 The boxplot shows the ratios of calculated versus reported electricity generation for the United States and Denmark. The orange line is the median, the box the 25th to 75th percentile, and the whisker the 2.5th to 97.5th percentile. Underlying data for Figure 3-6 can be found in Supporting Information S2.

This comparison shows that, although our electricity estimates are generally in line with empirical observations, they are not without uncertainty. First, a logistic function was used to calculate the power curve. Recent developments have shown that power curves can also be derived using process-based model approaches [165]. It could be interesting to evaluate whether alternative power curves are able to further improve the prediction of electricity production of a large range of wind turbines. Second, we used the ERA5 climate data which has the highest-resolution reanalysis data available on a global scale, with hourly time steps and $0.25 \times 0.25^{\circ}$ spatial resolution. There are uncertainties in the ERA5 wind data, such as incidental very high wind speeds at some locations [166] - at which our data set shows that no wind farms are present, and difficulties to capture the variations in wind speed in more complex terrain [167]. Despite these uncertainties, Ramon et al. [168] have shown that the ERA5 near-surface wind data set is the best global reanalysis data set available to provide wind speed at hub height. Due to their relative coarse resolution, reanalyses have difficulties to adequately represent local climatic conditions [169]. As electricity production depends on the cube of the wind speed, small biases in wind speed data have a large effect on electricity production estimations and hence the GHG footprint. Applying bias correction using more detailed spatial information does not improve results significantly [169]

and the ERA-5 reanalysis data used here has been found to be better at estimating electricity production from wind, in a country-wise comparison as well as on a perturbine basis, than other global data sets, such as MERRA-2 [167, 169]. When wind speed is overestimated, the GHG footprint is underestimated and vice versa. Efforts have been made to derive country-wise correction factors to apply to reanalysis data so that the country-wide electricity production better matches historic production [170]. Applying such a country-wide correction factor to our wind farmspecific data would however lead to over- or underestimations of production where our calculations match reported production and therefore not improve overall results. Furthermore, we accounted for the wind turbine wake effect in a simplified manner. Findings of previous studies vary, but generally wake effects depend on atmospheric stability and the distance between turbines and between wind farms. Here, turbines have been assumed to be placed at a distance of 9 diameters, which is slightly higher than the often seen 7 diameters (see section A.4 for more details). However, wind parks are not usually built in a square but have a larger front facing the main wind direction with varying spacing between cross- and downwind direction [171]. To counteract this effect, we assume a larger turbine spacing. If turbines are placed closer together, power production will decrease [136]. Placing turbines at 5 diameters distance instead of 9 diameters in a 10 by 10 array reduces the efficiency to 70% instead of 86%. In larger arrays, the effect thus becomes more pronounced. A higher wake effect thus results in lower electricity generation and therefore higher GHG footprints. Finally, the electricity generation of a wind turbine is directly dependent on its lifetime. Here, we assume a lifetime of 30 years, which is representative for recent turbines [155], but in the past shorter lifetimes of 20 to 25 years have been assumed [59, 172, 173]. A shorter lifetime increases the GHG footprint because less electricity is produced.

3.5 Conclusions

The GHG footprint of the global wind farm fleet has been calculated in a locationspecific manner ranging 1.1 orders of magnitude [2.5th-97.5th range] between individual wind farms. Our metamodel showed that the GHG footprint of electricity produced by a specific wind farm can be approximated by a limited number of technological and meteorological variables. The variation in GHG footprint of wind electricity was mostly explained by the variation in wind speed across different locations. The metamodel developed can also be used to calculate the GHG footprint of new wind farms and to straightforwardly derive potential well-suited locations for these new wind farms. Furthermore, our results can also be used to compare the GHG footprint of wind farms to one another and to other sources of electricity in a location-specific manner. Finally, the method described here can be extended to other impact categories, to identify potential environmental trade-offs of placing wind farms in certain locations.

Acknowledgments

This work is part of project number 016.Vici.170.190, which is financed by The Netherlands Organisation for Scientific Research (NWO).



4. Greenhouse Gas Footprints of Utility-scale Photovoltaic Facilities at the Global Scale

J.H.C. Bosmans, L.C. Dammeier, M.A.J. Huijbregts (2021). *Environmental Research Letters* 16: 094056

J.H.C. Bosmans, L.C. Dammeier, M.A.J. Huijbregts (2023). Corrigendum: Greenhouse gas footprints of utility-scale photovoltaic facilities at the global scale (2021 *Environ. Res. Lett. 16 094056*). *Environmental Research Letters 18: 059501*

Abstract

Technological characteristics and meteorological conditions determinants of the greenhouse gas (GHG) footprints of photovoltaic facilities. By accounting for technological and meteorological differences, we quantified the GHG footprints of 9,992 utility-scale photovoltaic facilities worldwide. We obtained a median greenhouse gas footprint of 58.7 g CO₂eg/kWh, with a 3-fold spread (28.2-94.6 g CO₃eg/kWh, 2.5th and 97.5th percentiles). Differences in panel type appeared to be the most important determinant of variability in the GHG footprint, followed by irradiation and a facility's age. We also provided a metamodel based on these three predictors for users to determine the facility-specific greenhouse gas footprint. The total cumulative electricity produced by the utility-scale photovoltaic fleet worldwide is 457 TWh/yr, 99.6% of which is produced at footprints below 100 g CO₂eg/kWh. Compared to earlier studies, the footprints we computed of global utility-scale facilities show a relatively large spread. In order to further improve the accuracy of facility-specific footprints, more information on panel type as well as production country is required.

4.1 Introduction

Photovoltaic solar power (PV) is an important source of renewable energy, producing electricity at much lower greenhouse gas (GHG) emissions than conventional fossil-based technologies [174]. By 2019, global PV capacity reached 580 GW [175] and generated ~720 TWh of electricity, roughly 3% of current global electricity production [176]. PV is now the third-largest renewable electricity source after hydropower and onshore wind [177], and its share is growing rapidly, with a potential 877 GW added by 2024, accounting for 60% of the expected growth of all renewables [176].

Various studies have investigated how life cycle GHG emissions of PV compare to emissions from fossil-based electricity sources. One approach in such studies is to perform a meta-analysis by gathering case studies reported in literature and harmonize their findings to represent standardized system boundaries for irradiation, lifetime, performance ratio and/or module efficiency [54 - 57]. The GHG footprints in these papers, expressed as life cycle GHG emissions per unit of electricity produced, range from ~14 to 82 g CO₃eq/kWh under harmonized conditions, with the greatest source of variation being the type of panel [56, 59, 60, 61]. Typically, thin film panels such as cadmium telluride, copper indium gallium diselenide and amorphous silicon have lower GHG footprints than mono- and polycrystalline silicon panels.

Meta-analyses provide insights in the sources of life cycle GHG emissions related to PV, but because of the harmonization process they do not show how footprints can vary in reality. Location of installation determines the amount of irradiation received by the panels, and location of production determines the GHG emissions during manufacturing, both important factors in the PV GHG footprints [60, 62, 63, 64, 67]. Furthermore, intra-type variation in module efficiency, type of mounting system, lifetime, degradation and capacity can explain variations in PV GHG footprints [54, 65, 66, 68 - 71]. With higher irradiation, for instance, footprints reduce due to higher electricity production [54, 60, 62 - 66]. Spatial differences in environmental footprints of PV are assessed by Louwen et al. [72] for rooftop PV in Eurasia and Africa, Ito et al. [73] for two sites in France and Morocco, and Pérez-López et al. [74], Perez-Lopez et al. [75] for utility-scale PV globally. These studies indicate that GHG footprints of PV vary significantly with location. Placing a PV facility at a location with high irradiation can reduce the GHG footprint by up to ~75% [72], and even within a country such as France choosing a location with higher irradiation can reduce the footprint by ~25% [74]. While providing valuable insights into the geographic variation of PV footprints, these studies do not use data on the actual fleet of PV facilities and therefore cannot assess the footprint of actual PV electricity.

Here, we quantified life cycle GHG footprints of the global utility-scale PV fleet, including ~10,000 facilities. With these GHG footprints we derived GHG emissionelectricity supply curves for the PV fleet and built a regression model to analyse which technological and/or climatological variables are most important for determining the GHG footprint. In addition, this regression model can be used for quick estimation of GHG footprints of PV. We use 30 years of the most recent highresolution climate reanalysis dataset ERA5 [144] at ~0.25° spatial and hourly time resolution, as well as a global dataset on facility-specific location and technological characteristics of existing and planned utility-scale facilities, combined with regionalized life cycle inventory data for PV production.

4.2 Materials and methods

4.2.1 GHG footprint

We compute the GHG environmental footprint EF_{GHG} as impact I per unit of electric power P:

$$EF_{GHG} = \frac{I}{P} \tag{4-1}$$

where we consider life cycle impact I in g CO₂eq, and lifetime electricity output P of a PV facility in kWh. For a location-specific EF, we use a dataset of 9,992 utilityscale photovoltaic parks across the globe (see section 4.2.2), market shares by origin countries per continent [178] and production location-specific impact I (this section), as well as a high-resolution global climate reanalysis dataset (see section 4.2.3). Figure 4-1 provides an overview of our methods.

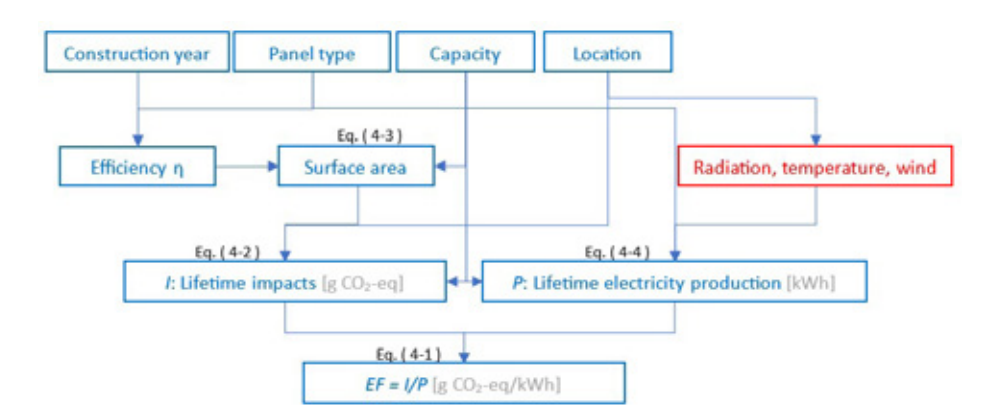


Figure 4-1 Overview of methods. Blue boxes refer to facility-specific technological characteristics (section 4.2.2), mainly from Wiki-Solar, the red box refers to input from the ERA5 climate reanalysis dataset (section 4.2.3). The equations refer to the computations described in section 4.2.1.

Life cycle greenhouse gas emissions, or impact I in equation (4-1), are derived using market shares by origin countries per continent [178] and production locationspecific impact (see Appendix B section B.2 for further details) and a facility's panel surface area:

$$I = I_{m^2} \cdot A \tag{4-2}$$

with surface area A (m²) depending on a facility's capacity and efficiency:

$$A = \frac{W_p}{rsds_{STC} \cdot \eta} \tag{4-3}$$

following Bhandari et al. [56]. Capacity in Wp is available from the Wiki-Solar dataset ('Wp' for Watt-peak, indicating direct current output under standard testing conditions), rsds_{stc} is surface downward solar radiation under standard testing conditions (1,000 Wm^{-2}) and η is panel efficiency (as a fraction of solar radiation that the panel can convert into electricity). n depends on panel type and year, following Chen et al. [179], see Appendix B section B.1.

We derived for each panel type considered (mono-crystalline silicon, polycrystalline silicon, amorphous silicon, cadmium telluride and copper indium (gallium) diselenide life cycle GHG emissions (I_m²) representing a continent-specific weighted average of production countries, as data on the production location for each individual facility is unavailable. Market shares by producing countries per continent are obtained from Absolute Reports [178]. We use 2016 market shares

for current facilities, and 2019 market shares for planned facilities. Type-specific impacts per producing country (China, EU, US, Malaysia and Korea) are obtained from literature (see Appendix B Table B-3).

Besides the impacts per m² of panel, a PV facility's impact derives from the so-called 'balance of systems' (BOS). The BOS includes the mounting system, wiring and inverters [54]. Here we use EcoInvent 3.5 values per m² of open ground mounting system as well as the impacts of inverters and electrical installation per unit capacity, independent of panel type and production location.

For more detail on life cycle GHG emissions, see Appendix B section B.2.

The electricity output of a PV facility depends on multiple variables, including the panel type, irradiation and temperature. Here we follow the PV power computations of Jerez et al. [180], based on Mavromatakis et al. [181]. Jerez et al. [180] define the PV power generation potential PVpot, a dimensionless magnitude accounting for the performance of a PV cell with respect to the power capacity (here expressed in MWac, obtained from the WikiSolar database). PVpot depends on radiation rad and cell temperature T_{cell}, the latter depending on air temperature, radiation and wind [30] as well as panel type. We furthermore account for losses due to panel degradation. In short, the instantaneous PV power production provided to the grid (in alternating current) is given by:

$$P(t) = PVpot(rad, T_{cell}) \cdot MWac \cdot f_{loss}$$
 (4-4)

For PVpot we use the location-specific hourly ERA5 climate variables for 1988-2017 (see section 4.2.3), thus obtaining a power output representative of current climate. Loss ratio f_{loss} is applied to account for panel degradation and is set to 0.899, representing a loss of 0.7%/yr over a 30-years lifetime [74, 182]. A 30-year lifetime is assumed to be representative of modern PV [182]. The full equations for computing generated electricity are given in Appendix B section B.3.

4.2.2 Facility-specific technology and location data

To compute facility-specific impact I and power output P, we need to know a facility's age (construction year), panel type, capacity and location-specific climate variables (see Figure 4-1). We use the Wiki-Solar dataset (http://wiki-solar.org) which provides technological characteristics of utility-scale PV projects around the globe, with a minimum, median and maximum capacity of 3, 10 and 3,000 MWp. Wiki-Solar includes 10,268 PV facilities, of which 9,992 with a known location. 7,982

facilities are operating or were in late stages of construction at the time of datagathering (2019) and 2,010 are planned. The median construction year is 2016. The total capacity in these 9,992 facilities is 367 GWp. Figure 4-2 shows the location and capacities of all facilities.

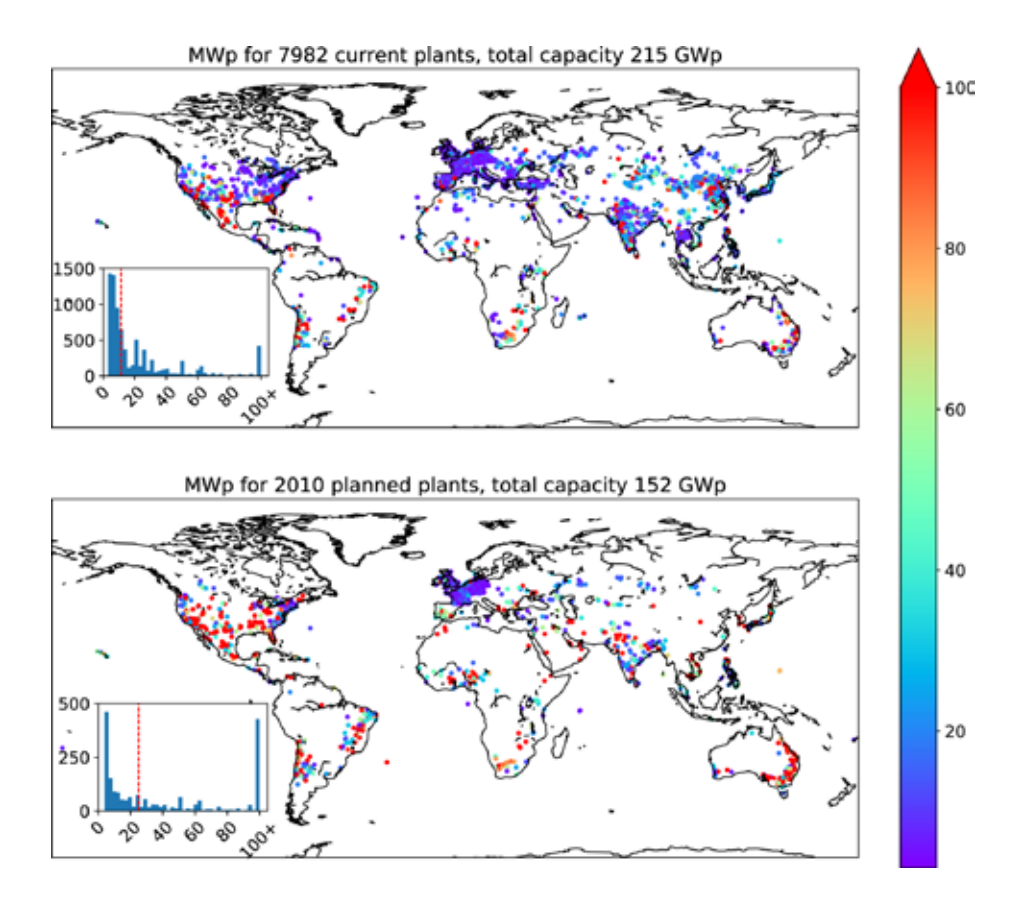


Figure 4-2 Location (map) and histogram (inset) of capacity, in MWp, available from the Wiki-Solar database for currently operating facilities (top) and planned facilities (bottom). The red dashed line in the histogram indicates the median capacity.

The Wiki-Solar dataset provides information on the panel type for 1,249 out of 9,992 facilities. We consider the five most common types [183]; mono-crystalline silicon, poly-crystalline silicon, amorphous silicon, cadmium telluride and copper indium (gallium) diselenide. To increase the number of facilities with known panel type, we gathered extra information from PV suppliers in Wiki-Solar as well as US EIA and GEO datasets [184, 185]. We found specific panel types for 99 additional facilities and narrowed the panel type to either crystalline or thin film for 1,443 and

17 facilities, respectively. Where a specific type is unknown, we computed the GHG footprint for the two crystalline types in case of crystalline panels, the three thin film types in case of thin film panels, or all five types where no information on panel type was found. The results represent an average footprint of these types weighted by 2016 production data for current facilities and 2019 production data for planned facilities (see Appendix B Table B-2). As described above in section 4.2.1, results also represent a continent-specific weighted average of I panel by production countries.

For capacity, Wiki-Solar provides both MWac and MWp for 2,046 facilities. For these facilities, the median performance ratio (PR = MWac/MWp) is 0.8, which is also the IEA recommended value [182]. For all remaining facilities, either MWac or MWp is given, and the PR value of 0.8 is used to derive the missing MWac or MWp.

For more detail on the Wiki-Solar dataset and gap filling, see Appendix B section B.1 (available online at https://stacks.iop.org/ERL/16/094056/mmedia).

4.2.3 Climate data

For power output computation, we use the most recent and highest-resolution global re-analysis dataset representing current climate at 0.25° × 0.25° (roughly 30 × 30 km at equator) [144], obtained through the Copernicus Climate Change Service [186]. Hourly resolution allows us to include the daily cycle of radiation as well as temporal variation in cell efficiency due to cell temperature (including air temperature, radiation and wind) see Appendix B section B.3 [187]. Hourly data gives improved estimates of PV power generation compared to lower-resolution data [188] (for more detail see Appendix B section B.4).

4.2.4 GHG emission—supply curves

To create GHG emission—supply curves, we ordered all 9,992 by their GHG footprint and computed the cumulative power production. Furthermore, we applied a bootstrapping technique to determine the uncertainty introduced by panel type, which is unknown for a large number of facilities. Instead of using weighted footprints at facilities where panel is unknown, we created 10,000 instances of our dataset, where each time a facility's footprint (if unknown) is set to that of one of the panel types, selected using 2016 (2019) production data as weights for current (planned) facilities (Fraunhofer ISE [183], also used in the weighted footprints in section 4.3.1). 2016 is the median construction year for facilities with unknown type in the Wiki-Solar database, 2019 is the latest year for which type-specific production data is available (see Appendix B Table B-2).

4.2.5 Regression analyses

After computing the GHG footprint for utility-scale PV facilities, we created a linear regression model to help determine which of the predictors we take into account (age, panel type, capacity and location-specific climate variables, see Figure 4-1) explains most of the variance in EF_{GHG}. We build this model on the 1,348 facilities for which panel type is known. Note that we cannot currently take production location into account in this regression, as facility-specific production location is unknown (instead we used continent-specific weighted averages of production countries based on market shares). For the climate variables, we use location-specific 30-year mean day-time irradiation I, temperature T and wind speed u as well as coefficient of variation (CV) for each variable to represent intra-year variation (see Appendix B equation (B-7)). The correlation matrix of the predictors (supplementary Figure B-1) shows that there are no significant correlations between the variables, and the variance inflation factors (vifs) are all below 5. Capacity is log-transformed because its distribution is right-skewed. We also log-transformed the response variable (EF_{GHG}). The model includes the interaction between panel type and construction year, because these together determine efficiency η used in the life cycle GHG emissions (equation (4-3), Appendix B section B.1).

After determining the best model, based on the Akaike Information Criterion, we assess the importance of each predictor using predictor randomization. Each predictor is randomized in turn, after which the model is re-built. The larger the drop in the model's R², the more important a predictor is. Results are shown in section 4.3 and more details on the regression model can be found in Appendix B section B.5.

4.3 Results

4.3.1 GHG footprints

The GHG footprint of all PV facilities is 58.7 (28.2-94.6) g CO₂eq/kWh (median, 2.5%-97.5% quantiles). 9,810 out of the 9,992 facilities (98.2%) have a GHG footprint below 100 g CO₂eq/kWh. Figure 4-3 shows that the spatial pattern is mostly dominated by latitude, with facilities at higher latitudes having higher GHG footprints due to lower irradiation and electricity output. The latitudinal pattern also emerges by looking at GHG footprints per continent (boxplots in Figure 4-3); Europe has the highest footprint, with a median EF_{GHG} of 76.9 (46.1-112.2) g CO₂eq/kWh (based on current and planned facilities combined). Lowest footprints are found in lowlatitude continents; South America (45.4 [30.6-62.3] g CO₂eq/kWh) and Africa (49.1 [31.5-61.0] g CO₂eq/kWh).

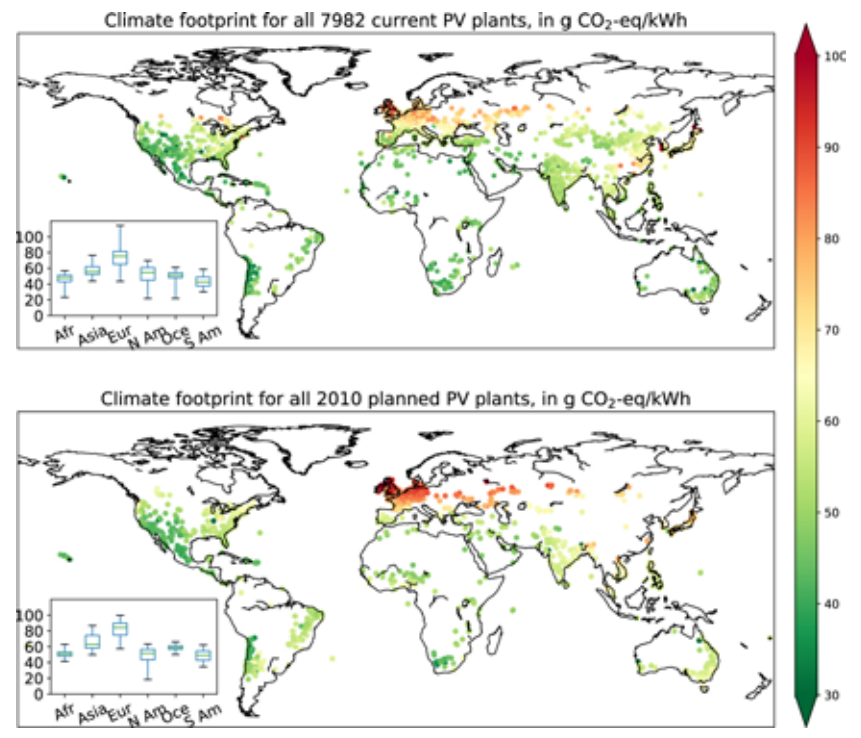


Figure 4-3 GHG footprint in g CO₂eq/kWh for currently operating (top) and planned (bottom) facilities. The boxplots show the median (red line), 25th and 75th percentile (blue box) as well as the 2.5th and 97.5th percentile (whiskers) of the footprints per continent (Afr: Africa, Asia, Eur: Europe, N Am: North America, S Am: South America, Oce: Oceania). The footprints reflect those of the panel type where known, and that of a weighted average of types based on 2016 and 2019 production data where panel type is not (fully) known (see Appendix B section B.1). They furthermore reflect continent-specific weighted averages of impacts from various production countries (see Appendix B section B.2).

Besides latitude, panel type also has a great influence on EF_{GHG} . As a sensitivity analysis, we assessed the non-weighted footprints of the 7,148 facilities of unknown type, for which footprints were computed for all five types, across types and continents. This indicates that panel type can have a larger effect on GHG footprints than location of installation; choosing cadmium telluride in Europe can result in lower footprints (35.9 [23.0-51.7] g CO_2 eq/kWh) than choosing mono-crystalline panels in South America (57.9 [44.0-74.7] g CO_2 eq/kWh), despite facilities in South America receiving much higher irradiation than those in Europe (2,165 vs 1,135 kWh/m/yr, median values).

Differentiating between operating and planned facilities indicates slightly lower footprints for current facilities (58.4 [27.1-93.3] g CO₂eq/kWh) compared to planned facilities (60.1 [38.4-95.6] g CO₂eq/kWh). This increase occurs despite an increase in panel efficiency, which causes lower footprints for newer facilities of all individual

panel types. However, across all facilities, the increase in market share of mono-Si panels (see Appendix B Table B-2), which have the highest impacts of all panel types, causes footprints to increase. Also, in Europe a higher share of planned facilities is produced in China, further increasing EF_{GHG}. In North America the opposite happens; footprints drop as imports shift from China to production locations with lower impacts.

4.3.2 GHG emission – supply curves

The GHG emission supply curves show that all facilities together produce 457 TWh/ yr with a maximum GHG footprint of 138 g CO₂eq/kWh. The majority of power, 455 TWh/yr (99.6%), is produced with a footprint below 100 g CO₃eq/kWh, in 9,810 facilities. 262 TWh/yr is produced by current facilities (see Figure 4-4a)), and 194 TWh/yr by planned facilities (see Figure 4-4b)). For current facilities, 7,818 out of 7,934 facilities (97.9%) have a footprint below 100 g CO₂eq/kWh. For planned facilities, 1,992 out of 2,010 (99.1%) have a footprint below 100 g CO₂eq/kWh.

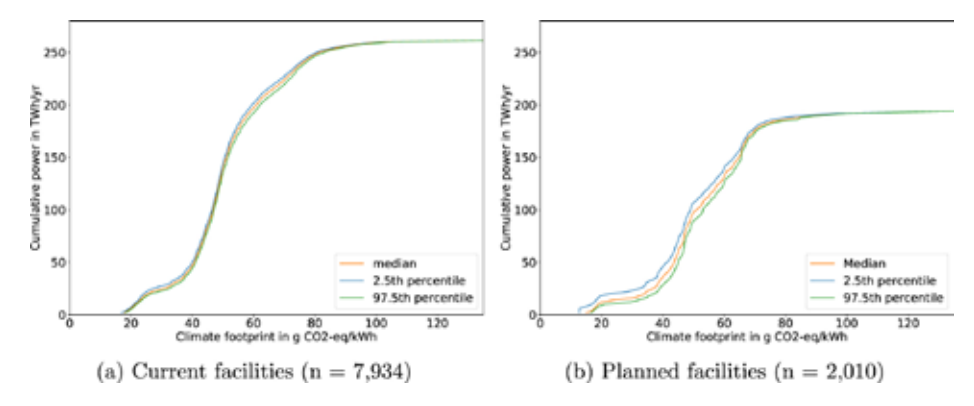


Figure 4-4 Cumulative power production (TWh/yr, y-axis) versus GHG footprint (g CO_eq/kWh, x-axis), for current (a) and planned (b) facilities. The bootstrapping technique described in the text (Materials and Methods section 4.2.4) was used to determine the 2.5th and 97.5th percentile and median footprint at very 2 TWh/yr power production. The plots extend to the median values of the maximum power and the maximum EF_{GHG} of each bootstrap.

Furthermore, by applying a bootstrapping technique we find that for current facilities, uncertainty in panel type does not have a strong effect on the GHG emission-supply curve (see Figure 4-4a)). The spread induced by unknown panel types (difference between the 2.5th and 97.5th percentiles) is less than 5 g CO₂eq/kWh and is highest at low footprints (~10%). Near total cumulative production the spread reduces to ~1%. For planned facilities, the spread is larger (see Figure 4-4b)), because a large part of these facilities (94.0%) has an unknown panel type. At low footprints the spread reaches 50%, or 11 g CO₂eq/kWh. The spread reduces to ~5%

in the upper regions of the emission-supply curve and reduces further towards the total cumulative production.

4.3.3 Regression analyses

The best linear regression model to fit the EF_{GHG} based on the facility-specific predictors we take into account, is

$$\begin{split} log(EF_{GHG}) = 65.07 - 0.03125 \cdot Year + \beta_{type} - 0.0002518 \cdot I_{mean} + 0.0007004 \cdot T_{mean} \\ - 0.003853 \cdot u_{mean} - 0.1678 \cdot I_{CV} + \beta_{Y-type} \cdot Year \end{split} \tag{4-5}$$

where β_{tvpe} and β_{Y-tvpe} have a type-specific value, because PV panel type is a categorical variable. β_{tvoe} is -48.85 for mono-Si, -48.62 for poly-Si, -13.07 for CdTe, –51.28 for CI(G)S and 0 for a-Si. $\beta_{\text{Y-type}}$ is 0.02435 for mono-Si, 0.02416 for poly-Si, 0.006379 for CdTe, 0.02543 for Cl(G)S and 0 for a-Si. The model's R^2 is 0.9868, see Appendix B Figure B-2. Year should be given in absolute value (i.e. 2009, 2017), irradiation I_{mean} in kWh/m²/yr, daytime temperature T_{mean} in °C, and daytime wind speed u_{mean} in m/s, I_{CV} as a fraction (see Appendix B section B.5).

The fact that equation (4-5) does not include capacity and variation in temperature and wind indicates that these are not important predictors of EF_{GHG} (see Appendix B section B.5). Randomizing each predictor in equation (4-5) in turn indicates that PV type is the most important predictor, as the change in R² is largest, followed by mean irradiation (see Figure 4-5). Year, or age of facility (used together with panel type to determine panel efficiency), is the third most important predictor of EF_{GHG}.

This regression model and importance analyses thus indicates that with only panel type, yearly irradiation and age of a facility, data which should easily be available to a user interested in a specific PV facility, one can quickly make an estimate of the GHG footprint, representing a globally weighted average for PV-producing countries across the world. Reducing the regression model to these three predictors results in the following metamodel:

$$log(EF_{GHG}) = 64.30 - 0.03088 \cdot Year + \beta_{type} - 0.000232 \cdot I_{mean} + \beta_{Y-type} \cdot Year$$
 (4-6)

where β_{type} is –12.68 for CdTe, -49.43 for Cl(G)S, -48.87 for mono-Si, -47.63 for poly-Si and 0 for a-Si. β_{Y-type} is 0.006182 for CdTe, 0.02451 for Cl(G)S, 0.02436 for mono-Si, 0.02367 for poly-Si and 0 for a-Si. Year should be given in absolute value (i.e. 2009, 2017), irradiation I_{mean} in kWh/m²/yr. This model has an R² of 0.9862, very close to the best model with $R^2 = 0.9868$.

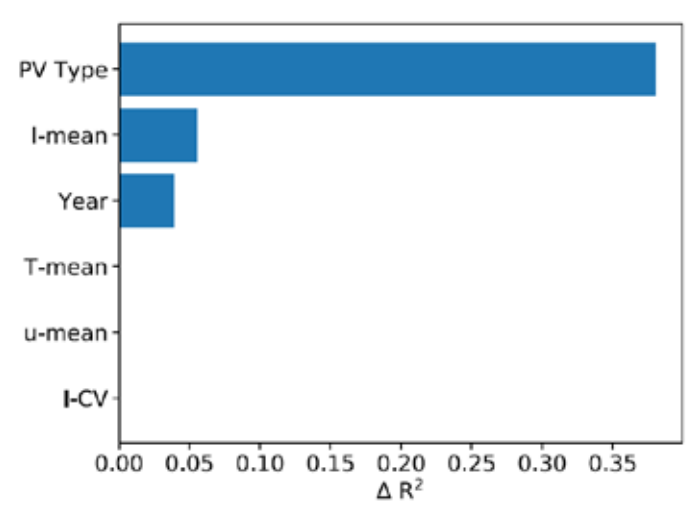


Figure 4-5 Importance of predictors of EF_{CHG}. The change in R² is computed by the R² of the original model (equation (4-5)) minus the equation (4-5) if that specific predictor is randomized.

4.4 Discussion

4.4.1 Interpretation

Our study confirms that photovoltaic solar power can produce electricity at much lower GHG footprints than fossil fuel, which has footprints in the range of 710-950 g CO₂eg/kWh for coal or 410-650 g CO₂eg/kWh for gas. When carbon capture and storage (CCS) is considered, the majority of the fossil-based electricity still has a higher footprint than PV (70-290 g CO₂eq/kWh) [59, 174].

Compared to published studies or meta-analyses, our footprints are on the same order of magnitude but are generally higher (Figure 4-6). Our range is often larger than that reported in other studies, because we consider a large range of system boundaries such as irradiation and age (efficiency). Some studies also consider a range of system boundaries; see Appendix B Table B-8 to Table B-11 for parameters used in the literature discussed here and shown in Figure 4-6. Similar ranges of EF_{GHG} are reported by Ludin et al. [71]. For poly-Si and CdTe they even extend slightly above our values, which could be related to including lower panel efficiencies and shorter lifetimes. Leccisi et al. [60] also report a range of footprints, representing a range of irradiation similar to ours, as well as production countries. Their lower GHG footprints could be related to higher panel efficiencies (compared to our median values) as well as relatively low impacts I. However, other studies with lower panel efficiencies (such as Hertwich et al. [59], Bergesen et al. [68] for CdTe and CI(G)S) also report lower GHG footprints, with similar lifetimes and irradiation, likely related to different boundary conditions, inventory data or assessment methods. Nian [62] report a similar range, across a similar range of irradiation. High efficiencies may explain why their footprints are overall lower. See Appendix B section B.6 for more details on comparing our footprints to those in literature.

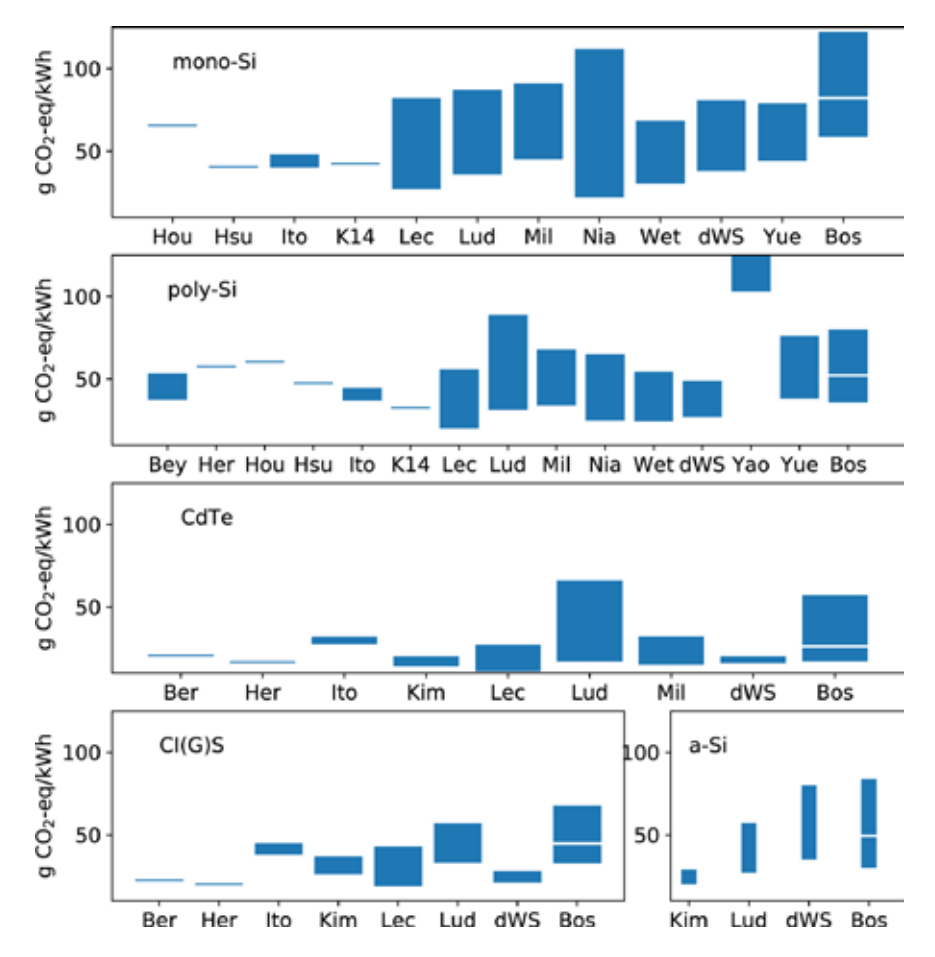


Figure 4-6 Reported GHG footprints of PV electricity in literature compared to ours (Bos, for Bosmans et al.). Ber: Bergesen et al. [68], Bey: Beylot et al. [69], Her: Hertwich et al. [59], Hou: Hou et al. [63], Hsu: Hsu et al. [54], Ito: Ito et al. [73], Kim: Kim et al. [61], K14: Kim et al. [189], Lec: Leccisi et al. [60], Lud: Ludin et al. [71], Mil: Miller et al. [64], Nia: Nian [62], Wet: Wetzel and Borchers [66], dWS: de Wild-Scholten [190], Yao: Yao et al. [191], Yue: Yue et al. [192]. From our study (Bos) we report the median (white line and 2.5-97.5th percentile (bar extent), based on the subset of facilities where panel type is known (450 facilities with mono-Si, 402 with poly-Si, 416 with CdTe, 73 with Ci(G)S, 43 with a-Si). Appendix B section B.6 and Table B-8 to Table B-11 give an overview of system boundaries used in the studies represented here. Note that the poly-Si footprints of Yao et al. [191] are beyond the range shown here (cropped for visibility).

4.4.2 Production location

One important source of variability in PV environmental footprints, and in different footprints reported in literature, is the location where the panels are produced. Several studies compare footprints of PV produced in different locations, mostly due to different background electricity mixes [60, 62, 64, 70, 75, 190, 193, 194, 195]. Furthermore, changes in manufacturing efficiencies and/or import of materials can affect the impacts and footprints for a single production location [63, 64, 67, 191, 192]. Of all studies providing footprints (shown in Figure 4-6) and/or impact I we summarized the system boundaries, including production location if provided, in Appendix B Table B-8 to Table B-11 (see also Appendix B section B.6). A large range of impact I is shown, often related to production location. Locations (countries) with a low GHG background electricity mix such as France or Germany are typically associated with low GHG emissions during production (impact I), while countries with electricity mixes strongly based on e.g. coal, such as China, typically have the highest GHG life cycle emissions. Even for one production country a large range of emissions is reported; for instance, for poly-Si from China Leccisi et al. [60] report 165 kg CO₂eg/m² while Grant et al. [195] report 519 kg CO₂eg/m².

The exact impact I, and subsequently the GHG footprint, thus strongly depends on the production location as well as the chosen system boundaries, life cycle inventories, impact assessment methods etc. [67]. We included variation in production location by using continent-specific weighted averages of the most important production countries based on market shares but acknowledge that in order to derive facility-specific footprints, more information on facility-specific supply chains is necessary.

Note that we did not include variation in BOS production location. Nian [62] report variation in impacts I and footprints for both panels and BOS, showing that changing production location for BOS has an effect, but the effect of changing panel production location is larger. Overall, the impacts associated with panels are larger than the impacts associated with BOS, particularly for crystalline panels [67, 189].

4.4.3 Limitations

A number of assumptions and uncertainties may influence our results.

Some of the input (Figure 4-1) was unknown, particularly for panel type. Our results as well as those of others [60, 74] indicate that panel type is an important predictor of EF_{GHG} . We used an average footprint if type is unknown, weighted by production values of the five most common types considered, which we believe results in a representative variation of ${\rm EF}_{\rm GHG}$ of global PV electricity production. Also, the global emission-supply curve is not strongly affected by uncertainty in panel type. Having more data on panel type will however reduce the uncertainty in facility-specific EF_{GHG}.

When computing life cycle GHG emissions (I in equation (4-1)), we did not include facility-specific supply chains, but continent-specific weighted averages of production countries based on market shares. Variation in production location can be an important source of variation in GHG footprints, as described in the previous section. If facility-specific supply chains are known, production country can be added to the regression analysis, improving the prediction of facility-specific GHG footprints.

Another important predictor of EF_{GHG} is panel efficiency. In this study, efficiency varies based on construction year and panel type, but further variation in efficiency can be introduced among different manufacturers or models of the same type. Besides improved panel efficiencies, $\mathrm{EF}_{\mathrm{GHG}}$ also decreases over time due to improved material and energy utilization in the production process, [e.g. [191, 196]]. The latter is not considered in our study.

Furthermore, 'balance of system' components (BOS) were assumed to be the same for all facilities, but we acknowledge that different mounting structures can affect the GHG emissions of a PV facility [56, 69]. We also ignored differences in BOS due to tilt angles or tracking systems. Of all facilities from the Wiki-Solar database, ~10% uses 1- or 2-way tracking. Although this increases the power output of a facility [197, 198], it also increases environmental impacts due to increased electricity and material needs. Sinha et al. [198] report that therefore the EF_{GHG} of fixed and tracking systems are comparable, while Leccisi et al. [60] find that EF GHG is reduced for an East-West-tracking system, particularly for crystalline panels. Miller et al. [64] find that whether the PV GHG footprint is in- or decreased when a tracking system is included strongly depends on the panel type as well as irradiation and cloud cover.

When computing the lifetime electricity output (P in equation (4-1)), we included location-specific high-resolution climate variables, as well as a loss factor to take panel degradation into account. Using an IEA-recommended fixed loss factor of 0.7% [182] we ignore that panel degradation can vary between locations and panel types [64, 72, 199, 200, 201]. We also ignore that power production can be reduced by shading or soiling through e.g. dust or snow as well as faulty installation or lack of maintenance [72, 200, 202, 203].

Third, we assume a fixed lifetime of 30 years for all facilities. A shorter or longer lifetime will directly affect the footprint, as shown by [54, 61, 66]. We use the ERA5 reanalysis data from 1988 to 2017 to obtain a representative power output under current climate. We tested that power output is not sensitive to the exact years chosen; for 1,460 locations we compared average power output for 2008-2017 to that of 1988-2017 and found that the difference is less than 1% for 88% of the locations, and all differences are less than 3%. We did not account for the panel type-specific effects of low irradiance, variation in spectral irradiance or angle of incidence on PV electricity production [188]. Furthermore, our footprint is expressed per kWh produced, while the amount of power ultimately consumed will be lower due to losses in the power grid as well as potential mismatches between PV production and power demand. Adding battery storage would allow for less power losses, but will likely increase environmental footprints, depending on the battery type [204]. The inclusion of batteries may increase payback times and global warming potential by up to 30% [205].

Lastly, we computed electric power output for all facilities assuming flat panels. Louwen et al. [72]. Chen et al. [206] show that the tilt of a facility can have a large range within which electricity production remains very similar, but we acknowledge that especially at higher latitudes we may underestimate electricity output.

4.4.4 Outlook

Our conclusions hold for GHG footprints, but this type of analysis could be expanded to other impact categories, such as material scarcity or eco-toxicity. Furthermore, the regression model we built can be used to estimate GHG footprints for individual facilities even with limited input. Computational efforts can be reduced by not using temporarily detailed climate data, as the regression model indicated that climate variables other than mean irradiation do not strongly affect a PV facility's life cycle GHG footprint. It is however important to fill data gaps concerning the panel type used and production location.

Our GHG emission-supply curves of cumulative PV production can also be used in integrated assessment models (IAMs), in addition to cost-supply curves [207], to include both financial and environmental constraints in renewable energy scenarios. For future scenarios, one should take into account reduced impacts I during manufacturing due to technological advances as well as the decarbonization of energy supply (e.g. [141, 196]).

4.5 Conclusion

In this study we computed the GHG footprint for 9,992 utility-scale PV facilities across the globe, based on facility-specific construction year, capacity, panel type and high-resolution climate data, as well as variation in production location. We find utility-scale PV GHG footprints of 58.7 (28.2-94.6) g CO₂eg/kWh (median, 2.5-97.5th quantiles). Spatially, locations with higher irradiation logically have lower footprints, but panel type is the most important predictor of EF_{cuc}. Placing a cadmium telluride panel, with low life cycle GHG emissions, in Europe can result in a lower GHG footprint than placing a mono-crystalline silicon panel, with high life cycle GHG emissions, in South America, despite the much larger irradiation at facilities in the latter continent [72, 74]. Panel efficiency (here determined through a facilities age) is the third most important predictor of GHG footprints.

We acknowledge that with more data, more accurate facility-specific footprints can be computed. Efforts should mainly focus on adding panel type and production country. We do find that the uncertainty in panel type does not strongly affect the global PV GHG emission-electricity supply curves.

4.6 Data availability statement

The data generated and/or analysed during the current study are not publicly available for legal/ethical reasons but are available from the corresponding author on reasonable request.

The facility-specific technological characteristics and locations from Wiki-Solar are proprietary and can be obtained from https://wiki-solar.org. The continent-specific market shares by origin countries are also proprietary and can be obtained through https://www.marketreportsworld.com/TOC/12344406#TOC. We used Chapter 8 (Global Solar Photovoltaic (PV) Market Analysis, by Geography) [178]. The climate data used in this study [208] can be obtained from the Copernicus Climate Change Service [186] for free. We used ERA5's hourly single level data.

Acknowledgments

This work is part of Grant 016. Vici. 170. 190, financed by the Netherlands Organisation for Scientific Research (NWO). NWO had no role in this study's design. We thank Philip Wolfe from Wiki-Solar and Suraj Patil from Absolute Reports. We would furthermore like to thank Aafke Schipper and Marlee Tucker for their help with the regression model, as well as the Weather & Climate Models group at the Royal Netherlands Meteorological Institute (KNMI) for their help obtaining and processing the ERA5 data. We also thank Folmer Krikken at KNMI and the Computer & Communications Department at Radboud University's Faculty of Science for their help with Python and R packages. We used Python 3.5.2 for our computations and used the maplotlib. pyplot package [209] (hosted at https://zenodo.org/record/3633844#.XpgHli2YN7M) for plotting. For our regression model we used R version 3.2.3.

We thank the referees and editor for their input which helped to improve the manuscript.



5. Greenhouse Gas Footprints of Individual Hydropower Facilities in the United States of America

L.C. Dammeier, V. Barbarossa, A.B.G. Janssen, S. Kosten, J.H.C. Bosmans, M.A.J. Huijbregts (2025) *In preparation*

Abstract

Hydropower is the largest source of renewable energy in the United States of America (US). While it is generally considered to be a low-carbon electricity source, technological and site-specific differences can lead to large variations in hydropower's greenhouse gas (GHG) footprints. Here, we quantified greenhouse gas footprints of 1,812 individual hydropower facilities in the US, accounting for facilityspecific differences in electricity production as well as differences in life cycle GHG emissions during the construction and operation of the hydropower facility. We found that the GHG footprint of hydropower facilities in the US range from 5.6·10⁻³ to 1.1 kg CO₂eg/kWh (5-95th percentile), with a median of 2.8·10⁻² kg CO₂eg/kWh. Our results show that the GHG footprint of hydropower from natural storage areas is systematically lower compared to man-made storage areas. Variation in GHG footprints of hydropower from man-made storage areas can be large and is mainly caused by differences in size, trophic state and climate zone. Our results can be used to identify hotspots of GHG footprints of hydropower production on the level of individual facilities. Our method can also be used as a blueprint to quantify the GHG footprints of existing and planned hydropower facilities worldwide.

5.1 Introduction

There is strong scientific evidence that the emission of greenhouse gasses (GHG) caused by anthropogenic activities is the main driver of climate change and that ambitious and global action is required to limit global warming to 1.5 to 2 °C, including large-scale transformations in the energy system towards renewable, low-carbon energy sources [210]. Hydropower is one of the most prominent renewable energy technologies worldwide. In 2023, 14.3% of the global electricity was supplied by hydropower and in 20 countries it provides more than 75% of the electricity produced [211]. In the United States of America (US), hydropower generated 5.5% of the electricity [212]. Hydropower is predicted to increase in the global primary energy mix in many energy scenarios [213]. As hydropower is a flexible source of electricity that can generate electricity when there is little wind and solar power and may in the case of pumped storage also be used to store excess electricity, it can be applied to mitigate the intermittent nature of solar and wind electricity production.

A common metric to compare GHG emissions of different power technologies is the GHG footprint, which is defined as the life cycle GHG emissions per unit of electricity produced (in kg CO₂eg/kWh). Life cycle emissions are usually quantified making use of life cycle assessments (LCAs), which is a standardized methodology to calculate emissions of a service or production during all life cycle stages. It has been shown that GHG footprints of hydropower production can vary greatly, ranging from 2·10⁻⁴ to 6.6 kg CO₃eq/kWh [76 - 93]. The reported range of 4.5 orders of magnitude in GHG footprint of hydropower facilities can be caused by differences in various environmental and technological factors. Different types of hydropower exist, from small run-of-river facilities to large dams creating vast reservoirs. Each of these types has different technological characteristics and even within the same type, there are large differences in technology, due to differences in topology at the site of the plant [38, 98].

Hydropower facilities without a man-made storage area have GHG emissions related to dam construction as well as operation and maintenance of the dam itself, including downstream emissions and emissions from dam spillways. Hydropower facilities that have a man-made storage area also have biogenic GHG emissions from that storage area during the operation of the facility. Emissions from the storage areas themselves heavily depend on the storage area's lifetime and the climate zone in which the hydropower facility is located, as well as pre-impoundment land cover type [94]. Earlier studies have shown that the ratio of GHG emissions from the dam itself compared to those of the storage area lies anywhere between 100% for diversion dams to 0.01% for tropical reservoirs [91].

One way to assess the GHG footprint of a technology on a larger scale is to harmonize outcomes of previous studies in a meta-analysis. However, one drawback of such meta-analyses is that due to the harmonization step detail is lost on how GHG footprints vary in reality. Little research has been done on quantifying facilityspecific GHG footprints of hydropower at large geographical scales. Being able to quantify the GHG footprint at the level of individual hydropower facilities can help to identify hotspots of GHG footprints of current hydropower production. Most studies focus, however, on one or a few facilities, focusing on a specific type of dam and associated technology. Wang et al. [95] assessed carbon emission and water consumption of hydropower plants in China, but they did not relate the impacts to the plants' electricity generation. A study by Harrison et al. [96] used the G-res tool to calculate GHG emissions from reservoirs on a global scale but neglected dam construction and also do not relate the emissions to electricity production. Scherer and Pfister [97] modelled the biogenic carbon footprint of hydropower reservoirs and reported an average GHG footprint of 0.273 kg/kWh, again focussing solely on the reservoir and not accounting for dam construction. Gemechu and Kumar [98] assessed LCA studies of hydropower and found that a wide range of emission intensities reported (1.5·10⁻³-3.7 kg CO₂eg/kWh) is caused by inconsistency in how LCA is used, high variability in key reservoir characteristics and data limitations.

Here, we quantified the GHG footprint of 1,812 hydropower facilities in the US, derived from the National Inventory of Dams (NID) [214] and amended with information from Hydrosource [215] and the WRI global power plan database [216]. The hydropower facilities' lifetime electricity production was estimated by a newly developed regression model, linking the historic electricity production data from the US Energy Information Administration (EIA) to high-resolution streamflow data from FLO1K [217] and the dams' height and capacity taken from the NID [214]. We derived facility-specific GHG emission factors, depending on the climate zone and the storage area's trophic state.

5.2 Materials and methods

5.2.1 Greenhouse gas footprint

The GHG footprint of a hydropower facility is defined as its life cycle GHG emissions divided by its electricity generation (P in kWh/year). The GHG emissions of a hydropower facility depend on two components: the construction of the facility (I_s, in kg CO₃eq/kWh) as well as the storage area emissions, including downstream emissions, during operation (I_o, in kg CO₂eq/year). Hence, the GHG footprint (F_{GHG}, in kg CO₃eq/kWh) can be calculated from

$$F_{GHG} = I_c + \frac{I_o}{P}$$
 (5-1)

Figure 5-1 gives an overview of the approach to quantify GHG emissions and electricity production of the 1,812 hydropower facilities in the US included in our calculations.

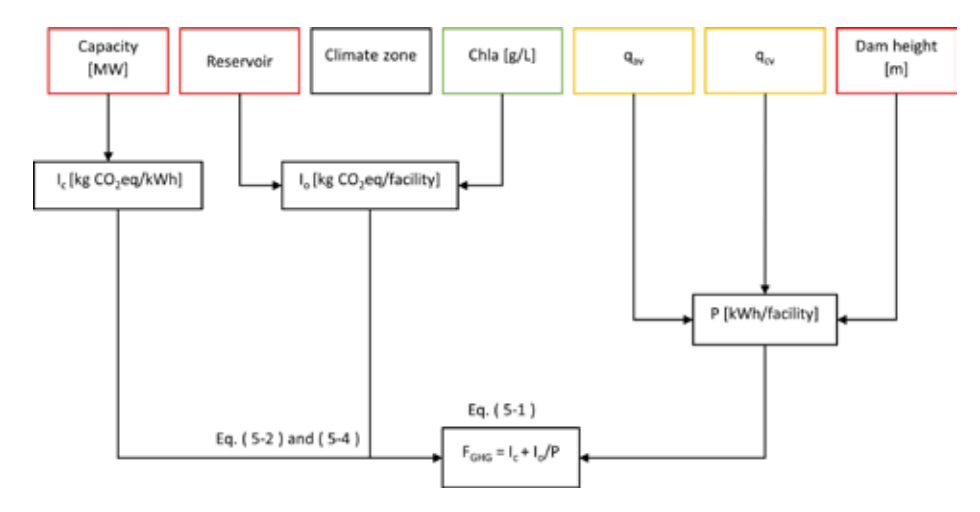


Figure 5-1 Overview of the method. Red boxes refer to facility-specific information [214, 215, 216]. Yellow boxes refer to information derived from FLO1K [217], which is a dataset providing streamflow data. The green box refers to information on chlorophyll-a data [218]. Equations (5-1), (5-2) and (5-4) are described further below in this section; abbreviation can be found in Table C-1. Capacity is used to derive the construction phase emissions from Kadiyala et al. [219].

5.2.2 GHG emissions of hydropower

Construction

We included emissions from the dam construction phase (I in kg CO₃eq/kWh) based on Kadiyala et al. [219], who quantified GHG emissions for small (<0.1 MW), medium (0.1-30 MW) and large (>30 MW) hydropower facilities based meta-analysis (for more information see Table C-2 in Appendix C). In our database, 16 facilities are classified as small, 948 facilities as medium and 316 facilities as large, based on information from the National Inventory of Dams (NID) [214] and Hydrosource [215]. When the capacity was not reported (n = 532), we calculated a weighted average of the GHG footprint for dam construction, based on the classification of Kadiyala et al. [219] and the relative occurrence of small, medium and large dams in our database, see section C.2.2 for more information.

Operation

During the operational phase of hydropower facilities based on man-made storage areas, most emissions come from the storage area itself and downstream of the spillway, caused by the decomposition of organic material in the water, which depends on the climate zone [91]. Information on the climate zone in which the hydropower facilities are located has been gathered from the IPCC [220] and is reported in section C.3. We based the GHG emissions in the operational phase of man-made storage areas on IPCC emission factor guidelines [221], assuming a hydropower facility lifetime of 100 years [222]:

$$I_{o} = A_{res} \cdot \left(\left(EF_{CH_{4}, a \le 20, j} \cdot 0.2 + EF_{CH_{4}, e > 20, j} \cdot 0.8 \right) \cdot \alpha \cdot GWP_{CH_{4}} \cdot (1 + R_{d}) + EF_{CO_{2}, a \le 20, j} \cdot 0.2 \right)$$
(5-2)

facilities' storage areas have been classified as man-made or natural storage area based on the classification of HydroLAKES [223]. Because in accordance with [224] run-of-river facilities can also have storage areas, albeit most often much smaller, we have not excluded emissions from these storage areas for run-of-river facilities here and apply equation (5-2) or (5-4) depending on whether or not these storage areas are classified as man-made or natural. Deemer et al. have shown that there is no significant difference between surface emissions between man-made storage areas and natural lakes [225]. In cases where no storage area is present, equation (5-4) is applied.

EF_{CHA as 20 i} is the methane emission factor of man-made storage areas in the first 20 years of operation, situated in climate zone j (kg CH₄/km²/year) (see Table C-2). EF_{CH4, a>20.1} is the methane emission factor of man-made storage areas in the period of 20 to 100 years of operation, situated in climate zone j (kg CH₄/km²/year) (see Table C-2).

EF_{CO2, a<20.1} is the CO₂ emission factor of man-made storage areas in the first 20 years of operation, situated in climate zone j (see Table C-2). Note that CO₂ emissions from storage areas are considered to be only relevant for the initial 20 years of a storage area's life [221].

a is the emission factor adjustment for the trophic state of the storage area in climate zone j and GWP_{CH4} is the global warming potential of methane for a 100year time horizon (34 kg CO_2 eq/kg CH_4) [226]. R_d is a dimensionless constant equal to the fraction of downstream emissions of CH₄ compared to the total flux of CH₄ from the storage area surface, here set equal to 9% [221].

The emission factor adjustment for the trophic state of a storage area α was calculated via [221]:

$$\alpha_i = 0.26 \cdot Chl - a_i \tag{5-3}$$

with Chl-a, the mean annual chlorophyll-a concentration in storage area i in g/L. The Chl-a, is taken from a database which gives the Chl-a, concentrations on a 50 by 50 km grid for the US in 2010 [218].

More information on how equation (5-2) is derived can be found in appendix C.2.1.

For hydropower facilities built on natural storage areas, we assume that the area's surface does not change upon construction of the hydropower facility and thus the size of the storage area attributed to anthropogenic use is considered negligible, because relevant information was not available. Therefore, emissions related to land use change during the first 20 years of operations are not relevant and since the storage area's surface is assumed to not change emissions from the surface cannot be attributed to hydropower operation. In accordance with the IPCC [221], reservoir emissions can thus be calculated via:

$$I_o = A_{res} \cdot EF_{CH_4,\alpha > 20,f} \cdot 0.8 \cdot \alpha \cdot GWP_{CH_4} \cdot R_d \qquad (5-4)$$

5.2.3 Electricity generation

We imputed the electricity generation data for the hydropower facilities by developing a linear mixed-effect regression model fitted to yearly electricity data. We used hydropower facility-specific electricity generation from the EIA [163]. We matched the EIA hydropower facilities to the NID hydropower facilities via the Oak Ridge National Laboratory hydropower dataset [227], which provides the matching IDs of NID and EIA datasets. Yearly electricity generation data for the period 1989 to 2015 could be retrieved for 960 (out of 1,812) hydropower facilities from the NID dataset and a total of 15,191 observations (dams-years).

Since power generation is dependent on hydraulic head, design discharge, capacity and load factors, we used proxies that approximate these variables as predictors in our model [228]. Namely, we employed dam height, storage area surface area, yearly average streamflow, yearly streamflow seasonality (see appendix C.4.1 for how this was calculated) and Gross Domestic Product (GDP) of the administrative unit connected to the hydropower facility. Dam height was used as proxy for hydraulic head. Storage area size and average flow at the dam location were used as proxies for design discharge. Seasonality of streamflow and GDP of the administrative unit were used as proxies for the load factor. Dam height and storage area size were retrieved directly from the NID. Yearly streamflow metrics were sampled from the FLO1K dataset (see appendix C.4.2 for the sampling procedure, [217]). The GDP of the administrative unit where the dam is located was computed by averaging GDP data [229] over the administrative units provided by https://gadm.org/data.html.

Due to harmonization across datasets, re-allocation to the river network and exclusion of outliers, the final set of observations consisted of 14,295 dams year for a total of 942 NID facilities. Prior to fitting the model, we log-transformed the response variable and applied a Yeo-Johnson transformation to the predictors to resemble a Gaussian distribution as these were all highly skewed (Figure C-1 and Figure C-2). In addition, we standardized all variables to zero mean and unit variance to improve the comparability of the regression coefficients. We checked for multicollinearity of the predictor set and found that all Pearson's r was below 0.7 and therefore retained the full set of predictors (Figure C-3). We considered the hydropower facility ID as a random term in the mixed-effect model to account for non-independence of yearly electricity generation coming from the same power plant and allowed all first-order interaction terms. We used an automated procedure for model selection that uses a genetic algorithm to find the optimal combination of predictors with the lowest Bayesian Information Criterion (BIC) [230]. We preferred BIC over Akaike Information Criterion as BIC tends to outperform alternatives particularly if the sampling size is large [231]. We ranked the models based on BIC and chose the model with the lowest complexity (i.e., the lowest number of predictors) within the first 10 BIC interval points (see Table C-5 for the results). To assess model reliability, we used 10-fold cross-validation across all observations (i.e., number of dams-years, see Table C-6) and across hydropower sites (i.e., by excluding 10% of the power plants in each fold, see Table C-7) and reported coefficients of determination R² and root mean square error (RMSE).

The model to predict a hydropower facilities electricity generation was

$$P = -0.025 \cdot H^{0.546} + q_{av}^{0.388} + q_{av} \cdot H^{0.051} + (q_{ma} \cdot q_{av})^{-0.018}$$
(5-5)

with H the dam height as given in the NID in m and $\boldsymbol{q}_{_{\boldsymbol{n}\boldsymbol{a}}}$ and $\boldsymbol{q}_{_{\boldsymbol{m}\boldsymbol{a}}}$ the average and maximum annual streamflow in m³/s, respectively.

5.3 Results

5.3.1 Yearly GHG emissions during operation

Yearly GHG emissions during operation from the 1,812 hydropower dams in the US as included in our study range from 286 to 53.5·106 kg CO₃eq/yr [5-95 percentile], with a median of 57·10³ kg CO₂eg/yr (Figure 5-2). In total, these hydropower facilities are expected to cause GHG emissions of 34·10³ kt CO₃eq/year. Facilities situated on man-made storage areas (n = 632) account for 98% of the yearly GHG emissions during operation, with a median of 2.2·10⁶ kg CO₂eg/yr [5.2·10³-206·10⁶ kg CO₂eg/yr the 5-95 percentile]. Those facilities having natural storage areas (n = 1,180) account for 2% of GHG emissions during operation, with a median of 18·10³ kg CO₃eq/yr [155-1.1·10⁶ kg CO₃eq/yr the 5-95 percentile]. 90% of the total emissions during operation are from 96 high-emitting hydropower facilities, which is 5% of all facilities. Of these 96 facilities, all but three have man-made storage areas.

5.3.2 Electricity generation

Figure 5-3 shows the distribution of electricity generation of the 1,812 hydropower dams in the US that are part of our database. They are expected to generate a total of 223 TWh electricity each year. 90% of the electricity is produced by 361 hydropower facilities, which is 20% of all facilities. Hydropower facilities with man-made storage areas (n = 632) account for 43% of the yearly electricity generation. Electricity generation ranges from 3.2 to 637.2 GWh, with a median of 31.6 GWh. Hydropower facilities having natural storage areas (n = 1,180) generate 57% of the yearly electricity production, ranging from 2.0 to 224.5 GWh, with a median of 8.7 GWh.

5.3.3 GHG footprints

GHG footprints of hydropower facilities in the US (n = 1,812) range from $5.6 \cdot 10^{-3}$ to 1.1 kg CO₃eq/kWh (5-95 percentile), with a median of 2.8·10⁻² kg CO₃eq/kWh. The GHG footprints per facility are shown in Figure 5-4. GHG footprints vary greatly between dams with or without a man-made storage area, generally being higher for facilities located at man-made storage areas compared to those located on natural storage areas, as can be seen from the boxplot in Figure 5-5. Hydropower facilities with man-made storage areas have a median GHG footprint of 7.9· 10^{-2} kg CO₂eq/kWh, ranging from 6.4· 10^{-3} to 4.3 kg CO₂eq/kWh [5-95 percentile]. Those facilities with natural ones have a median GHG footprint of 2.6·10⁻² kg CO_2 eq/kWh, ranging from $5.6 \cdot 10^{-3}$ to $6.5 \cdot 10^{-2}$ kg CO_2 eq/kWh [5-95 percentile].

The boxplot in Figure 5-5 shows the distribution of GHG emissions grouped by climate zone and type of storage area (man-made vs. natural). With the exception of boreal climate zones, hydropower facilities on man-made storage areas in all climate zones have higher GHG footprints than those located on natural storage areas. Facilities located in tropical dry/montane areas have the highest average GHG footprints, both for natural storage areas as man-made storage areas. Underlying data for Figure 5-5 is given in Table C-8.

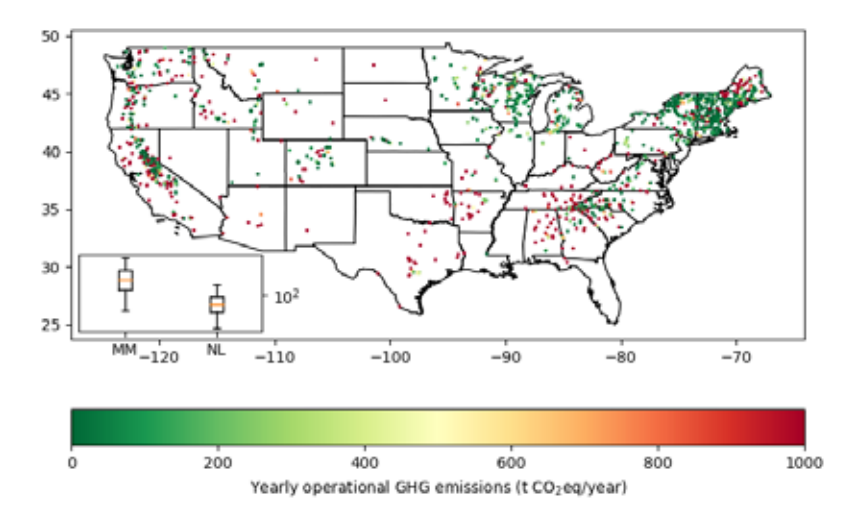


Figure 5-2 Yearly operational GHG emissions (t CO_2 eq/year) from hydropower facilities in the US. The boxplot shows the distribution of GHG emissions from facilities with man-made (MM) storage areas or natural ones (NL). The orange line represents the median, the boxes the 25-75th percentile and the whiskers the 5-95th percentiles.

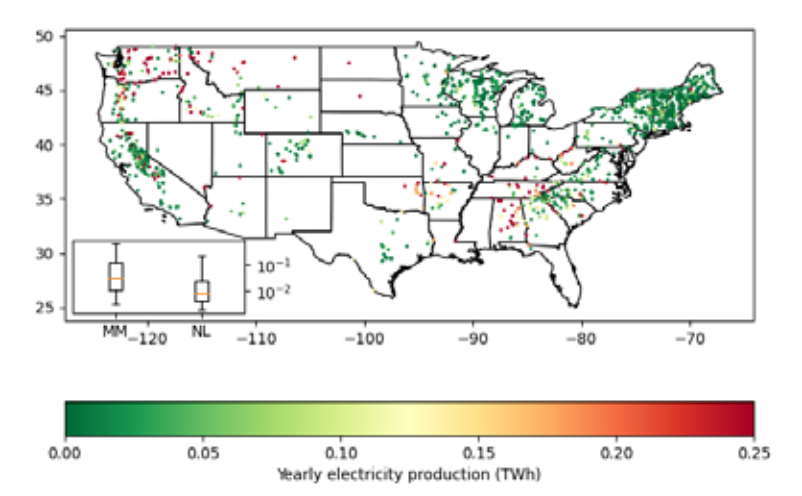


Figure 5-3 Yearly electricity generation (TWh/year) by hydropower facilities in the US. The boxplot shows the distribution of electricity generation by facilities with man-made (MM) storage areas or natural ones (NL). The orange line represents the median, the boxes the 25-75th percentile and the whiskers the 5-95th percentiles.

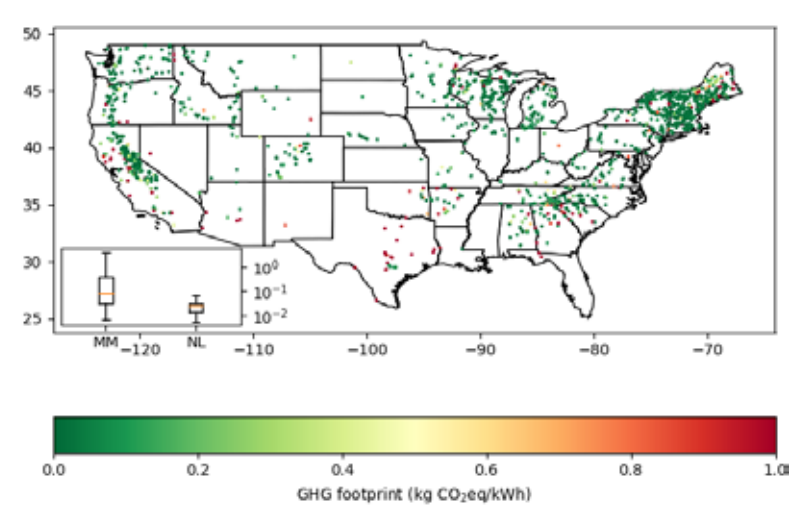


Figure 5-4 GHG footprints (kg CO₂eg/kWh) of hydropower facilities in the US. The boxplot shows the distribution of GHG footprints of facilities with man-made (MM) storage areas or natural ones (NL). The orange line represents the median, the boxes the 25-75th percentile and the whiskers the 5-95th percentiles.

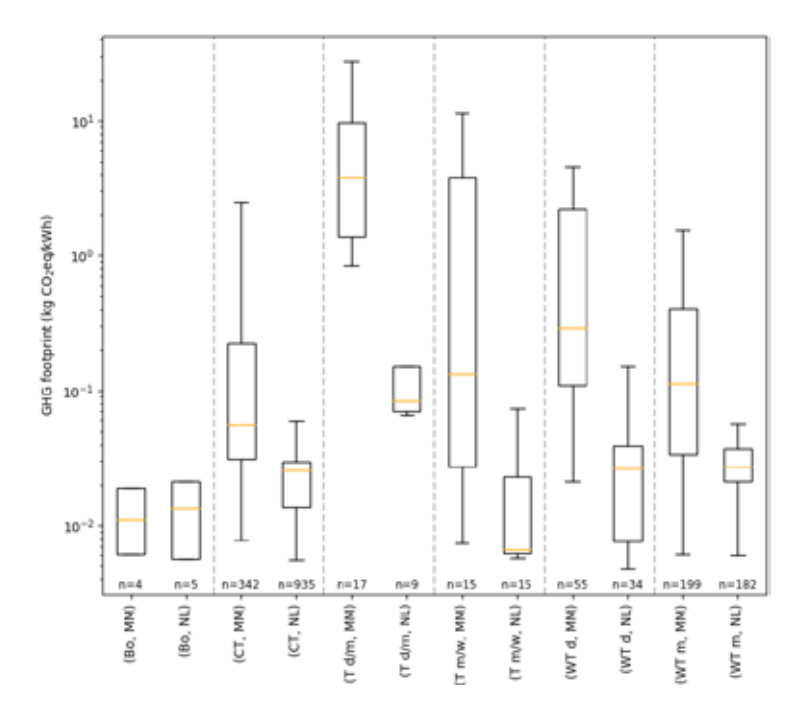


Figure 5-5 Boxplot showing the distribution of GHG emissions grouped by climate zone and storage area type. The orange line represents the median, the boxes the 25-75th percentile and the whiskers the 5-95th percentiles. Below each category, the number of observations is given. Climate zones are Bo: boreal, CT: cool temperate, T d/m: tropical dry/montane, T m/w: tropical moist/wet, WT d, warm temperate dry, WT m: warm temperate moist. Storage area types are MM: man-made and NL: natural.

5.4 Discussion

We calculated GHG footprints for hydropower facilities in the US ranging from 5.6·10⁻³ to 1.1 kg CO₂eg/kWh (5-95 percentile), with a median of 2.8·10⁻² kg CO₂eg/kWh. This range is in line with what is reported in literature [98]. The study by Song et al. [91] reports footprints to be higher, but they also consider dam demolition, which is omitted here. A study by Li and He [232] report a median carbon intensity from hydropower reservoirs of 63 g CO₂eg/kWh, which also is higher than in our study. They find that higher GHG footprints are found for eutrophic reservoirs and those with shallow depth (<20 m), a factor that we did not include in our study.

While in general, the GHG footprints presented in this study are in line with results found in previous studies, we see extreme outliers, over- or underestimating the GHG footprints from hydropower. The discussion tries to explain the causes of these outliers as well as examine sources of uncertainty in the results.

5.4.1 GHG emissions

Construction emissions

GHG emissions from the construction phase are difficult to quantify because the type of dam built depends on site-specific characteristics. For example, the geography of the site has a large effect on the type of dam to be built and the size of it [91]. Here, we derived the construction GHG emissions (in kg CO₂eq/kWh) from a classification made by Kadiyala et al. [219], which is based on the capacity of the hydropower facility and whether it is operated as a reservoir or run-of-river facility.

Information on the capacity and the mode of operation was not known 29.5% of the hydropower facilities included in our analysis. Using a weighted average based on the distribution of these attributes in the dataset where capacity and/ or the mode of operation is not known introduces uncertainty in the estimation of GHG emissions connected to the construction phase. The construction phase emissions reported in Kadiyala range from 3.45·10⁻³ kg CO,eq/kWh for large runof-river facilities to 4.782·10⁻² kg CO₂eq/kWh for small run-of-river facilities [219]. Additional information on capacity and mode of operation of these facilities can reduce this uncertainty.

Beyond capacity and mode of operation, other factors may also influence construction phase GHG emissions from hydropower facilities, such as information on different structural types of hydropower dams (e.g., embankment dams, arch dams, gravity dams and buttress dams). Dams differ in their shape as well as the type and amount of materials used [91]. Combined with information on the size of the dam, such as height, width, and volume, GHG emissions during the construction phase can be further improved. Note that the NID also provides information on dam structure and the type of materials used [214], but due to data limitations this information was not used here.

Operational emissions

Man-made storage areas appear to be an important source of GHG emissions from hydropower facilities for most climate zones [233]. It is therefore highly relevant to classify water bodies as man-made or natural for GHG footprint predictions of hydropower facilities. Information on whether a reservoir is man-made or natural was unavailable in the NID and therefore had to be derived from the HydroLAKES database [223].

We used the coordinates of the pour points in HydroLAKES to match with the coordinates of the dams under the assumption that if a new dam has been constructed, it has been constructed on an existing river and that if an existing lake has been dammed, it is dammed at the natural pour point. However, due to the complexity of some hydropower projects, which can consist of cascades of dams or where the waterflow can partially be diverted over a turbine further downhill to increase head, mismatches might occur in areas with relatively large number of waterbodies.

We also assumed that whenever a storage area was man-made, that all emissions occurring would not have occurred otherwise. A review by Prairie et al. [234] indeed suggested that almost all CH₄ emissions from reservoirs are new, although only part of the CO₂ emissions would not have occurred otherwise. Organic matter that is trapped and dissolved in a storage area after its construction would otherwise have been dissolved somewhere else, further downstream along the river. Hence, the CO₂ emissions may only be displaced and not new. Other studies have also evaluated the GHG emissions from reservoirs in the US. A recent study from Hansen et al. [235], who applied the G-res emissions model to a subset of hydropower dams in the US, showed that the dominant emission pathways are CO, diffusion and CH₄ ebullition. Note that in our calculations, the vast majority of the GHG emissions due to the operation phase is explained by CH₂ emissions.

Given that hydropower is a long-lived technology, with the oldest facilities being commissioned in the late 19th century, climate change as well as changes in the land use and development of the catchment areas of storage areas are likely to occur, which are in our case neglected in the quantification of storage area emissions. Changes in the surroundings can also lead to changes in the influx of organic material into the reservoir. While these changes can be involuntary, this implies that by explicitly managing the influx of materials into a reservoir can affect and lower emissions from reservoirs. Tigli et al. [236] showed that efforts made to lower the trophic status of a storage area indeed lead to lower GHG emissions, as also suggested by Meerhoff et al. [237] and Aben et al. [238], who advocate that reducing nutrient loadings through, for example, better agricultural practices or wastewater treatment, is not only good for water quality but also from a climate perspective.

Other factors influencing emissions and leading to uncertainty in the calculations are the use of emission factors for six aggregated climate zones, instead of the 12 climate zones known to the IPCC, the use of average yearly Chl-a data, which is known to vary temporally between seasons as well as spatially within a lake [236], and assuming a standard emission factor for downstream CH₄ emissions, which may well become more and more important in the future [239] as hydropower facilities age and therefore, CO₂ emissions from the storage area become less prominent. These were not included here due to data limitations.

Finally, it should be noted that an important aspect in LCA is the allocation of emissions to a specific activity. In the case of hydropower, the reservoir or run-ofriver facility might be used for additional purposes next to electricity generation, such as recreation, fishing, municipal and agricultural water supplies, and flood control [91]. Here, we assigned the full emissions to electricity generation due to a lack of information on other uses of the storage area which causes an overestimation of emissions allocated to hydropower in case it is used for multiple purposes. Scherer and Pfister [97] applied an allocation based on the ranking of hydropower compared to other uses, which could also be included to allocate emissions in future studies, but was not used here because the ranking of the facilities' purposes was not known in our case.

5.4.2 Electricity generation

The amount of electricity generated as an important factor in the quantification of GHG footprints of hydropower facilities. The decision to release water and thus produce electricity in most cases does not solely depend on the need for electricity but also depends on other uses such as irrigation or general water management strategies. Recently, Baratgin et al. [240] have developed a model to reproduce hydropower electricity production in France by including amongst others water demands and non-energy demands. A similar model could be developed for the US.

Furthermore, hydraulic head is commonly accepted to be estimated by dam height, but it has also been discussed to not always be an accurate representation of the actual head of a reservoir, because water intake and the location of the turbine usually are not at the top and bottom of the dam, respectively, see for example [241]. As electricity generation linearly depends on the height, height is an important parameter in determining the power output.

Another potential source of uncertainty is the relocation of dams, which took place to match the dams to FLO1K data. In areas with many waterways, this can potentially lead to erroneous flow information and hence electricity production estimates, either over- or underestimating the electricity generated.

However, we see that the modelling of the amount of electricity produced is in the same order of magnitude as the actual production of electricity from hydropower in the US (223 vs.240 TWh, respectively [242], or 93%) and comparison of the average annual electricity production data we estimate with the study conducted by Turner et al. [243] shows a very good fit, with the exception of two extreme outliers (see Appendix C.6 for more information). Therefore, while improvements to quantify electricity production from hydropower may be achieved moving forward, we are confident that the model developed here provides a good approximation for the GHG footprint calculations.

5.5 Conclusions and outlook

We quantified the GHG footprint of individual hydropower facilities in the US and found a range of 2 orders of magnitude [5th-95th percentile] between individual hydropower facilities. This range is in line with other GHG footprints reported in literature [98]. While in many cases, the GHG footprints of hydropower are comparable to those of other renewable electricity sources, such as wind power and solar power, some hydropower plants have GHG footprints that exceed those of conventional electricity generation [91]. High GHG footprints are typically found for hydropower facilities with eutrophic man-made storage areas.

Our method can be used to identify dams with large GHG footprints, which could then potentially be combined with floating PV, which has been shown to potentially decrease the GHG intensity of hydropower reservoirs [244]. It can also be applied to identify locations where non-hydropower dams can be repurposed to generate low-carbon electricity or where new hydropower facilities with low GHG footprints could be constructed.

Acknowledgments

This work is part of project number 016.Vici.170.190, which is financed by The Netherlands Organisation for Scientific Research (NWO).



6. Synthesis

6.1 Introduction

The aim of this thesis was to quantify facility-specific GHG footprints of renewable electricity sources at large spatial scales. Accounting for technological and meteorological variability, facility-specific GHG footprints of the three most important non-biomass renewable energy technologies were derived: wind (chapter 2 and 3), solar (chapter 4) and hydropower (chapter 5). In this synthesis, the main sources of variability are discussed. Section 6.2 covers the technological variability in GHG footprints, section 6.3 is about spatial variability and section 6.4 about temporal variability. Finally, section 6.5 includes conclusions and recommendations for future research.

6.2 Technological variability

In my thesis, I quantified GHG footprints for wind farms and utility-scale PV facilities at the global scale, while for hydropower facilities the assessment was done for the United States of America (US). The differences between the renewable electricity technologies are summarized in Figure 6-1. GHG footprints for wind are shown separately for on- and offshore wind farms. For utility-scale PV, a distinction between crystalline and thin-film panels is made. The GHG footprints for hydropower facilities are split into man-made storage areas and natural storage areas. To compare the GHG footprints to conventional electricity generation technologies, information on coal- and gas-fired power plants is added from [245] and [246], respectively, and information on nuclear power comes from Le Boulch et al. [247]. From Figure 6-1 it becomes apparent that the GHG footprints have a larger variability between different technologies than within the same technology.

Overall, wind power has the lowest GHG footprints of the technologies assessed in my thesis, with offshore wind farms on average having a lower GHG footprint than onshore wind farms. Note that offshore wind farms show a larger range of GHG footprints than onshore wind farms, with the 5th percentile being lower than the 5th percentile of onshore wind farms and the 90th percentile exceeding the 90th percentile of onshore wind. For solar power, thin-film panels have lower GHG footprints than crystalline ones, with the 90th percentile of thin-film panels being lower than the median of their crystalline counterparts. This is in line with literature on solar [59, 60, 64, 71, 73, 190] and wind power [52, 59, 248]. However, a recent study has shown that increasing distance to shore increases the GHG footprint of wind power [249]. Man-made storage area-based hydropower facilities have higher GHG footprints than those located on natural storage areas. Hydropower facilities based on natural storage areas have GHG footprints in the range of wind and solar power. Those with man-made storage areas can have GHG footprints as low as wind power but can also have GHG footprints exceeding those of natural gas and coal. Other studies confirm this observation [91, 98, 250].

Even though wind power on average has the lowest GHG footprints, its 90th percentile overlaps with the 5th percentile of solar and hydropower, showing that there are instances when thin-film PV or hydropower can have GHG footprints as low as wind power. Similarly, there are instances where hydropower facilities can have a lower GHG footprint than solar power.

Wind, solar and hydropower all have lower median GHG footprints than coal- and gas-fired power plants. The 90th percentile of wind and solar power as well as natural storage area-based hydropower GHG footprints is lower than the 5th percentile of the GHG footprints of coal-fired power plants. However, there are hydropower facilities located on man-made storage areas with GHG footprints exceeding the 90th percentile of coal-fired power plants. Nuclear power has GHG footprints that are in the same range as those of wind power, with the median being lower than both on- and offshore wind power [247].

This shows that my results can be used to choose electricity sources with the lowest GHG footprints using facility-specific data for a certain location, which can increase gains in GHG emission reduction compared to choosing a technology based on the lowest average GHG footprint.

The metamodels developed for wind and solar power indicated the importance of technological aspects on the intra-technology variability of GHG footprints. For wind, in addition to whether or not a facility is onshore or offshore, the turbines' hub heights, rated power and the number of turbines in a wind farm are explaining differences in GHG footprints of wind turbines [251]. The panel type and the module efficiency are the two main technological variables determining differences in the GHG footprints of PV facilities [30].

No metamodel for the GHG footprint of hydropower facilities has been developed yet, but Figure 6-1 indicates that intra-technological variations, such as whether a facility has a man-made or natural storage area, could be used as proxies in the development of such a model. Furthermore, dam height and reservoir surface area were used to predict a hydropower facilities' electricity generation, implying that they might be important technological variables to include in a metamodel.

My results imply that it is always important to include facility-specific information, no matter whether GHG footprints of different technologies are to be compared to each other, or the GHG footprint of the same technology is to be assessed in different locations.

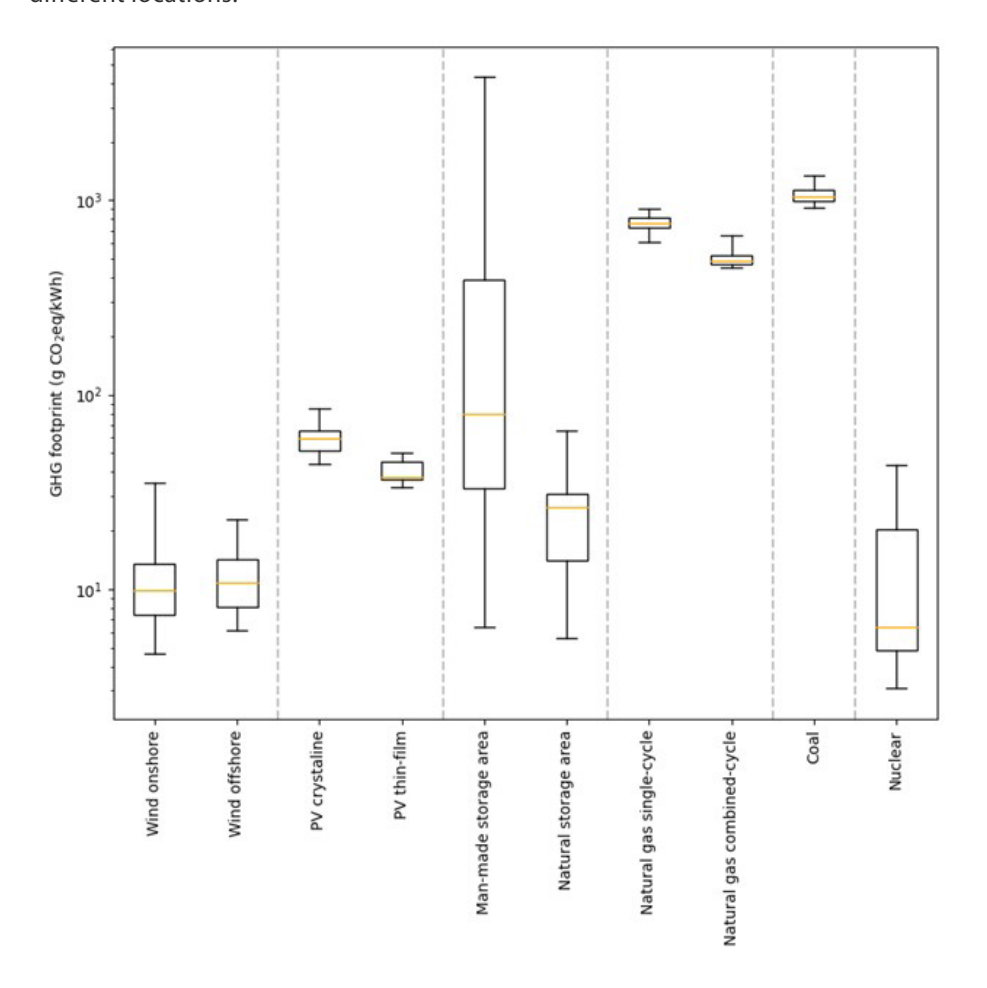


Figure 6-1 GHG footprints of the different technologies assessed in this thesis with comparison to coal [245], gas [246], and nuclear power [247]. The orange line represents the median, the boxes the 25-75th percentile and the whiskers the 5-95th percentiles.

6.3 Spatial variability

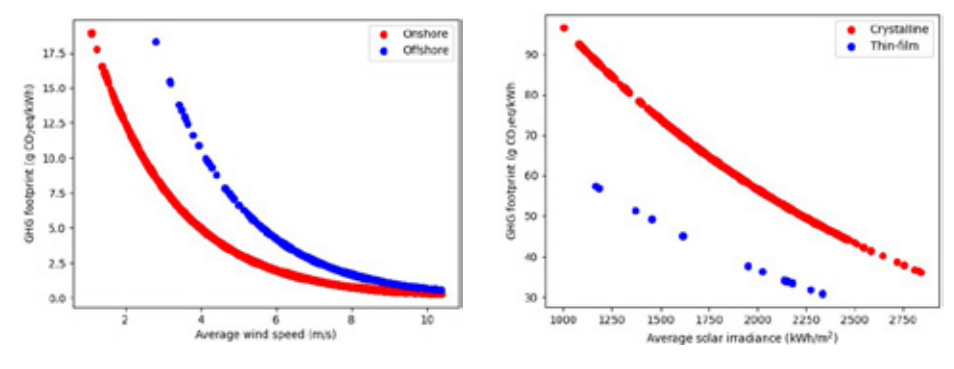
The importance of spatial resolution of the meteorological data has been investigated in chapter 2, where I have shown that a resolution of 30 by 30 km for wind speed data is a small enough resolution to predict a wind turbine's GHG

footprint. We built on that analysis in chapter 3, where I showed that wind speed is the most important variable in determining a facility's GHG footprint. This is caused by the fact that – within its operational wind speed range – the electricity production of a wind turbine is roughly related to the cubed wind speed, meaning that even a small increase in wind speed can create a large increase in the electricity production and thus a strong reduction in the GHG footprint (see Figure 6-2a).

For solar power, the relationship between irradiation and electricity production is linear, and hence we see that irradiation is an important variable to determine a facilities GHG footprint in the metamodel developed in chapter 4 (see Figure 6-2b). This finding is in line with Louwen et al. [72] who also showed that solar irradiance is an important factor in the environmental assessment of PV, with temperature being another important aspect as it can affect a PV panel's efficiency. Temperature was also included in the metamodel developed in chapter 4, but the importance analysis showed that using only irradiation as predictor sufficiently well estimated the results.

For hydropower facilities, flow data has been used to impute electricity production, but as I have not developed a metamodel for the GHG footprint, I have not assessed the importance of meteorological variables on the GHG footprint. Other spatially explicit variables included in the GHG footprint prediction are the storage area's chlorophyll a (Chl-a) concentration and the climate zone a hydropower facility is located in. [252] and [225] have shown that these are important factors influencing GHG emissions and thus GHG footprints. However, to date spatial and temporal variability of temperature and chlorophyll a concentration in water bodies is difficult to capture on large spatial scales, but recently Zhao et al. used highresolution satellite images to develop a Chl-a retrieval algorithm [253]. They found that lake surface temperature was the most important factor in determining Chl-a concentration. These findings could be used in future research to develop a similar approach as taken for wind and solar power, which can then provide clarity on which factors determine spatial variability for hydropower GHG footprints.

Thus, spatial variability in meteorological conditions are strong predictors for GHG footprints of wind, solar and possibly hydropower. For wind power, wind speed seems to be more important than technological variability, due to the production being related to wind speed cubed. For solar power, irradiation is slightly less important than technological variability, due to the strong difference in energy needed for producing crystalline vs. thin film panels, which also depend on production location [254].



- a) Partial dependence plot for wind power.
- b) Partial dependence plot for solar power

Figure 6-2 Partial dependence plots for wind power (a) and solar power (b) showing the effect of the main spatial variable on the greenhouse gas (GHG) footprint of the facilities. A bigger change in GHG footprint means that the variable is more important.

6.4 Temporal variability

In chapter 2, I have investigated how temporal variation in wind speed affects the calculation of GHG footprints. I found that using daily data at a 30 by 30 km grid sufficiently represent the life cycle GHG emissions of wind turbines compared to higher resolution data.

While I used hourly wind speed data to calculate the facility-specific GHG footprints of wind power in chapter 2, the metamodel developed in chapter 3 uses locationspecific 30-year average wind speeds as the only non-technological predictor. For the solar power GHG footprint calculations in chapter 4, I initially used hourly irradiation, temperature and wind speed data. Again, the metamodel showed that location-specific yearly average irradiation, temperature and wind speed play a role in the estimation of solar power GHG footprints. An importance analysis showed that with only hourly irradiation GHG footprints can be well approximated.

In both instances, temporal variability was deemed to be of lesser importance in the estimation of facility-specific GHG footprints of the electricity generation technologies assessed in this thesis. However, the confidence in the metamodel is increased by using a methodology that first makes use of the detailed (i.e., hourly) information available before reducing the level of detail.

For hydropower, I followed a different approach, where metamodels were used to impute the facility-specific GHG footprints from the start. The electricity production of each hydropower facility was calculated using a regression model based on average

yearly flow data [217]. GHG emissions for the construction and operational phases of the facilities were derived from emission factors derived from literature [219]. Given the increasing availability of data and the rise of AI technologies, a similar approach to those used here for wind and solar power could be used when calculating GHG footprints of hydropower facilities on a global scale. Al could be applied to gap filling, using, for example, data scraping methods. Furthermore, temporal variability in chlorophyll concentration and temperature, which [252, 225] have shown to be important in a reservoir's GHG emission, could be included in the calculations once datasets covering larger spatial and temporal scales are available.

6.5 Conclusions and Recommendations

In conclusion, the main findings of my thesis are:

- In order to develop a metamodel that can predict greenhouse gas footprint information as specific as possible with a minimum of information, the first step always has to be a detailed, in-depth analysis. Conducting an in-depth analysis helps to understand where the limits lie of an acceptable approximation.
- Facility-specific GHG footprints for wind power, solar power and hydropower can be approximated by a limited number of technological and spatio-temporal variables, allowing for an easier comparison of GHG footprints for specific technologies at distinct locations.
- The variability in the GHG footprints of the renewable electricity generation technologies considered here is greater between the different technologies than within a technology.

Based on these main findings, several recommendations for future work can be made. Future research should:

- Explore a similar approach as taken for wind and solar power when attempting to calculate GHG footprints for hydropower facilities on a global scale in which time-, space, and technology-specific variables are first used in the highest-possible resolution to then determine the most important variables in hydropower's GHG footprint.
- · Improve the metamodels derived for wind and solar power by including additional location- and technology-specific information, made possible by increased data availability and improvements in AI technology, which can reduce the computational requirements.

- Develop GHG emission-supply curves for relevant electricity generation technologies to integrate into integrated assessment models in addition to costsupply curves.
- Expand the models developed here to other impact categories to facilitate the evaluation of environmental performance and trade-offs of different electricity generation technologies.
- Develop a tool that supports decision makers which electricity generation technology is best suited at a certain location to minimize environmental impacts and trade-offs.
- Determine how much can be gained in terms of GHG emission mitigation at each location by comparing facility-specific GHG footprints of one technology to other (non-)renewable electricity sources.



References

- [1] Our World in Data, "Energy Mix," January 2024. [Online]. Available: https://ourworldindata. org/energy-mix. [Accessed 21 March 2025].
- [2] IPCC, "Climate Change 2022: Mitigation of Climate Change. Working Group III contribution to the Sixth Assessment Report of the Intergovernmental Panel on Climate Change," Cambridge University Press, Cambridge, United Kingdom and New York, NY, USA, 2022.
- [3] Our World in Data, "Greenhouse gas emissions by sector, World," 2024. [Online]. Available: https://ourworldindata.org/grapher/ghg-emissions-by-sector. [Accessed 21 March 2025].
- [4] J. Kimball, Physics of Sailing, Boca Raton: CRC Press, 2009.
- [5] T. F. Glick, S. Livesey and F. Wallis, Medieval science, technology adn medicine: an encyclopedia, Routledge, 2014.
- [6] United Nations, "What is renewable energy?," [Online]. Available: https://www.un.org/en/ climatechange/what-is-renewable-energy. [Accessed 22 6 2023].
- [7] Our World in Data, "Share of global primary energy consumption by source," 2024. [Online]. Available: https://ourworldindata.org/grapher/global-primary-energy-share-inc-biomass. [Accessed 21 March 2025].
- [8] L.-M. Eitler, "Sensation: Österreicher baute bereits vor 140 Jahren das erste Windrad," 2 August 2023. [Online]. Available: https://www.igwindkraft.at/media.php?filename= download%3D%2F2023.08.02%2F1690963041050772.pdf&rn=202300802%20PA%20 Erstes%20Windrad%20stand%20in%20O%CC%88sterreich.pdf. [Accessed 23 April 2024].
- [9] Z. Shahan, "History of Wind Turbines," 21 November 2014. [Online]. Available: https://www. renewableenergyworld.com/storage/grid-scale/history-of-wind-turbines/. [Accessed 24 April 2024].
- [10] A. Memija, "World's First 26 MW Offshore Wind Turbine Rolls Off Production Line," 14 October 2024. [Online]. Available: https://www.offshorewind.biz/2024/10/14/worlds-first-26-mwoffshore-wind-turbine-rolls-off-production-line/. [Accessed 22 March 2025].
- [11] Office of Energy Efficiency & Renewable Energy, "How Do Wind Turbines Work?," [Online]. Available: https://www.energy.gov/eere/wind/how-do-wind-turbines-work. [Accessed 23 April 2024].
- [12] IRENA, "Renewable Power Generation Costs in 2022," International Renewable Energy Agency, Abu Dhabi, 2023.
- [13] Q. Hassan, S. Algburi, A. Z. Sameen, H. M. Salman and M. Jaszczur, "A review of hybrid renewable energy systems: Solar and wind-powered solutions: Challenges, opportunities, and policy implications," Results in Engineering, vol. 20, p. 101621, 2023.
- [14] A. Bose, T. Dürr, R. A. Klenke and K. Henle, "Predicting strike susceptibility and collision patterns of the common buzzard at wind turbine structures in the federal state of Brandenburg, Germany," PLOS ONE, vol. 15, no. 8, p. e0238269, 2020.
- [15] T. Allison, J. E. Diffendorfer, E. Baerwald, J. Beston, D. Drake, A. Hale, C. Hein, M. M. Huso, S. Loss, J. E. Lovich, D. Strickland, K. Williams and V. Winder, "Impacts to wildlife of wind energy siting and operation in the United States," Issues in Ecology, vol. 21, pp. 1-24, 2019.
- [16] J. D. Lloyd, R. Butryn, S. Pearman-Gillman and T. D. Allison, "Seasonal patterns of bird and bat collision fatalities at wind turbines," PLOS ONE, vol. 18, no. 5, p. e0284778, 2023.
- J. Rydell, L. Bach, M.-J. Dubourg-Savage, M. Green, L. Rodrigues and A. Hedenström, "Bat [17] Mortality at Wind Turbines in Northwestern Europe," Acta Chiropterologica, vol. 12, no. 2, pp. 261-274, 2010.

- [18] R. Haac, R. Darlow, K. Kaliski, J. Rand and B. Hoen, "In the shadow of wind energy: Predicting community exposure and annoyance to wind turbine shadow flicker in the United States," *Energy Research & Social Science*, vol. 87, p. 102471, 2022.
- [19] F. J. Y. Müller, V. Leschinger, G. Hübner and J. Pohl, "Understanding subjective and situational factors of wind turbine noise annoyance," *Energy Policy*, vol. 173, p. 113361, 2023.
- [20] J. Rogers, "Optimal strategies for wind turbine environmental curtailment," Wind Energy, vol. 23, pp. 1331-1350, 2020.
- [21] L. C. Dammeier, J. M. Loriaux, Z. J. Steinmann, D. A. Smits, I. L. Wijnant, B. van den Hurk and M. A. Huijbregts, "Space, Time, and Size Dependencies of Greenhouse Gas Payback Times of Wind Turbines in Northwestern Europe," *Environmental Science and Technology*, vol. 53, no. 15, pp. 9289-9297, 2019.
- [22] C. Jung and D. Schindler, "Modeling wind turbine-related greenhouse gas payback times in Europe at high spatial resolutions," Energy Conversion and Management, vol. 243, p. 114334, 2021.
- [23] IEA, "Renewables," IEA, 2023. [Online]. Available: https://www.iea.org/energy-system/renewables. [Accessed 23 April 2024].
- [24] L. Chen, M. Baghoolizadeh, A. Basem, S. H. Ali, B. Ruhani, A. J. Sultan, S. Salahshour and A. Alizadeh, "A comprehensive review of building-integrated photovoltaic system (BIPV)," International Communications in heat and Mass Transfer, vol. 159, no. B, p. 108056, 2024.
- [25] Y. Yun, S. Moon, S. Kim and J. Lee, "Flexible fabric-based GaAs thin-film solar cell for wearable energy harvesting applications," Solar Energy Materials and Solar Cells, vol. 246, p. 111930, 2022.
- [26] D. M. Chapin, C. S. Fuller and G. L. Pearson, "A New Silicon p-n Junction Photocell for Converting Solar Radiation into Electrical Power," *Journal of Applied Physics*, vol. 25, no. 5, pp. 676-677, 1954.
- [27] NASA, "Vanguard Satellite, 1958," 17 March 2015. [Online]. Available: https://www.nasa.gov/image-article/vanguard-satellite-1958/. [Accessed 24 April 2024].
- [28] Office of Energy Efficiency & Renewable Energy, "How Does Solar Work?," [Online]. Available: https://www.energy.gov/eere/solar/how-does-solar-work. [Accessed 23 April 2024].
- T. Gill, "The world's biggest solar farms," 12 March 2024. [Online]. Available: https://www.theecoexperts.co.uk/solar-panels/biggest-solar-farms. [Accessed 22 March 2025].
- [30] J. H. Bosmans, L. C. Dammeier and M. A. Huijbregts, "Greenhouse gas footprints of utility-scale photovoltaic facilities at the global scale," *Environmental Research Letters*, vol. 16, no. 9, p. 094056, 2021.
- [31] T. Semeraro, A. Pomes, C. Del Giudice, D. Negro and R. Aretano, "Planning ground based utility scale solar energy as green infrastructure to enhance ecosystem services," *Energy Policy*, vol. 117, pp. 218-227, 2018.
- [32] E. J. Nordberg, J. M. Caley and L. Schwarzkopf, "Designing solar farms for synergistic commercial and conservation outcomes," *Solar Energy*, vol. 228, pp. 586-593, 2021.
- [33] EPA, "Best Practices for Siting Solar Photovoltaics on Municipal Solid Waste Landfills," United States Environmental Protection Agency, Washington, D.C., 2022.
- [34] Y. Jin, Hu, Shijie, A. D. Ziegler, L. Gibson, J. E. Campbell, R. Xu, D. Chen, K. Zhu, Y. Zheng, B. Ye, F. Ye and Z. Zeng, "Energy production and water savings from floating solar photovoltaics on global reservoirs," *Nature Sustainability*, vol. 6, pp. 865-874, 2023.
- [35] NHA, "History," National Hydropower Association, 2024. [Online]. Available: https://www.hydro.org/about/history/. [Accessed 24 April 2024].

- [36] Office of Energy Efficiency & Renewable Energy, "Hydropower Basics," [Online]. Available: https://www.energy.gov/eere/water/hydropower-basics. [Accessed 24 April 2024].
- [37] Office of Energy Efficiency & Renewable Energy, "How Hydropower Works," [Online]. Available: https://www.energy.gov/eere/water/how-hydropower-works. [Accessed 23 April 2024].
- [38] D. Egré and J. C. Milewski, "The diversity of hydropower projects," Energy Policy, vol. 30, pp. 1225-1230, 2002.
- [39] P. Moghaddasi, K. Gavahi, H. Moftakjari and H. Moradkhani, "Unraveling the hydropower vulnerability to drought in the United States," Environmental Research Letters, vol. 19, no. 8, p. 084038, 2024.
- [40] A. Kumar, T. Schei, A. Ahenkorah, R. C. Rodriguez, J.-M. Devernay, M. Freitas, D. Hall, A. Killingtveit and Z. Liu, "Hydropower," in IPCC Special Report on Renewable Energy Sources and Climate Change Mitigation, Cambridge, United Kingdom and New York, NY, USA, Cambridge University Press, 2011, pp. 437-496.
- [41] International Organization for Strandardization, "ISO 14040:2016," [Online]. Available: https://www.iso.org/standard/37456.html. [Accessed 19 April 2019].
- [42] International Organization for Standardization, "ISO 14044:2006," [Online]. Available: https:// www.iso.org/standard/38498.html. [Accessed 24 April 2024].
- [43] L. Golsteijn, "Life Cycle Assessment (LCA) explained," PRé Sustainability, 17 July 2022. [Online]. Available: https://pre-sustainability.com/articles/life-cycle-assessment-lca-basics/. [Accessed 3 April 2025].
- [44] A. Bonou, A. Laurent and S. O. Olsen, "Life cycle assessment of onshore and offshore wind energy-from theory to application," Applied Energy, vol. 180, pp. 327-337, 2016.
- [45] M. Caduff, M. A. Huijbregts, H.-J. Althaus, A. Köhler and S. Hellweg, "Wind Power Electricity: The Bigger the Turbine, The Greener the Electricity?," Environmental Science & Technology, vol. 46, no. 9, pp. 4725-4733, 2012.
- [46] G. Q. Chen, Q. Yang and Y. H. Zhao, "Renewability of wind power in China: A case study of nonrenewable energy cost and greenhouse gas emission by a plant in Guangxi," Renewable and Sustainable Energy Reviews, vol. 15, no. 5, pp. 2322-2329, 2011.
- [47] B. Guezuraga, R. Zauner and W. Pölz, "Life cycle assessment of two different 2 MW class wind turbines," Renewable Energy, vol. 37, no. 1, pp. 37-44, 2012.
- [48] S. White and G. Kulcinski, "Net energy payback and CO2 emissions from wind-generated electricity in the Midwest," 1998.
- [49] S. W. White, "Net Energy Payback and CO2 Emissions from Three Midwestern Wind Farms: An Update," Natural Resources Research, vol. 15, pp. 271-281, 2006.
- [50] N. Demir and A. Taşkın, "Life cycle assessment of wind turbines in Pınarbaşı-Kayseri," Journal of Cleaner Production, vol. 54, pp. 253-263, 2013.
- [51] P. Padey, R. Girard, D. le Boulch and I. Blanc, "From LCAs to Simplified Models: A Generic Methodology Applied to Wind Power Electricity," Environmental Science & Technology, vol. 43, no. 3, pp. 1231-1238, 2013.
- [52] R. Sacchi, R. Besseau, P. Pérez-López and I. Blanc, "Exploring technologically, temporally and geographically-sensitive life cycle inventories for wind turbines: A parameterized model for Denmark," Renewable Energy, vol. 132, pp. 1238-1250, 2019.
- [53] R. Besseau, R. Sacchi, I. Blanc and P. Pérez-López, "Past, present and future environmental footprint of the Danish wind turbine fleet with LCA_WIND_DK, an online interactive platform," Renewable and Sustainable Energy Reviews, vol. 108, pp. 274-288, 2019.

- [54] D. D. Hsu, P. O'Donoughue, V. Fthenakis, G. A. Heath, H. Chul Kim, P. Sawyer, J.-K. Choi and D. E. Turney, "Life Cycle Greenhouse Gas Emissions of Crystalline Silicon Photovoltaic Electricity Generation," *Journal of Industrial Ecology*, vol. 16, no. \$1, pp. \$122-\$135, 2012.
- [55] H. Chul Kim, V. Fthenakis, J.-K. Choi and D. E. Turney, "Life Cycle Greenhouse Gas Emissions of Thin-film Photovoltaic Electricity Generation," *Journal of Industrial Ecology*, vol. 16, no. s1, pp. S110-S121, 2012.
- [56] K. P. Bhandari, J. M. Collier, R. J. Ellingson and D. S. Apul, "Energy payback time (EPBT) and energy return on energy invested (EROI) of solar photovoltaic systems: A systematic review and meta-analysis," *Renewable and Sustainable Energy Reviews*, vol. 47, pp. 133-141, 2015.
- [57] A. Louwen, W. G. van Sark, A. P. Faaij and R. E. Schropp, "Re-assessment of net energy production and greenhouse gas emissions avoidance after 40 years of photovoltaics development," *Nature Communications*, vol. 7, p. 13728, 2016.
- [58] R. Bhandari, B. Kumar and F. Mayer, "Life cycle greenhouse gas emission from wind farms in reference to turbine sizes and capacity factors," *Journal of Cleaner Production*, vol. 277, p. 123385, 2020.
- [59] E. G. Hertwich, T. Gibon, E. A. Bouman, A. Arvesen, S. Suh, G. A. Heath, J. D. Bergesen, A. Ramirez, M. I. Vega and L. Shi, "Integrated life-cycle assessment of electricity-supply scenarios confirms global environmental benefit of low-carbon technologies," *Proceedings of the National Academy of Sciences*, vol. 112, no. 20, pp. 6277-6282, 2014.
- [60] E. Leccisi, M. Raugei and V. Fthenakis, "The Energy and Environmental Performance of Ground-Mounted Photovoltaic Systems—A Timely Update," *Energies*, vol. 9, no. 8, p. 622, 2016.
- [61] H. C. Kim, V. Fthenakis, J.-K. Choi and D. E. Turney, "Life Cycle Greenhouse Gas Emissions of Thin-film Photovoltaic Electricity Generation," *Journal of Industrial Ecology*, vol. 16, no. 1, pp. S110-S121, 2012.
- [62] V. Nian, "Impacts of changing design considerations on the life cycle carbon emissions of solar photovoltaic systems," Applied Energy, vol. 183, pp. 1471-1487, 2016.
- [63] G. Hou, H. Sun, Z. Jiang, Z. Pan, Y. Wang, X. Zhang, Y. Zhao and Q. Yao, "Life cycle assessment of grid-connected photovoltaic power generation from crystalline silicon solar modules in China," *Applied Energy*, vol. 164, pp. 882-890, 2016.
- [64] I. Miller, E. Gencer, H. S. Vogelbaum, P. R. Brown, S. Torkamani and F. M. O'Sullivan, "Parametric modeling of life cycle greenhouse gas emissions from photovoltaic power," *Applied Energy*, vol. 238, pp. 760-774, 2019.
- [65] D. Nugent and B. K. Sovacool, "Assessing the lifecycle greenhouse gas emissions from solar PV and wind energy: A critical meta-survey," *Energy Policy*, vol. 65, pp. 229-244, 2014.
- [66] T. Wetzel and S. Borchers, "Update of energy payback time and greenhouse gas emission data for crystalline silicon photovoltaic modules," *Progress in Photovoltaics: Research and Applications*, vol. 23, no. 10, pp. 1429-1435, 2014.
- [67] V. Muteri, M. Cellura, D. Curto, V. Franzitta, S. Longo, M. Mistretta and M. L. Parisi, "Review on Life Cycle Assessment of Solar Photovoltaic Panels," *Energies*, vol. 13, no. 1, p. 252, 2020.
- [68] J. D. Bergesen, G. A. Heath, T. Gibon and S. Suh, "Thin-Film Photovoltaic Power Generation Offers Decreasing Greenhouse Gas Emissions and Increasing Environmental Co-benefits in the Long Term," Environmental Science & Technology, vol. 48, no. 16, pp. 9834-9843, 2014.
- [69] A. Beylot, J. Payet, C. Puech, N. Adra, P. Jacquin, I. Blanc and D. Beloin-Saint-Pierre, "Environmental impacts of large-scale grid-connected ground-mounted PV installations," *Renewable Energy*, vol. 61, pp. 2-6, 2014.

- [70] N. Gazbour, G. Razongles, E. Monnier, M. Joanny, C. Charbuillet, F. Burgun and C. Schaeffer, "A path to reduce variability of the environmental footprint results of photovoltaic systems," Journal of Cleaner Production, vol. 197, no. Part 1, pp. 1607-1618, 2018.
- [71] N. A. Ludin, N. I. Mustafa, M. M. Hanafiah, M. A. Ibrahim, M. A. M. Teridi, S. Sepeai, A. Zaharim and K. Sopian, "Prospects of life cycle assessment of renewable energy from solar photovoltaic technologies: A review," Renewable and Sustainable Energy Reviews, vol. 96, pp. 11-28, 2018.
- [72] A. Louwen, R. E. Schropp, W. G. van Sark and A. P. Faaij, "Geospatial analysis of the energy yield and environmental footprint of different photovoltaic module technologies," Solar Energy, vol. 155, pp. 1339-1353, 2017.
- [73] M. Ito, S. Lespinats, J. Merten, P. Malbranche and K. Kurokawa, "Life cycle assessment and cost analysis of very large-scale PV systems and suitable locations in the world," Progress in Photovoltaics: Research and Applications, vol. 24, no. 2, pp. 159-174, 2015.
- [74] P. Pérez-López, B. Gschwind, P. Blanc, R. Frischknecht, P. Stolz, Y. Durand, G. Heath, L. Ménard and I. Blanc, "ENVI-PV: an interactive Web Client for multi-criteria life cycle assessment of photovoltaic systems worldwide," Progress in Photovoltaics: Research and Applications, vol. 25, no. 7, pp. 484-498, 2016.
- [75] P. Perez-Lopez, B. Gschwind, R. Frischknecht, P. Stolz, C. Mehl, M. Payeur, G. Heath and I. Blanc, "Combining region-specific supply chains with geo-located PV electricity production for Life Cycle Assessment of worldwide crystalline silicon photovoltaic systems in ENVI-PV 2.0," in 36th European Photovoltaic Solar Energy Conference and Exhibition, Marseille, FR, 2019.
- [76] D. M. Ribeiro and G. Anderi, "Life-cycle inventory for hydroelectric generation: a Brazilian case study," Journal of Cleaner Production, vol. 18, pp. 44-54, 2010.
- P. Denholm and G. L. Kulcinsku, "Life cycle energy requirements and greenhouse gas [77] emissions from large scale energy storage systems," Energy Conversion and Management, vol. 45, no. 13-14, pp. 2153-2172, 2004.
- [78] J. Gallagher, D. Styles, A. McNabola and A. P. Williams, "Life cycle environmental balance and greenhouse gas mitigational protential of micro-hydropower energy recovery in the water industry," Journal of Cleaner Production, vol. 99, pp. 152-159, 2015.
- [79] L. Gagnon and J. F. van der Vate, "Greenhouse gas emissions from hydropower. The state of research in 1996," Energy Policy, vol. 25, no. 1, pp. 7-13, 1997.
- [80] M. Pehnt, "Dynamic life cycle assessment (LCA) of renewable energy technologies," Renewable Energy, vol. 31, no. 1, pp. 55-71, 2006.
- [81] M. B. Rule, Z. J. Worth and C. A. Boyle, "Comparison of Life Cycle Carbon Dioxide Emissions and Embodied Energy in Four Renewable Electricity Generation Technologies in New Zealand," Environmental Science and Technology, vol. 43, no. 16, pp. 6106-6413, 2012.
- [82] K. Flury and R. Frischknecht, "Life Cycle Inventories of Hydroelectric Power Generation," ESUservices Ltd., Uster, CH, 2012.
- [83] V. Goel, R. Prakash and I. K. Bhat, "Life cycle greenhouse gas emissions estimation for small hydropower schemes in India," Energy, vol. 44, no. 1, pp. 498-508, 2012.
- [84] S. Arnøy and I. S. Modahl, "Life Cycle Data for Hydroelectric Generation at Embretsfoss 4 (E4) Power Station," Ostfold Research, Fredrikstad, 2013.
- [85] Axpo, "Environmental Product Declaration - Au-Schonberg Small-Scale Hydro Power Plant," Axpo, Baden, CH.
- [86] S. Arnøy and I. S. Modahl, "Life Cycle Data for Hydroelectric Generation at Trollheim Power Station," Ostfold Research, Fredrikstad, 2013.

- [87] Axpo, "Environmental Product Declaration: Wildegg-Brugg run-of-river Power Plant, Update 2019," Axpo, Baden, CH, 2019.
- [88] J. Gallagher, D. Styles, A. McNabola and A. P. Williams, "Current and Future Environmental Balance of Small-Scale Run-of-River Hydropower," *Environmental Science and Technology*, vol. 49, no. 10, pp. 6344-6351, 2015.
- [89] W. Suwanit and S. H. Gheewala, "Life cycle assessment of mini-hydropower plants in Thailand," *The International Journal of Life Cycle Assessment*, vol. 16, pp. 849-858, 2011.
- [90] C. R. Donnelly, A. Carias, M. Morgenroth, M. Ali, A. Bridgeman and N. Wood, "An Assessment of the Life Cycle Costs and GHG Emissions for Alternative Generation Technologies," in International World Energy Council Conference, Montreal, Quebec, Canada, 2010.
- [91] C. Song, K. H. Gardner, S. J. Klein, S. Pereira Souza and W. Mo, "Cradle-to-grave greenhouse gas emissions from dams in the United States of America," *Renewable and Sustainable Energy Reviews*, vol. 90, pp. 945-956, 2018.
- [92] H. L. Raadal, L. Gagnon, I. S. Modahl and O. J. Hanssen, "Life cycle greenhouse gas (GHG) emissions from the generation of wind and hydro power," *Renewable and Sustainable Energy Reviews*, vol. 15, pp. 3417-3422, 2011.
- [93] A. Briones-Hidrovo, J. Uche and A. Martínez-Graxia, "Accounting for GHG net reservoir emissions of hydropower in Ecuador," *Renewable Energy*, vol. 112, pp. 209-221, 2017.
- [94] Y.T. Prairie, S. Mercier-Blais, J. A. Harrison, C. Soued, P. del Giorgio, A. Harby, J. Alm, V. Chanudet and R. Nahas, "A new modelling framework to assess biogenic GHG emissions from reservoirs: The G res tool," *Environmental Modelling & Software*, vol. 143, p. 105117, 2021.
- [95] J. Wang, X. Chen, Z. Liu, V. F. Frans, X. Qui, F. Xu and Y. Li, "Assessing the water and carbon footprint of hydropower stations at the national scale," *Science of The Total Environment*, vol. 676, pp. 595-612, 2019.
- [96] J. A. Harrison, Y. T. Praire, S. Mercier-Blais and C. Soued, "Year-2020 Global Distribution and Pathways of Reservoir Methane and Carbon Dioxide Emissions According to the Greenhouse Gas From Reservoirs (G-res) Model," Global Biogeochemical Cycles, vol. 35, no. 6, p. e2020GB006888, 2021.
- [97] L. Scherer and S. Pfister, "Hydropower's Biogenic Carbon Footprint," PLOS One, vol. 11, no. 9, p. e0161947, 2016.
- [98] E. Gemechu and A. Kumar, "A review of how life cycle assessment has been used to assess the environmental impacts of hydropower energy," *Renewable and Sustainable Energy Reviews*, vol. 167, p. 112684, 2022.
- [99] International Energy Agency, "Next Generation Wind and Solar Power From cost to value," Paris, FR, 2016.
- [100] World Wind Energy Association, "Wind Power Capacity Reaches 600 GW, 53.9 GW Added in 2018," [Online]. Available: https://wwindea.org/blog/2019/02/25/wind-power-capacity-worldwide-reaches-600-gw-539-gw-added-in-2018/. [Accessed 10 April 2019].
- [101] International Energy Agency, "World Energy Outlook 2015," Paris, FR, 2015.
- [102] Global Wind Energy Council, "Global Wind Energy Outlook 2016," Brussels, BE, 2016.
- [103] S. L. Dolan and G. A. Heath, "Life cycle greenhouse gas emissions of utility-scale wind power," Journal of Industrial Ecology, vol. 16, no. s1, pp. S136-S154, 2012.
- [104] P. M. Elshout, R. van Zelm, J. Balkovic, M. Obersteiner, E. Schmid, R. Skalsky, M. van der Velde and M. A. Huijbregts, "Greenhouse-gas payback times for crop-based biofuels," *Nature Climate Change*, vol. 5, pp. 604-610, 2015.

- Royal Netherlands Meteorological Institute, "KNW (KNMI North sea Wind) Atlas," [Online]. Available: http://projects.knmi.nl/knw/. [Accessed 10 April 2019].
- The Wind Power.net, "Wind farms database," [Online]. Available: http://www.thewindpower. [106] net/index.php. [Accessed 21 August 2018].
- [107] B. B. Nalukowe, J. Liu, W. Damien and T. Lukawski, "Life Cycle Assessment of a Wind Turbine," 2006.
- [108] Vestas Wind Systems A/S, "Life Cycle Assessment of Electricity Production from a V80-2.0 MW Gridstreamer Wind Plant," Randers, DK, 2011.
- Elsam Engineering A/S, "Life Cycle Assessment of offshore and onshore sited wind farms (Engl. Transl.)," Copenhagen, DK, 2004.
- Vestas Wind Systems A/S, "Life Cycle Assessment of Electricity Production from an onshore [110] V126-3.3 MW Wind Plant," Randers, DK, 2014.
- [111] Vestas Wind Systems A/S, "Life Cycle Assessment of Electricity Produced from an onshore V100-2.0 MW Wind Plant," Randers, DK, 2015.
- K. R. Haapala and P. Prempreeda, "Comparative life cycle assessment of 2.0 MW wind [112] turbines," International Journal of Sustainable Manufacturing, vol. 3, no. 2, pp. 170-185, 2014.
- ecoinvent Centre, "Life cycle inventories of energy systems: Results for current systems in [113] Switzerland and other UCTE countries," Dübendorf, CH, 2007.
- A. Rashedi, I. Sridhar and K. Tseng, "Life cyle assessment of 50MW wind firms and strategies for impact reduction," Renewable and Sustainable Energy Reviews, vol. 21, pp. 89-101, 2013.
- [115] Bundesamt für Energie BFE, "Ökobilanzierung von Schweizer Windenergie," Bern, CH, 2015.
- [116] E. Pick, H.-J. Wagner and O. Bunk, "Kumulierter Energieaufwand von Windkraftanlagen," Brennstoff-Wärme-Kraft, vol. 50, pp. 52-55, 1998.
- Vestas Wind Systems A/S, "Life Cycle Assessment of Electricity Production from a V90-2.0 MW Gridstreamer Wind Plant," Randers, DK, 2011.
- [118] Vestas Wind Systems A/S, "Life Cycle Assessment of Electricity Production from a V112 Turbine Wind Plant," Randers, DK, 2011.
- A. Arvesen and E. G. Hertwich, "Assessing the life cycle environmental impacts of wind [119] power: A review of present knowledge and research needs," Renewable and Sustainable Energy Reviews, vol. 16, no. 8, pp. 5994-6006, 2012.
- S. Arlot and A. Celisse, "A survey of cross-validation procedures for model selection," Statistics [120] Survey, vol. 4, pp. 40-79, 2010.
- [121] European Wind Energy Association, "The Economics of Wind Energy A report by the European Wind Energy Association," Brussels, BE, 2009.
- [122] A. Betz, Introduction to the Theory of Flow Machines, Oxford, UK: Pergamon Press, 1966.
- D. P. Dee, S. M. Uppala, A. J. Simmons, P. Berrisford, P. Poli, S. Kobayashi, U. Andrae, M. A. [123] Balmaseda, G. Balsamo, P. Bauer, P. Bechtold, A. C. Beljaars, L. van de Berg, J. Bidlot, N. Bormann, C. Delsol, R. Dragani, M. Fuentes, A. J. Heer, L. Haimberger, S. B. Healy, H. Hersbach, E. V. Hólm, L. Isaksen, P. Kållberg, M. Köhler, M. Matricardi, A. P. McNally, B. M. Monge-Sanz, J.-J. Morcrette, B.-K. Park, C. Peubey, P. de Rosnay, C. Tavolato, J.-N. Thépaut and F. Vitart, "The ERA-Interim reanalysis: configuration and performance of the data assimilation system," Quarterly Journal of the Royal Meteorological Society, vol. 137, no. 656, pp. 553-597, 2011.
- R. Bubnová, G. Hello, P. Bénard and J.-F. Geleyn, "Integration of the Fully Elastic Equations Cast in the Hydrostatic Pressure Terrain-Following Coordinate in the Framework of the ARPEGE/Aladin NWP System," Monthly Weather Review, vol. 123, no. 1, pp. 515-535, 1995.

- [125] Y. Seity, P. Brousseau, S. Malardel, G. Hello, P. Bénard, F. Bouttier, C. Lac and V. Masson, "The AROME-France Convective-Scale Operational Model," *Monthly Weather Review*, vol. 139, no. 3, pp. 976-991, 2011.
- [126] A. Stepek, M. Savenije, H. W. van den Brink and I. L. Wijnant, "Validation of KNW atlas with publicly available mast observations (Phase 3 of KNW project)," De Bilt, NL, 2015.
- [127] I. L. Wijnant, G. J. Marseille, A. Stoffelen, H. W. van den Brink and A. Stepek, "Validation of KNW atlas with scatterometer winds (Phase 3 of KWN project)," Royal Netherlands Meteorological Institute, De Bilt, NL, 2015.
- [128] H. Kling, M. Fuchs and M. Paulin, "Runoff conditions in the upper Danube basin under an ensemble of climate change scenarios," *Journal of Hydrology*, Vols. 424-425, pp. 264-277, 2012.
- [129] I. Gonzáles-Aparicio, F. Monforti, P. Volker, A. Zucker, F. Careri, T. Huld and J. Badger, "Simulating European wind power generation applying statistical downscaling to reanalysis data," Applied Energy, vol. 199, pp. 155-168, 2017.
- [130] D. Dee, J. Fasullo, D. Shea, J. Walsh and NCAR Staff, "The Climate Data Guide: Atmospheric Reanalysis: Overview & Comparison Tables," [Online]. Available: https://climatedataguide.ucar.edu/climate-data/atmospheric-reanalysis-overview-comparison-tables. [Accessed 10 April 2019].
- [131] G. Flato, J. Marotzke, B. Abiodun, P. Braconnot, S. C. Chou, W. Collins, P. Cox, F. Driouech, S. Emori, V. Eyring, C. Forest, P. Gleckler, E. Guilyardi, C. Jakob, V. Kattsov, C. Reason and M. Rummukainen, "Evaluation of Climate Models," in *Climate Change 2013: The Physical Science Basis, Contribution of Working Group I to the Fifth Assessment Report of the IPCC*, T. F. Stocker, D. Qin, G. Plattner, M. Tignor, S. K. Allen, J. Boschgun, A. Nauels, Y. Xia, V. Bex and P. M. Midgley, Eds., Cambridge, UK, Cambridge University Press, 2013.
- [132] The NCAR Command Language, version 6.4.0, Boulder, Colorado, 2017.
- [133] R. Fajber, A. H. Monahan and W. J. Merryfield, "At What Time of Day Do Daily Extreme Near-Surface Wind Speeds Occur?," *Journal of Climate*, vol. 27, no. 11, pp. 4226-4244, 2014.
- [134] E. Son, S. Lee, B. Hwang and S. Lee, "Characteristics of turbine spacing in a wind farm using an optimal design process," *Renewable Energy*, vol. 65, pp. 245-249, 2014.
- [135] R. J. Barthelmie, S. C. Pryor, S. T. Frandsen, K. S. Hansen, J. G. Schepers, K. Rados, W. Schlez, A. Neubert, L. E. Jensen and S. Neckelmann, "Quantifying the Impact of Wind Turbine Wakes on Power Output of Offshore Wind Farms," *Journal of Atmospheric and Oceanic Technology*, vol. 27, no. 8, pp. 1302-1317, 2010.
- [136] E. Dupont, R. Koppelaar and H. Jeanmart, "Global available wind energy with physical and energy return on investment constraints," *Applied Energy*, vol. 209, pp. 322-338, 2018.
- [137] C. Jung and D. Schindler, "The role of air density in wind energy assessment A case study from Germany," *Energy*, vol. 171, pp. 385-392, 2019.
- [138] S. Germer and A. Kleidon, "Have wind turbines in Germany generated electricicty as would be expected from the prevailing wind conditons in 2000-2014?," *PLOS One*, vol. 14, no. 2, p. e0211028, 2019.
- [139] N. Dailili, A. Edrisy and R. Carriveau, "A review of surface engineering issues critical to wind turbine performance," *Renewable and Sustainable Energy Reviews*, vol. 13, no. 2, pp. 428-438, 2009.
- [140] K. Siler-Evans, I. Lima Azevedo, M. G. Morgan and J. Apt, "Regional variations in the health, environmental, and climate benefits of wind and solar generation," *Proceedings of the National Academy of Sciences of the United States of America*, vol. 110, no. 29, pp. 11768-11773, 2013.

- [141] M. Pehl, A. Arvesen, F. Humpenöder, A. Popp, E. G. Hertwich and G. Luderer, "Understanding future emissions from low-carbon power systems by integration of life-cycle assessment and integrated energy modelling," Nature Energy, vol. 2, pp. 939-945, 2017.
- [142] A. Dabbaghiyan, F. Fazelpour, M. Dehghan Abnavi and M. A. Rosen, "Evaluation of wind energy potential in province of Bushehr, Iran," Renewable and Sustainable Energy Reviews, vol. 55, pp. 455-466, 2016.
- A. Allouhi, O. Zamzoum, M. R. Islam, R. Saidur, T. Kousksou, A. Jamil and A. Derouich, [143] "Evaluation of wind energy potential in Morocco's coastal regions," Renewable and Sustainable Energy Reviews, vol. 72, pp. 311-324, 2017.
- ECMWF, "ERA5," [Online]. Available: https://www.ecmwf.int/en/forecasts/datasets/ [144] reanalysis-datasets/era5. [Accessed 10 April 2019].
- M. D. Vieira, T. C. Ponsioen, M. J. Goedkoop and M. A. Huijbregts, "Surplus Ore Potential as a Scarcity Indicator for Resource Extraction," Journal of Industrial Ecology, vol. 21, no. 2, pp. 381-390, 2016.
- [146] S. Pfister, D. Saner and A. Koehler, "The environmental relevance of freshwater consumption in global power production," The International Journal of Life Cycle Assessment, vol. 16, pp. 580-591, 2011.
- [147] P. A. Arias, N. Bellouin, E. Coppola, R. G. Jones, G. Krinner, J. Marotzke, V. Naik, M. D. Palmer, G.-K. Plattner, J. Rogelj, M. Rojas, J. Sillmann, T. Storelvmo, P. W. Thorne and B. Trewin, "Technical Summary," in Climate Change 2021: The Physical Science Basis. Contribution of Working Group I to the Sixth Assessment Report of the Intergovernmental Panel on Climate Change, Cambridge, United Kingdom and New York, NY, USA, Cambridge University Press, 2021, pp. 35-144.
- P. J. Simons and W. M. Cheung, "Development of a quantitative analysis system for greener and economically sustainable wind farms," Journal of Cleaner Production, vol. 133, pp. 886-898, 2016.
- [149] IRENA, "Future of wind: Deployment, investment, technology, grid integration and socioeconomic aspects (A Global Energy Transformation paper)," Abu Dhabi, 2019.
- Global Wind Energy Council, "Global Wind Report 2019," Brussels, BE, 2020. [150]
- H. Ritchie, M. Roser and P. Rosado, "Renewable energy," 2020. [Online]. Available: https:// [151] ourworldindata.org/renewable-energy#breakdown-of-renewables-in-the-energy-mix.
- A. Alsaleh and M. Sattler, "Comprehensive life cycle assessment of large wind turbines in the US," Clean Technologies and Environmental Policy, vol. 21, pp. 887-903, 2019.
- B. Mendecka and L. Lombardi, "Life cycle environmental impacts of wind energy technologies: A review of simplified models and harmonization of the results," Renewable and Sustainable Energy Reviews, vol. 111, pp. 462-480, 2019.
- ECMWF, "ERA5," [154] 2020. [Online]. Available: https://cds.climate.copernicus.eu/#!/ search?text=ERA5&type=dataset. [Accessed 4 October 2020].
- R. H. Wiser and M. Bolinger, "Benchmarking Anticipated Wind Project Lifetimes: Results from a Survey of U.S. Wind Industry Professionals," 2019.
- [156] 4C Offshore, "4C Offshore," [Online]. Available: https://www.4coffshore.com/. [Accessed 5 January 2022].
- [157] IRENA, "Wind energy," [Online]. Available: https://www.irena.org/wind. [Accessed 5 January 2022].
- D. Villanueva and A. Feijóo, "Comparison of logistic functions for modeling wind turbine power curves," Electric Power Systems Research, vol. 155, pp. 281-288, 2018.

- [159] SciPy.org, "scipy.optimize.curve_fit," [Online]. Available: https://docs.scipy.org/doc/scipy/reference/generated/scipy.optimize.curve_fit.html. [Accessed 24 February 2020].
- [160] A. Ulazia, J. Sánez, G. Ibarra-Berastegi, S. J. González-Rojí and S. Carreno-Madinabeitia, "Global estimations of wind energy potential considering seasonal air density changes," *Energy*, vol. 187, p. 115938, 2019.
- [161] J. Beauson, A. Laurent, D. P. Rudolph and J. Pagh Jensen, "The complex end-of-life of wind turbine blades: A review of the European context," *Renewable and Sustainable Energy Reviews*, vol. 155, p. 111847, 2022.
- [162] A. J. Pimm, J. Palczewski, E. R. Barbour and T. T. Cockerill, "Using electricity storage to reduce greenhouse gas emissions," *Applied Energy*, vol. 282, no. Part A, p. 116199, 2021.
- [163] EIA, "Form EIA-923 detailed data with previous form data (EIA-906/920)," [Online]. Available: https://www.eia.gov/electricity/data/eia923. [Accessed 9 January 2022].
- [164] Danish Energy Agency, "Overview of the energy sector," [Online]. Available: https://ens. dk/en/our-services/statistics-data-key-figures-and-energy-maps/overview-energy-sector. [Accessed 9 January 2022].
- [165] Y.-M. Saint-Drenan, R. Besseau, M. Jansen, I. Staffell, A. Troccoli, L. Dubus, J. Schmitd, K. Gruber, S. G. Simoes and S. Heier, "A parametric model for wind turbine power curves incorporating environmental conditions," *Renewable Energy*, vol. 157, pp. 754-768, 2020.
- [166] ECMWF, "ERA5: data documentation," [Online]. Available: https://confluence.ecmwf.int/display/CKB/ERA5%3A%2Bdata%2Bdocumentation.
- [167] J. Olausen, "ERA5: The new champion of wind power modelling?," *Renewable Energy*, vol. 126, pp. 322-331, 2018.
- [168] J. Ramon, L. Lledó, V. Torralba, A. Soret and F. J. Doblas-Reyes, "What global reanalysis best represents near-surface winds?," *Quarterly Journal of the Royal Meteorological Society,* vol. 145, no. 724, pp. 3236-3251, 2019.
- [169] K. Gruber, P. Regner, S. Wehrle, M. Zeyringer and J. Schmidt, "Towards global validation of wind power simulations: A multi-country assessment of wind power simulation from MERRA-2 and ERA-5 reanalyses bias-corrected with the global wind atlas," *Energy*, vol. 238, no. Part A, p. 121520, 2022.
- [170] I. Staffell and S. Pfenninger, "Using bias-corrected reanalysis to simulate current and future wind power output," *Energy*, vol. 114, pp. 1224-1239, 2016.
- [171] G. Gualtieri, "A novel method for wind farm layout optimization based on wind turbine selection," Energy Conversion and Management, vol. 193, pp. 106-123, 2019.
- [172] Gamesa, "Electricity from: European GAMESA G128-5.0 MW onshore wind farm," 2015.
- [173] Gamesa, "Electricity from: European GEAMES G132-5.0 MW onshore wind farm," 2015.
- [174] T. Bruckner, I. A. Bashmakov, Y. Mulugetta, H. Chum, A. de la Vega Navarro, J. Edmonds, A. Faaij, B. Fungtammasan, A. Garg, E. Hertwich, D. Honnery, D. Infield, M. Kainuma, S. Khennas, S. Kim, H. B. Nimir, K. Riahi, N. Stachan, R. Wiser and X. Zhang, "Energy Systems," in Climate Change 2014: Mitigation of Climate Change. Contribution of Working Group III to the Fifth Assessment Report of the Intergovernmental Panel on Climate Change, O. Edenhofer, R. Pichs-Madruga, Y. Sokona, E. Farahani, S. Kadner, K. Seyboth, A. Adler, I. Baum, S. Brunner, P. Eickemeier, B. Kriemann, J. Savolainen, S. Schlömer, C. von Stechow, T. Zwickel and J. C. Minx, Eds., Cambridge, UK and New York, NY, USA, Cambridge University Press, 2014.
- [175] IRENA, "Renewable Capacity Statistics 2020," IRENA, Abu Dhabi, 2020.

- [176] IEA, "Fuels & Technologys: Solar," [Online]. Available: www.iea.org/fuels-and-technologies/ solar. [Accessed 2020].
- [177] IEA, "Solar PV," [Online]. Available: www.iea.org/reports/solar-pv. [Accessed 2020].
- [178] Absolute Reports, "Global Solar Photovoltaic (PV) Market Growth, Trends and Forecasts (2018-2023). Chapter 8: Global Solar Photovoltaic (PV) Market Analysis, by Geography," 2018.
- [179] Y. Chen, P. P. Altermatt, D. Chen, X. Zhang, G. Xu, Y. Yang, Y. Wang, Z. Feng, H. Shen and P. J. Verlinden, "From Laboratory to Production: Learning Models of Efficiency and Manufacturing Cost of Industrial Crystalline Silicon and Thin-Film Photovoltaic Technologies," IEEE Journal of Photovoltaics, vol. 8, pp. 1531-1538, 2018.
- S. Jerez, I. Tobin, R. Vautard, J. P. Montávez, J. M. López-Romero, F. Thais, B. Bartok, O. B. [180] Christensen, A. Colette, M. Déqué, G. Nikulin, S. Kotlarski, E. van Meijgaard, C. Teichmann and M. Wild, "The impact of climate change on photovoltaic power generation in Europe," Nature Communications, vol. 6, p. 10014, 2015.
- F. Mavromatakis, G. Makrides, G. Georghiou, A. Pothrakis, Y. Franghiadakis, E. Drakakis and E. [181] Koudoumas, "Modeling the photovoltaic potential of a site," Renewable Energy, vol. 35, no. 7, pp. 1387-1390, 2010.
- R. Frischknecht, P. Stolz, G. Heath, M. Raugei, P. Sinha and M. de Wild-Scholten, "Methodology [182] Guidelines on Life Cycle Assessment of Photovoltaic," IEA PVPS, 2020.
- Frauenhofer Institute for Solar Energy Systems (ISE), "Photovoltaics Report," ISE, 2020. [183]
- EIA, "EIA-860 2018 data," U.S. Energy Information Administration, [Online]. Available: https:// www.eia.gov/electricity/data/eia860/. [Accessed 30 September 2019].
- R. Gupta and H. Shankar, "Global Energy Observatory (GEO)," [Online]. Available: https:// [185] globalenergyobservatory.org. [Accessed 12 November 2019].
- [186] Copernicus Climate Change Service, "ERA5: Fifth genenration of ECMWF atmospheric reanalyses of the global climate," Copernicus Climate Change Service (C3S) Climate Data Store (CDS), [Online]. Available: https://cds.climate.copernicus.eu/cdsapp#!/home.
- K. Kawajiri, T. Oozeki and Y. Genchi, "Effect of Temperature on PV Potential in the World," [187] Environmental Science & Technology, vol. 45, no. 20, pp. 9030-9035, 2011.
- T. Huld, R. Gottschalg, H. G. Beyer and M. Tobic, "Mapping the performance of PV modules, [188] effects of module type and data averaging," Solar Energy, vol. 84, no. 2, pp. 324-338, 2010.
- B.-j. Kim, J.-y. Lee, K.-h. Kim and T. Hur, "Evaluation of the environmental performance of sc-Si and mc-Si PV systems in Korea," Solar Energy, vol. 99, pp. 100-114, 2014.
- [190] M. J. de Wild-Scholten, "Energy payback time and carbon footpring of commercial photovoltaic systems," Solar Energy Materials and Solar Cells, vol. 119, pp. 296-305, 2013.
- [191] Y. Yao, Y. Chang and E. Masanet, "A hybrid life-cycle inventory for multi-crystalline silicon PV module manufacturing in China," Environmental Research Letters, vol. 9, p. 114001, 2014.
- D. Yue, F. You and S. B. Darling, "Domestic and overseas manufacturing scenarios of silicon-[192] based photovoltaics: Life cycle energy and environmental comparative analysis," Solar Energy, vol. 105, pp. 669-678, 2014.
- K. Kawajiri and Y. Genchi, "The Right Place for the Right Job in the Photovoltaic Life Cycle," Environmental Science & Technology, vol. 46, no. 13, pp. 7415-7421, 2012.
- [194] L. Serrano-Luján, N. Espinosa, J. Abad and A. Urbina, "The greenest decision on photovoltaic system allocation," Renewable Energy, vol. 101, pp. 1348-1356, 2017.

- [195] C. A. Grant and A. L. Hicks, "Effect of manufacturing and installation location on environmental impact payback time of solar power," *Clean Technologies and Environmental Policy*, vol. 22, pp. 187-196, 2020.
- [196] V. Fthenakis and E. Leccisi, "Updated sustainability status of crystalline silicon-based photovoltaic systems: Life-cycle energy and environmental impact reduction trends," Progress in Photovoltaics: Research and Applications, vol. 29, no. 10, pp. 1068-1077, 2021.
- [197] O. Perpiñan, E. Lorenzo, M. A. Castro and R. Eyras, "Energy payback time of grid connected PV systems: Comparison between tracking and fixed systems," *Progress in Photovoltaics: Research and Applications*, vol. 17, no. 2, pp. 137-147, 2008.
- [198] P. Sinha, M. Schneider, S. Dailey, C. Jepson and M. de Wild-Scholten, "Eco-Efficiency of CdTe Photovoltaics with Tracking Systems," in *IEEE 39th Photovoltaic Conference (PVSC)*, 2013.
- [199] D. C. Jordan and S. R. Kurtz, "Photovoltaic Degradation Rates an Analytical Review," *Progress in Photovoltaics: Research and Applications*, vol. 21, no. 1, pp. 12-29, 2011.
- [200] M. Santhakumari and N. Sagar, "A review of the environmental factors degrading the performance of silicon wafer-based photovoltaic modules: Failure detection methods and essential mitigation techniques," Renewable and Sustainable Energy Reviews, vol. 110, pp. 83-100, 2019.
- [201] I. Kaaya, M. Koehl, A. P. Mehilli, S. de Cardona Mariano and K. A. Weiss, "Modeling Outdoor Service Lifetime Prediction of PV Modules: Effects of Combined Climatic Stressors on PV Module Power Degradation," *IEEE Journal of Photovoltaics*, vol. 9, no. 4, pp. 1105-1112, 2019.
- [202] B. Kim and C. Kim, "Estimating the effect of module failures on the gross generation of a photovoltaic system using agend-based modeling," Renewable and Sustainable Energy Reviews, vol. 91, pp. 1019-1024, 2018.
- [203] M. Dida, S. Boughali, D. Bechki and H. Bouguettaia, "Output power loss of crystalline silicon photovoltaic modules due to dust accumulation in Saharan environment," *Renewable and Sustainable Energy Reviews*, vol. 124, p. 109787, 2020.
- [204] J. Das, A. P. Abraham, P. C. Ghosh and R. Banerjee, "Life cycle energy and carbon footprint analysis of photovoltaic battery microgrid system in India," *Clean Technologies and Environmental Policy*, vol. 20, pp. 65-80, 2018.
- [205] M. Raugei, E. Leccisi and V. M. Fthenakis, "What Are the Energy and Environmental Impacts of Adding Battery Storage to Photovoltaics? A Generalized Life Cycle Assessment," *Energy Technology*, vol. 8, no. 11, p. 1901146, 2020.
- [206] X. M. Chen, Y. Li, B. Y. Zhao and R. Z. Wang, "Are the optimum angles of photovoltaic systems so important?," *Renewable and Sustainable Energy Reviews*, vol. 124, p. 109791, 2020.
- [207] D. E. H. J. Gernaat, The role of renewable energy in long-term energy and climate scenarios, Utrecht: Utrecht University, 2019.
- [208] European Centre for Medium-range Weather Forecasts (ECMWF), "ERA5 Climate reanalysis," [Online]. Available: https://climate.copernicus.eu/climate-reanalysis. [Accessed 8 10 2019].
- [209] J. D. Hunter, "Matplotlib: A 2D Graphics Environment," Computing in Science & Engineering, vol. 9, no. 3, pp. 90-95, 2007.
- [210] IPCC, "Summary for Policymakers," in Climate Change 2023: Synthesis Report. Contribution of Working Groups I, II and III to the Sixth Assessment Report of the Intergovernmental Panel on Climate Change, Core Writing Team, H. Lee and J. Romero, Eds., Geneva, IPCC, 2023, pp. 1-34.
- [211] Our World in Data, "Share of electricity production from hydropower," 2024. [Online]. Available: https://ourworldindata.org/grapher/share-electricity-hydro?tab=table. [Accessed 22 March 2025].

- Ember, "Energy Institute Statistical Review of World Energy," Ember, 2024. [Online]. Available: https://ourowrldindata.org/renewable-energy#hydropower-in-the-energy-andelectric. [Accessed 6 12 2024].
- A. F. Hof, A. G. Dagnachew, P. L. Lucas and D. P. van Vuuren, "Insight into Energy Scenarios: [213] A comparison of key transition indicators of 2 C scenarios," PBL Publishers, The Hague, The Netherlands, 2019.
- U. A. C. o. Engineers, "National Inventory of Dams," 2020. [Online]. Available: https://nid. [214] usace.army.mil/#/. [Accessed 20 10 2022].
- [215] M. M. Johnson, S.-C. Kao, N. M. Samu and R. Uria-Martinez, "Existing Hydropower Assets (EHA), 2021," Oak Ridge National Laboratory, 2021. [Online]. Available: https://hydrosource. ornl.gov/dataset/EHA2021. [Accessed 22 10 2022].
- WRI, "global-power-plant-database," 11 June 2018. [Online]. Available: https://github.com/ [216] wri/global-power-plant-database. [Accessed 20 10 2022].
- [217] V. Barbarossa, M. A. Huijbregts, A. H. Beusen, H. E. Beck, H. King and A. M. Schipper, "FLO1K, global maps of mean, maximum and minimum annual streamflow at 1 km resolution from 1960 through 2015," Scientific Data, vol. 5, p. 180052, 2018.
- [218] A. B. Janssen, Personnal communication, 2022.
- [219] A. Kadiyala, R. Kommalapati and Z. Huque, "Evaluation of the Life Cycle Greenhouse Gas Emissions from Hydroelectricity Generation Systems," Sustainability, vol. 8, no. 6, p. 539, 2016.
- IPCC, "1st Corrigenda to the 2019 Refinement to the 2006 IPCC Guidelines for National [220] Greenhouse Gas Inventories," September 2021. [Online]. Available: https://www.ipcc-nggip. iges.or.jp/public/2019rf/corrigenda1.html. [Accessed 21 March 2025].
- C. E. Lovelock, C. Evans, N. Barros, Y. Prairie, J. Alm, D. Bastviken, J. J. Beaulieu, M. Garneau, A. [221] Harby, J. Harrison, D. Pare, H. L. Raadal, B. Sherman, C. Zhang and S. M. Ogle, "Wetlands," in 2019 Refinement to the 2006 IPCC Guidelines for National Greenhouse Gas Inventories, Geneva, Intergovernmental Panel on Climate Change, 2019, pp. 7.1-7.52.
- U. D. o. Energy, "Hydropower Setting a Course for Our Energy Future," U.S. Department of [222] Energy, Washington D.C., 2004.
- [223] M. L. Messager, B. Lehner, G. Grill, I. Nedeva and O. Schmitt, "Estimating the volume and age of water stored in global lakes using a geo-statistical approach," Nature Communications, vol. 7, p. 13603, 2016.
- R. McManamay, C. Oigbokie, S.-C. Kao and M. Bevelhimer, "Classification of US Hydropower Dams by their Modes of Operation," River Research and Applications, vol. 32, no. 7, pp. 1450-1468, 2016.
- B. R. Deemer, J. A. Harrison, S. Li, J. J. Beaulieu, T. DelSontro, N. Barros, J. F. Bezerra-Neto, S. M. Powers, M. A. Dos Santos and A. J. Vonk, "Greenhouse Gas Emissions from Reservoir Water Surfaces: A New Global Synthesis," BioScience, vol. 66, no. 11, pp. 949-964, 2016.
- G. Myhre, D. Shindell, F.-M. Breon, W. Collins, J. Fuglestvedt, J. Huang, D. Koch, J.-F. Lamarque, D. Lee, B. Mendoza, T. Nakajima, A. Robock, G. Stephens, T. Takemura and H. Zhang, "Anthropogenic and Natural Radiative Forcing," in Climate Change 2013: The Physical Science Basis. Contribution of Working Group I to the Fifth Assessment Report of the Intergovernmental Panel on Climate Change, Geneva, IPCC, 2014, pp. 659-740.
- [227] Oak Ridge National Laboratory, "Hydrosource," [Online]. Available: https://hydrosource.ornl. gov/. [Accessed 9 3 2025].

- [228] D. E. Gernaat, P. W. Bogaart, D. P. van Vuuren, H. Biemans and R. Niessink, "High-resolution assessment of global technical and economic hydropower potential," *Nature Energy*, vol. 2, pp. 821-828, 2017.
- [229] M. Kummu, M. Taka and J. H. Guillaume, Data from: Gridded global datasets for Gross Domestic Product and Human Development Index over 1990-2015, 2020.
- [230] V. Calcagno, glmulti: Model Selection and Multimodel Inference Made Easy, 2020.
- [231] L. E. Raffalovich, G. D. Deane, D. Armstrong and H.-S. Tsao, "Model selection procedures in social research: Monte-Carlo simulation results," *Journal of Applied Statistics*, vol. 35, no. 10, pp. 1093-1114, 2008.
- [232] M. Li and N. He, "Carbon intensity of global existing and future hydropower reservoirs," Renewable and Sustainable Energy Reviews, vol. 162, p. 112433, 2022.
- [233] S. Lu, W. Dai, Y. Tang and M. Guo, "A review of the impact of hydropower reservoirs on global climate change," *Science of the Total Environment*, vol. 711, p. 134996, 2020.
- [234] Y. T. Prairie, J. Alm, J. Baeulieu, N. Barros, T. Battin, J. Cole, P. del Giorgio, T. DelSontro, F. Guérin, A. Harby, J. Harrison, S. Mercier-Blais, D. Serca, S. Sobek and D. Vachon, "Greenhouse Gas Emissions from Freshwater Reservoirs: What Does the Atmosphere See?," *Ecosystems*, vol. 21, pp. 1058-1071, 2018.
- [235] C. Hansen, R. Pilla, B. Skinner, N. Griffiths and H. Jager, "Variability in modelled reservoir greenhouse gas emissions: comparison of selected US hydropower reservoirs against global estimates," Environmental Research Communications, vol. 4, no. 12, p. 121008, 2022.
- [236] M. Tigli, M. P. Bak, J. H. Janse, M. Strokal and A. B. Janssen, "The future of algal blooms in lakes globally is in our hands," *Water Research*, vol. 268, p. 122533, 2025.
- [237] M. Meerhoff, J. Audet, T. A. Davidson, L. De Meester, S. Hilt, S. Kosten, Z. Liu, N. Mazzeo, H. Paerl, M. Scheffer and E. Jeppesen, "Feedback between climate change and eutrophication: revisiting the allied attack concept and how to strike back," *Inland Waters*, vol. 12, pp. 187-204, 2022.
- [238] R. C. Aben, E. S. Oliveira Junior, A. R. Carlos, T. J. van Bergen, L. P. Lamers and S. Kosten, "Impact of plant species and intense nutrient loading on CH4 and N2O fluxes from small inland waters: An experimental approach," *Aquatic Botany*, vol. 180, p. 103527, 2022.
- [239] C. Soued, J. A. Harrison, S. Mercier-Blais and Y. T. Prairie, "Reservoir CO2 and CH4 emissions and their climate impact over the period 1900-2060," *Nature Geoscience*, vol. 15, pp. 700-705, 2022.
- [240] L. Baratgin, J. Polcher, P. Dumas and P. Quirion, "Modeling hydropower operations at the scape of a power grid: a demand-based approach," *Hydrology and Earth System Sciences*, vol. 28, no. 24, pp. 5479-5509, 2024.
- [241] O. J. Mdee, C. Z. Kimambo, T. K. Nielsen and J. Kihedu, "Measurement methods for hydropower resources: a review," Water Utiliuty Journal, vol. 18, pp. 21-38, 2018.
- [242] U.S. Energy Information Administration, "What is U.S. electricity generation by energy source?," U.S. Energy Information Administration, [Online]. Available: https://www.eia.gov/tools/faqs/faq.php?id=427&t=3. [Accessed 14 February 2025].
- [243] S. W. Turner, N. Voisin and K. Nelson, "Revised monthly energy generation estimates for 1,500 hydroelectric power plants in the United States," *Scientific Data*, vol. 9, p. 675, 2022.
- [244] R. M. Almeida, A.-U.-H. Chowdhury, H. Rodrigo, M. Li and R. J. Schmitt, "Offsetting the greenhouse gas footprint of hydropower with floating solar photovotaics," *Nature Sustainability*, vol. 7, pp. 1102-1106, 2024.

- Z. J. Steinmann, A. Venkatesh, M. Hauck, A. M. Schipper, R. Karuppiah, I. J. Laurenzi and M. A. Huijbregts, "How To Address Data Gaps in Life Cycle Inventories: A Case Study on Estimating CO2 Emissions from Coal-Fired Electricity Plants on a Global Scale," Environmental Science & Technology, vol. 48, no. 9, pp. 5282-5289, 2014.
- M. Hauck, Z. Steinmann, I. Laurenzi, R. Karuppiah and H. M.A.J, "How to quantify uncertainty [246] and variability in life cycle assessment: the case of greenhouse gas emissions of gas power generation in the US," Environmental Research Letters, vol. 9, p. 074005, 2014.
- [247] D. Le Boulch, M. Buronfosse, Y. Le Guern, P.-A. Duvernois and N. Payen, "Meta-analysis of the greenhouse gases emissions of nuclear electricity generation: learnings from process-based LCA," International Journal of Life Cycle Assessment, vol. 29, pp. 857-872, 2024.
- Y. Wang and T. Sun, "Life cycle assessment of CO2 emissions from wind power plants: [248] Methodology and case studies," Renewable Energy, vol. 43, pp. 30-36, 2012.
- [249] Y. Feng and L. Zhang, "The GHG Intensities of Wind Power Plants in China from a Life-Cycle Perspective: The Impacts of Geographical Location, Turbine Technology and Management Level," Sustainability, vol. 15, no. 5, p. 4449, 2023.
- [250] G. Elene, "Assessment of Greenhouse Gas Emissions from Hydropower Projects Using G-RES Tool," NTNU, Trondheim, 2023.
- L. C. Dammeier, J. H. Bosmans and M. A. Huijbregts, "Variability in greenhouse gas footprints of the global wind farm fleet," Journal of Industrial Ecology, vol. 27, no. 1, pp. 272-282, 2022.
- [252] T. DelSontro, J. J. Beaulieu and J. A. Downing, "Greenhouse gas emissions from lakes and impoundments: Upscaling in the face of global change," Limnology and Oceanography Letters, vol. 3, pp. 64-75, 2018.
- [253] D. Zhao, J. Huang, Z. Li, G. Yu and H. Shen, "Dynamic monitoring and analysis of chlorophyll-a concentrations in global lakes using Sentinel-2 images in Google Earth Engine," Science of The Total Environment, vol. 912, p. 169152, 2024.
- D. Polverini, N. Espinosa, U. Eynard, E. Leccisi, F. Ardente and F. Mathieux, "Assessing the carbon footprint of photovoltaic modules through the EU Ecodesign Directive," Solar Energy, vol. 257, pp. 1-9, 2023.
- [255] C. Jung, D. Taubert and D. Schindler, "The temporal variability of global wind energy Longterm trends and inter-annual variability," Energy Conversion and Management, vol. 188, pp. 462-472, 2019.
- [256] J. Li, S. Li and F. Wu, "Research on carbon emission reduction benefit of wind power project based on life cycle assessment theory," Renewable Energy, vol. 155, pp. 456-468, 2020.
- J.-b. Xie, J.-x. Fu, S.-y. Liu and W.-s. Hwang, "Assessments of carbon footprint and energy analysis of three wind farms," Journal of Cleaner Production, vol. 254, p. 120159, 2020.
- J. Chipindula, V. S. V. Botlaguduru, H. Du, R. R. Kommalapati and Z. Huque, "Life Cycle [258] Environmental Impact of Onshore and Offshore Wind Farms in Texas," Sustainability, vol. 10, no. 6, p. 2022, 2018.
- L. Schleisner, "Life cycle assessment of a wind farm and related externalities," Renewable Energy, vol. 20, no. 3, pp. 279-288, 2020.
- [260] K. Abeliotis and D. Pactiti, "Assessment of the Environmental Impacts of a Wind," International Journal of Renewable Energy Research, vol. 4, no. 3, pp. 580-585, 2014.
- [261] H.-J. Wagner, C. Baack, T. Eickelkamp, A. Epe, J. Lohmann and S. Troy, "Life cycle assessment of the offshore wind farm alpha ventus," Energy, vol. 36, no. 5, pp. 2459-2464, 2011.

- [262] A. Arvesen, C. Birkeland and E. G. Hertwich, "The Importance of Ships and Spare Parts in LCAs of Offshore Wind Power," *Environmental Science & Technology*, vol. 47, no. 6, pp. 2948-2956, 2013.
- [263] M. R. Gomaa, H. Rezk, R. J. Mustafa and M. Al-Dhaifallah, "Evaluating the Environmental Impacts and Energy Performance of a Wind Farm System Utilizing the Life-Cycle Assessment Method: A Practical Case Study," *Energies*, vol. 12, no. 17, p. 3263, 2019.
- [264] K. B. Oebels and S. Pacca, "Life cycle assessment of an onshore wind farm located at the northeastern coast of Brazil," *Renewable Energy*, vol. 53, pp. 60-70, 2013.
- [265] N. Demir and A. Taşkın, "Life cycle assessment of wind turbines in Pınarbaşı-Kayseri," *Journal of Cleaner Production*, vol. 54, pp. 253-263, 2013.
- [266] H. Hondo, "Life cycle GHG emission analysis of power generation systems: Japanese case," *Energy*, vol. 30, no. 11-12, pp. 2042-2056, 2005.
- [267] S. H. Al-Behadili and W. B. El-Osta, "Life Cycle Assessment of Dernah (Libya) wind farm," Renewable Energy, vol. 83, pp. 1227-1233, 2015.
- [268] L. Wang, Y. Wang, H. Du, J. Zuo, R. Y. M. Li, Z. Zhou, F. Bu and M. P. Garvlehn, "A comparative life-cycle assessment of hydro-, nuclear and wind power: A China study," *Applied Energy*, vol. 249, pp. 37-45, 2019.
- [269] J. Yang, Y. Chang, L. Zhang, Y. Hao, Q. Yan and C. Wang, "The life-cycle energy and environmental emissions of a typical offshore wind farm in China," *Journal of Cleaner Production*, vol. 180, pp. 316-324, 2018.
- [270] L. Xu, M. Pang, L. Zhang, W.-R. Poganietz and S. D. Marathe, "Life cycle assessment of onshore wind power systems in China," Resources, Conservation and Recycling, vol. 132, pp. 361-368, 2018.
- [271] A. Kadiyala, R. Kommalapati and Z. Huque, "Characterization of the life cycle greenhouse gas emissions from wind electricity generation systems," *International Journal of Energy and Environmental Engineering*, vol. 8, pp. 55-64, 2017.
- [272] F. Ardente, M. Beccali, M. Cellura and V. L. Brano, "Energy performances and life cycle assessment of an Italian wind farm," *Renewable and Sustainable Energy Reviews*, vol. 12, no. 1, pp. 200-217, 2008.
- [273] J. Yang and B. Chen, "Integrated evaluation of embodied energy, greenhouse gas emission and economic performance of a typical wind farm in China," Renewable and Sustainable Energy Reviews, vol. 27, pp. 559-568, 2013.
- [274] M. Pehnt, M. Oeser and D. J. Swider, "Consequential environmental system analysis of expected offshore wind electricity production in Germany," *Energy*, vol. 33, no. 5, pp. 747-759, 2008.
- [275] B. Tremeac and F. Meunier, "Life cycle analysis of 4.5 MW and 250 W wind turbines," Renewable and Sustainable Energy Reviews, vol. 13, no. 8, pp. 2104-2110, 2009.
- [276] Vestas Wind Systems A/S, "Life cycle assessment of offshore and onshore sited wind power plants based on Vestas V90-3.0MW turbines," Radners, DK, 2006.
- [277] J. Weinzettel, M. Reenaas, C. Solli and E. G. Hertwich, "Life cycle assessment of a floating offshore wind turbine," *Renewable Energy*, vol. 34, no. 3, pp. 742-747, 2009.
- [278] P. Garrett and K. Rønde, "Life cycle assessment of wind power: comprehensive results from a state-of-the-art approach," *The International Journal of Life Cycle Assessment*, vol. 18, pp. 37-48, 2013.
- [279] S. Dolan, "Life Cycle Assessment and Emergy Synthesis of Theoretical Offshore Wind Farm for Jacksonville, Florida," 2007.

- [280] B. Reimers, B. Özdirik and M. Kaltschmitt, "Greenhouse gas emissions from electricity generated by offshore wind farms," Renwable Energy, vol. 72, pp. 428-438, 2014.
- Y.-M. Lee and Y.-E. Tzeng, "Development and Life-Cycle Inventory Analysis of Wind Energy in [281] Taiwan," Journal of Energy Engineering, vol. 134, no. 2, pp. 53-57, 2008.
- [282] H. L. Raadal, B. I. Vold, A. Myhr and T. A. Nygaard, "GHG emissions and energy performance of offshore wind power," Renewable Energy, vol. 66, pp. 314-324, 2014.
- [283] M. Ozoemena, W. M. Cheung and R. Hasan, "Comparative LCA of technology improvement opportunities for a 1.5-MW wind turbine in the context of an onshore wind farm," Clean Technologies and Environmental Policy, vol. 20, pp. 173-190, 2018.
- Vestas Wind Systems A/S, "Life Cycle Assessment of electricity production from and Onshore [284] V112-3.45 MW Wind Plant," Randers, DK, 2017.
- Vestas Wind Systems A/S, "Life Cycle Assessment of Electricity Production from an Onshore V112-3.3 MW Wind Plant," Randers, DK, 2015.
- B. Burger and C. Bauer, "Windkraft," in Sachbilanzen von Energiesystemen: Grundlagen für den ökologischen Vergleich von Energiesystemen und den Einbezug von Energiesystemen in Ökobilanzen für die Schweiz. Final report, R. Dones, Ed., Dübendorf, CH, 2007.
- A. Schreiber, J. Marx and P. Zapp, "Comparative life cycle assessment of electricity generation by different wind turbine types," Journal of Cleaner Production, vol. 233, pp. 561-572, 2019.
- [288] R. H. Crawford, "Life cycle energy and greenhouse emissions analysis of wind turbines and the effect of size on energy yield," Renewable and Sustainable Energy Reviews, vol. 13, no. 9, pp. 2653-2660, 2009.
- M. Z. Jacobson, "Review of solutions to global warming, air pollution, and energy security," [289] Energy and Environmental Science, no. 2, pp. 149-173, 2009.
- [290] N. Jungbluth, C. Bauer, R. Dones and R. Frischknecht, "Life Cycle Assessment for Emerging Technologies: Case Studies for Photovoltaic and Wind Power (11 pp)," The International Journal of Life Cycle Assessment, vol. 10, pp. 24-34, 2005.
- [291] M. Lenzen and U. Wachsmann, "Wind turbines in Brazil and Germany: an example of geographical variability in life-cycle assessment," Applied Energy, vol. 77, no. 2, pp. 119-130, 2004.
- E. J. Libermann, "A Life Cycle Assessment and Economic Analysis of Wind Turbines Using [292] Monte Carlo Simulation," 2003.
- [293] E. Martínez, F. Sanz, S. Pellegrini, E. Jiménez and J. Blanco, "Life-cycle assessment of a 2-MW rated power wind turbine: CML method," The International Journal of Life Cycle Assessment, vol. 14, pp. 52-63, 2009.
- M. McCulloch, M. Raynolds and M. Laurie, "Life-Cycle Value Assessment of a Wind Turbine," [294] Drayton Valley, AB, CA, 2000.
- [295] S. Pacca and A. Horvath, "Greenhouse Gas Emissions from Building and Operating Electric Power Plants in the Upper Colorado River Basin," Environmental Science & Technology, vol. 36, no. 14, pp. 3194-3200, 2002.
- M. Pehnt, "Dynamic life cycle assessment (LCA) of renewable energy technologies," [296] Renewable Energy, vol. 31, no. 1, pp. 55-71, 2006.
- [297] B. M. Rule, Z. J. Worth and C. A. Boyle, "Comparison of Life Cycle Carbon Dioxide Emissions and Embodied Energy in Four Renewable Electricity Generation Technologies in New Zealand," Environmental Science & Technology, vol. 43, no. 16, pp. 6406-6413, 2009.
- C. J. Rydh, M. Jonsson and P. Lindahl, "Replacement of Old Wind Turbines Assessed from [298] Energy, Environmental and Economic Perspectives," 2004.

- [299] Y. Uchiyama, "Life Cycle Analysis of Photovoltaic Cell and Wind Power Plants," Tokyo, JP, 1996.
- [300] K. R. Voorspools, E. A. Brouwers and W. D. D'haeseleer, "Energy content and indirect greenhouse gas emissions embedded in 'emission-free' power plants: results for the Low Countries," *Applied Energy*, vol. 67, no. 3, pp. 307-330, 2000.
- [301] S. W. White and G. L. Kulcinski, "Birth to death analysis of the energy payback ratio and CO2 gas emission rates from coal, fission, wind, and DT-fusion electrical power plants," Fusion Engineering and Design, vol. 48, no. 3-4, pp. 473-481, 2000.
- [302] M. A. Huijbregts, Z. J. Steinmann, P. M. Elshout, G. Stam, F. Verones, M. Vieira, M. Zijp, A. Hollander and R. van Zelm, "ReCiPe 2016: A harmonized life cycle impact assessment method at midpoint and endpoint level Report I: Characerization," RIVM, Bilthoven, The Netherlands, 2016.
- [303] J. A. Crook, L. A. Jones, P. M. Forster and R. Crook, "Climate change impacts on future photovoltaic and concentrated solar power energy output," *Energy & Environmental Science*, vol. 4, pp. 3101-3109, 2011.
- [304] R. Chenni, M. Makhlouf, T. Kerbache and A. Bouzid, "A detailed modeling method for photovoltaic cells," *Energy*, vol. 32, no. 9, pp. 1724-1730, 2007.
- [305] G. TamizhMani, L. Ji, Y. Tang, L. Petacci and C. Osterwald, "Photovoltaic Module Thermal/ Wind Performance: Long-Term Monitoring and Model Development For Energy Rating," in NCPV and Solar Program Review Meeting Proceedings, Denver, Colorado, 2003.
- [306] R. Urraca, T. Huld, A. Gracia-Amillo, F. J. Martinez-de-Pison, F. Kaspar and A. Sanz-Garcia, "Evaluation of global horizontal irradiance estimates from ERA5 and COSMO-REA6 reanalysis using ground and satellite-based data," *Solar Energy*, vol. 164, pp. 339-354, 2018.
- [307] A. F. Zuur, E. N. Ieno, N. Walker, A. A. Saveliev and G. M. Smith, Mixed Effects Models and Extensions in Ecology with R, New York, NY: Springer, 2009.
- [308] L. Stoop, *Blackouts are not an option*, Utrecht: Utrecht University, 2018.
- [309] D. Yang, J. Liu, J. Yang and N. Ding, "Life-cycle assessment of China's multi-crystalline silicon photovoltaic modules considering international trade," *Journal of Cleaner Production*, vol. 94, pp. 35-45, 2015.
- [310] IHA, "Facts about hydropower," International Hydropower Association, 2022. [Online]. Available: https://www.hydrpower.org/iha/discover-facts-about-hydropwer. [Accessed 2 10 2022].
- [311] EIA, "Hydropower explained," 13 3 2022. [Online]. Available: https://www.eia.gov/energyexplained/hydropower. [Accessed 2 10 2022].
- [312] U. E. I. Administration, "Electricity Data Browser," EIA, [Online]. Available: https://www.eia.gov/electricity/data/browser/. [Accessed 20 10 2022].
- [313] E. C. J. R. Centre, "Soil Projects Support to Renewable Energy Directive," European Commission, 10 June 2010. [Online]. Available: https://esdac.jrc.ec.europa.eu/projects/ RenewableEnergy/. [Accessed 2010 2022].



Appendices

Appendix A Appendix for chapter 3 Appendix B Appendix for chapter 4 Appendix C Appendix for chapter 5

Appendix A Appendix for chapter 3

This appendix provides more information on how gap-filling was done for the different variables (section A.1), an overview of the completeness of the data set with regard to total installed capacity and a validation of the electricity production (section A.2), how the wind data was processed (section A.3), as well as what wake effect is and how it was accounted for (section A.4). Additional information on how the metamodel was developed is presented in section A.5, and section A.6 provides more detailed maps of the GHG footprint for different world regions. Section A.7 covers the capacity factor of the global wind farm fleet. Section A.8 covers which data was included in the literature comparison and section A.9 describes the applicability domain of the GHG emission regression model.

A.1 Gap filling of wind farm data

Whenever the data needed in the calculations was not available, the data gaps were filled according to the methods described in this section. Some information could be derived directly from other data from the database, other information had to be derived using regression analysis. Data on the global wind farm fleet has been provided by TheWindpower.net [106]. For 132 offshore wind farms, information on location was supplemented with updated information from [106] and [156]. For 26,821 of the 31,298 wind farms in the original data set, sufficient data was available to include the wind farm in the calculations. Summary Table A-1 shows which information was available for how many wind farms. How many of the missing values were added using which gap filling method is also included in Table A-1.

A.1.1 Hub height

For 4,572 wind farms where no information on hub height was available, a regression model was built to estimate turbine height (m) based on either the diameter (m) (321 farms):

$$H = 1.3 \cdot D^{0.9} \tag{A-1}$$

with an R² of 0.76 and a standard error of 0.22, or the rated power (MW) (4,380 farms):

$$H = 3.1 \cdot P_{rated}^{0.44} \tag{A-2}$$

with an R² of 0.74 and a standard error of 7.90.

A.1.2 Rotor diameter

The rotor diameter (m) was derived from a regression model based on the rated power (MW) (5,243 turbines):

$$D = 1.557 \cdot P_{rated}^{0.526} \tag{A-3}$$

which has an R² of 0.94 and a standard error of 6.78.

A.1.3 Rated power

The rated power (MW) can be calculated from the total power (MW) of all wind turbines in a wind farm and the number of turbines in that farm for 5,243 turbines without this information:

 $P_{rated} = \frac{P_{total}}{N_{rurbines}} \tag{A-4}$

A.1.4 Number of turbines

Similar to the rated power, the number of wind turbines can be calculated by dividing the total power (MW) of all wind turbines in a wind farm by the rated power (MW) of the individual wind turbines in it, which was done for one entry:

$$N_{turblnes} = \frac{P_{total}}{P_{rated}}$$
 (A-5)

A.1.5 Power curve: k and b

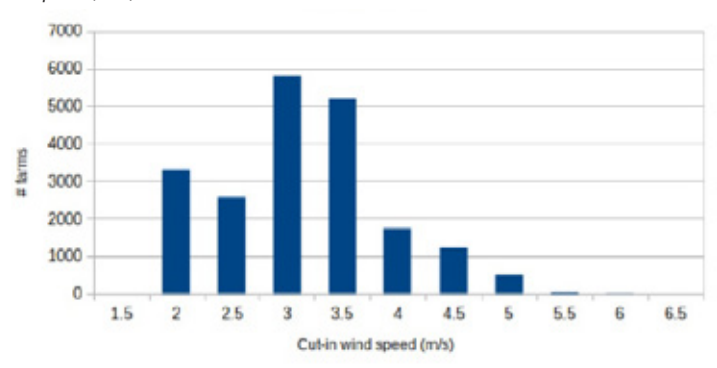
For 19,091 wind turbines information on the power curve was available. Thewindpower.net provides power outputs in 0.5 m/s intervals as given by the turbines' manufacturers. Wind turbines'power curves follow a so-called sigmoid function [158] and such a function was fit to the data provided by Thewindpower. net using SciPy's curve fit method with the sigmoid function [159].

This results in two variables, k and b, which describe the power curve of each given wind turbine. The average R² of the fitted curves is 0.996. For the wind turbines where data is not available (7,771 turbines), the average k and b of all wind turbines in the database are used (0.74 [the 2.5 and 97.5 percentiles are 0.58-0.94] and 8.57 [the 2.5 and 97.5 percentiles are 7.20-9.64], respectively).

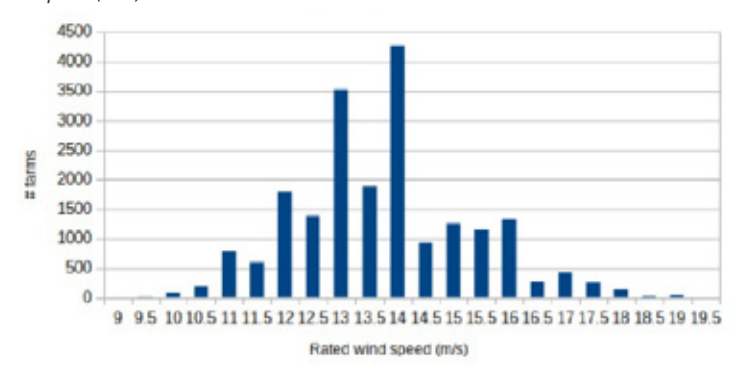
A.1.6 Cut-in, rated and cut-off wind speeds

Based on the histograms in Figure A-1, 3 m/s was used as the cut-in wind speed if it was unknown, 14 m/s was used in case the rated wind speed was not known and when the cut-off wind speed was missing, 25 m/s was used.

a) Cut-in wind speed (m/s)



b) Rated wind speed (m/s)



c) Cut-off wind speed (m/s)

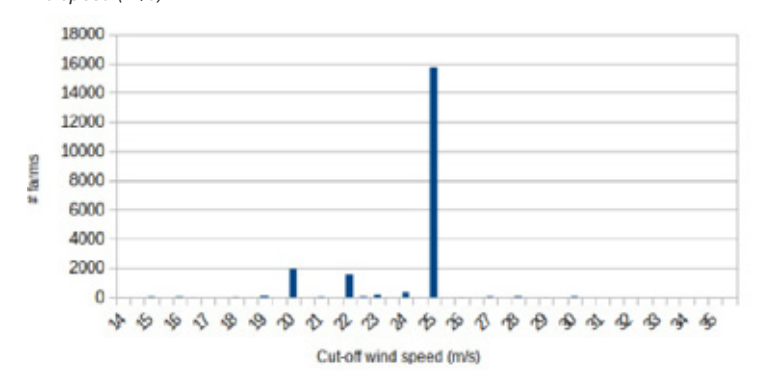


Figure A-1 Histogram of the distribution of cut-in (a), rated (b) and cut-off (c) wind speeds for all turbines in the database.

Onshore/offshore location

Upon loading the wind farms labelled as 'offshore' in qgis, some of them were seen to be located onshore. A global raster map distinguishing land and water was combined with all wind farms in the data set and all of them were reallocated to be either on- or offshore using qgis's point sampling tool. In total, 2,159 wind farms had to be relocated in this manner.

Summary table

Table A-1 gives an overview of how many wind farms in the data set used here had not all information available. Additionally, the number of data gaps filled by the different methods is provided.

Table A-1 Number of gaps filled by which method. Methods correspond to section numbers above.

Variable	Number of farms without this information	Number of farms information derived for (via equation/method)
Hub height	4,601	321 (eq. (A-1))/4,380 (eq. (A-2))
Rotor diameter	5,243	5,132 (eq. (A-3))
Rated power	5,243	5,132 (eq. (A-4))
Number of turbines	1	1 (eq. (A-5))
Total power	0	n.a.
Power curve		
• k	7,771	7,646 (m. A.1.5)
• b	7,771	7,646 (m. A.1.5)
Cut-in wind speed	5,643	5,532 (m. A.1.6)
Rated wind speed	5,769	5,658 (m. A.1.6)
Cut-off wind speed	5,653	5,524 (m. A.1.6)
On-/Offshore	n.a.	2,159 (m. A.1.7)

A.2 Completeness of turbine database and validation of the electricity production

We computed electricity production for all wind farms due to the lack of data on location-specific electricity production over its lifetime (30 years). For two countries, Denmark and the US, the electricity produced has been validated on a per-wind farm basis using data sets from the Danish Energy Agency [164] and the EIA [163]. The wind farms in our database were matched to the EIA database based on name, state and commissioning year. Matching with the Danish database was done based on name, commissioning year, manufacturer, hub height, rotor diameter, nameplate capacity and the number of turbines in a farm. While matching the Danish wind turbines to wind farms in our data set could be done with a high degree of certainty due to the availability of both technological and spatial information, matching was done purely on a limited number of spatial information for the US.

Since we calculated electricity production for whole years and the exact commissioning date was not known, the first year of production was excluded from the analysis. All wind farms that did not have continuous production records were also excluded. In total, 1,724 Danish wind farms were successfully matched to a farm in our data set and 657 US wind farms were matched.

Table A-2 gives an overview of the installed capacity per country. Data was available from Our World in Data [151] and IRENA [157].

Table A-2 Comparison of installed	capacity in our	study to dat	a from Our	world in data	[151] and
IRENA [157].					

Country	Installed capacity oud database (GW)	Installed capacity Our world in data (GW, 2020)	Installed capacity IRENA (GW, 2020)
Albania	0.15		
Algeria	0.01		0.01
Argentina	3.29	2.62	2.62
Armenia	0.004		0.002
Australia	10.33	9.46	8.60
Austria	2.86	3.22	3.22
Azerbaijan	0.01		0.07
Bahrain	0.001		0.0007
Bangladesh	0.0009		0.003
Belarus	0.003		0.11
Belgium	4.26	4.69	4.69
Bhutan	0.0006		0.0006

Table A-2 Continued

Country	Installed capacity oud database (GW)	Installed capacity Our world in data (GW, 2020)	Installed capacity IRENA (GW, 2020)
Bolivia	0.03		0.03
Bosnia & Herzegovina	0.13		0.09
Brazil	14.10	17.20	17.20
Bulgaria	0.52	0.70	0.70
Cambodia	0.0003		0.0003
Canada	12.62	13.58	13.58
Cape Verde	0.02		0.03
Chile	2.43	2.15	2.15
China	88.53	281.99	281.99
Colombia	0.02		0.51
Costa Rica	0.37	0.39	0.39
Croatia	0.87		0.79
Cuba	0.11		0.01
Curacao	0.03		0.05
Cyprus	0.19		0.16
Czech Republic	0.33		0.34
Denmark	6.92	6.24	6.24
Dominica	0.0002		0.0002
Dominican Republic	0.37		0.37
Ecuador	0.07		0.02
Egypt	1.30	1.38	1.38
El Salvador	0.05		
Eritrea	0.0008		0.0008
Estonia	2.71		0.32
Ethiopia	0.32		0.32
Faroe Islands	0.02		0.02
Fiji	0.01		0.01
Finland	4.09	2.47	2.47
France	19.91	17.38	17.38
Gambia	0.0002		0.001
Georgia	0.02		0.02
Germany	65.15	62.18	62.18
Greece	2.39	4.11	4.11
Guam	0.0003		0.0003
Guatemala	0.11		0.11
Honduras	0.18		0.24

Table A-2 Continued

Country	Installed capacity oud database (GW)	Installed capacity Our world in data (GW, 2020)	Installed capacity IRENA (GW, 2020)
Hungary	0.38		0.32
Iceland	0.004		0.002
India	16.41	38.56	38.56
Indonesia	0.15		0.15
Iran	0.28	0.30	0.31
Ireland	6.19	4.30	4.30
Israel	0.03		0.03
Italy	10.59	10.84	10.84
Jamaica	0.10		0.10
Japan	5.09	4.21	4.38
Jordan	0.47	0.52	0.51
Kazakhstan	0.45		0.49
Kenya	0.44		0.34
Kosovo	0.03		0.03
Kuwait	0.01		0.01
Latvia	0.05		0.08
Lithuania	0.72		0.54
Luxembourg	0.006		0.17
Mauritania	0.14		0.03
Mauritius	0.01		0.01
Mexico	5.09	8.13	8.13
Micronesia	0.0008		0.0008
Mongolia	0.05		0.16
Montenegro	0.12		0.12
Morocco	1.29	1.41	1.41
Mozambique	0.003		
Namibia	0.005		0.005
Netherlands	8.65	6.60	6.60
New Zealand	0.94	0.78	0.78
Nicaragua	0.14		0.19
Nigeria	0.01		0.003
North Macedonia	0.04		0.04
Norway	2.99	3.98	3.98
Oman	0.05		0.05
Pakistan	0.51	1.24	1.24
Panama	0.34		0.27

Table A-2 Continued

Country	Installed capacity oud database (GW)	Installed capacity Our world in data (GW, 2020)	Installed capacity IRENA (GW, 2020)
Peru	0.41		0.38
Philippines	0.46	0.44	0.44
Poland	9.49	6.27	6.27
Portugal	5.62	5.24	5.24
Puerto Rico	0.13		0.10
Romania	2.00	3.02	3.02
Russia	1.05	0.95	0.95
St. Kitts & Nevis	0.002		0.002
Saudi Arabia	0.42		0.003
Senegal	0.16		0.05
Serbia	0.60		0.40
Seychelles	0.006		0.006
Singapore	0.0001		0.0001
Slovakia	0.005		0.004
Slovenia	0.003		0.005
South Africa	3.04	2.64	2.64
South Korea	1.96	1.64	1.64
Spain	23.25	27.09	27.09
Sri Lanka	0.13		0.25
Sweden	12.65	9.69	9.69
Switzerland	0.17		0.09
Syria	0.003		0.0006
Taiwan	3.92	0.84	
Thailand	0.55	1.51	1.51
Tunisia	0.24	0.24	0.24
Turkey	5.96	8.83	8.83
Ukraine	1.15	1.40	1.40
United Arab Emirates	0.009		
United Kingdom	38.10	24.66	24.48
United States	102.44	117.74	117.74
Uruguay	1.35	1.51	1.51
Uzbekistan	0.0008		0.0008
Vanuatu	0.004		0.003
Venezuela	0.13		0.07
Vietnam	0.71		0.60

A.3 ERA 5

ERA5 climate data has been downloaded from the Copernicus Climate Data Store. Hourly data was used on a 0.25°x 0.25° resolution starting from 1988 until 2017. Wind data is available at 10 and 100 m height and in a u- and v-component (eastward and northward, respectively), both in m/s. To get the wind speed at hub height, two steps are necessary:

- 1. Combine u- and v-component to get one wind speed at 10 and 100 m for each grid cell and time step.
- 2. Extrapolate the wind speed at 10 m to the wind turbines' hub height.

A.3.1 Wind speed calculation

Calculating the wind speed (v, in m/s) at 10 and 100 m is done using

$$v = \sqrt{u^2 + v^2}$$
 (A-6)

A.3.2 Wind speed extrapolation

Extrapolating the 10 m wind speed to the turbines' hub height is more complex. Here, we assume that wind speed can be extrapolated using the power law

$$v_H = v_{10} \cdot \left(\frac{H}{10}\right)^{\alpha} \tag{A-7}$$

with v_H the wind speed at hub height (m/s), v_{10} the wind speed at 10 m (m/s), H the hub height (m) and α the wind shear exponent. α can be calculated for each grid point and each time step via

$$\alpha = log_{10} \left(\frac{v_{100}}{v_{10}} \right) \tag{A-8}$$

Additionally, wind speed also depends on air density (kg/m³) [255]. Air density at hub height is calculated according to

$$\rho_H = \frac{p_H}{R \cdot T_H} \tag{A-9}$$

with ρ_H the air pressure at hub height (Pa), T_H the temperature at hub height (K) and R the ideal gas constant of 8.31447 J/mol·K. Both ρ_H and T_H also vary with height and are usually measured above the ground. Therefore, they need to be extrapolated as well following the method described in [255]. Measured air pressure p_a is extrapolated to the hub height using

$$p_{H} = p_{a} \cdot \left(1 - \frac{0.0065 \cdot \Delta h}{T_{a}}\right)^{5.225} \tag{A-10}$$

with p_a the air pressure at mean sea level, Δh the height difference between the measurement height and the hub height (m) and T_a the temperature at 2 m (K). T_a is extrapolated to the temperature at hub height using

$$T_H = T_a - 0.0065 \cdot \Delta h$$
 (A-11)

Temperature and pressure are also available from the Copernicus Climate Data Store, given in K and Pa, respectively.

A.4 Wake effect

Wind turbines extract energy from the wind meaning that downwind of a wind turbine, the wind blows less hard than upwind. Hence, turbines that are located downwind of another wind turbine experience slower wind speeds, an effect that is especially pronounced in wind farms. This effect is called the wake effect. Quantifying the wake effect for wind turbines in wind farms is difficult as it depends on the exact lay-out of the farm, meaning for example the turbine spacing and general form of the farm, but also on local wind speed characteristics such as wind speed and direction. If wind turbines are, for example, placed in two rows of eight turbines each, with the rows in a north-south orientation, only one turbine is downwind of another turbine if the wind blows from the east or west. If, however, the wind comes from the north or south, 7 turbines are downwind of at least one other turbine and thus experience some form of wake effect.

When designing a wind farm, extensive research is done on the predominant wind direction and what the effects of different farm lay-outs and turbine spacing are on the power output. However, information on the farms' lay-outs and turbine spacing were not provided in the database. Therefore, a standard square wind farm lay-out was deployed here, following [136], who calculated wake effects for different wind farm sizes under various turbine spacing. Considering a square wind farm lay-out has the advantage that wind direction does not have a big influence on the results. Based on the table provided in [136], the following wake effect regression was derived, taking 9D as the distance between turbines:

$$f_w = -0.03532 \cdot ln(N_{turbines})$$
 (A-12)

A.5 Metamodel

In a first step to develop the metamodel, variation inflation factors (vifs) were calculated. If a vif is above 5, the multicolinearity is considered to be too high. For this reason, rotor diameter was excluded from the list of variables. Furthermore, in order to see if variables are correlated, a correlation matrix was made. If values are higher than 0.8, the variables are thought to be dependent and excluded. The correlation matrix of the variables included is shown in Figure A-2. It shows that all values are below 0.8 and therefore all variables are included.

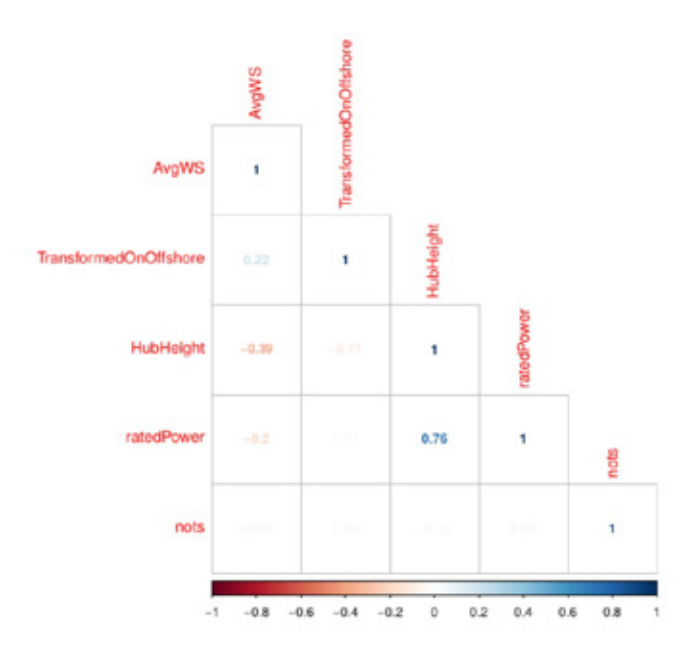


Figure A-2 Correlation matrix of the predictors included in the metamodel. All values are below 0.8.

Figure A-3 shows the residuals vs. fitted plot of the best model (based on the Akaike Information Criterion). The residual standard error for this model was 0.10 with an adjusted R² of 0.83.

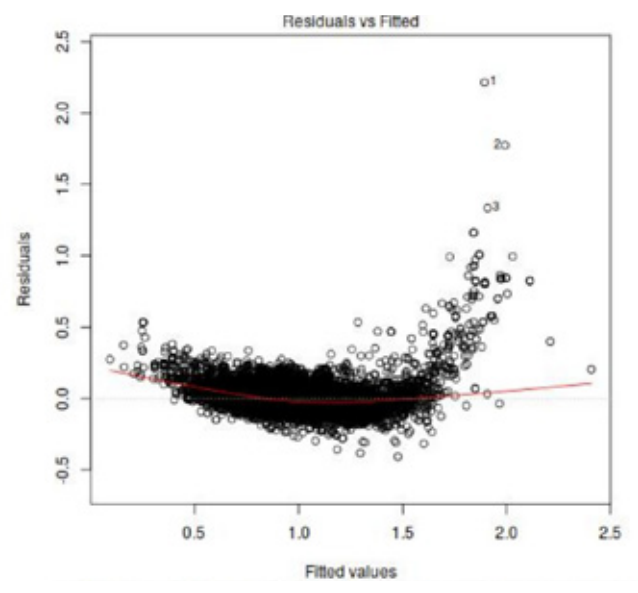


Figure A-3 Residuals vs. fitted plot of the best model based on the Akaike Information Criterion.

A.6 GHG footprint of world regions

Below, the GHG footprints of the different world regions are shown. Figure A-4 shows the GHG footprint of wind farms in Africa, Figure A-5 the footprint of those in America, Figure A-6 that of those in Asia, Figure A-7 the footprint of wind farms in Europe and Figure A-8 that of Oceanian wind farms.

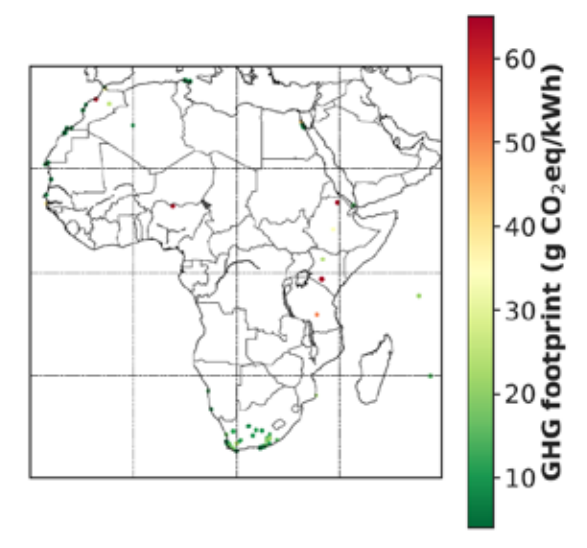


Figure A-4 GHG footprints of wind farms in Africa.

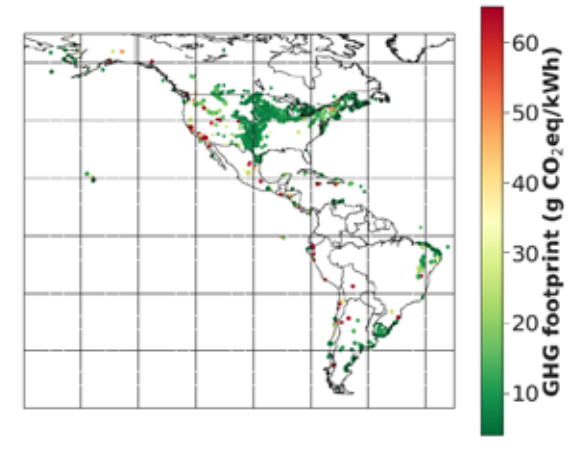


Figure A-5 GHG footprints of wind farms in America.

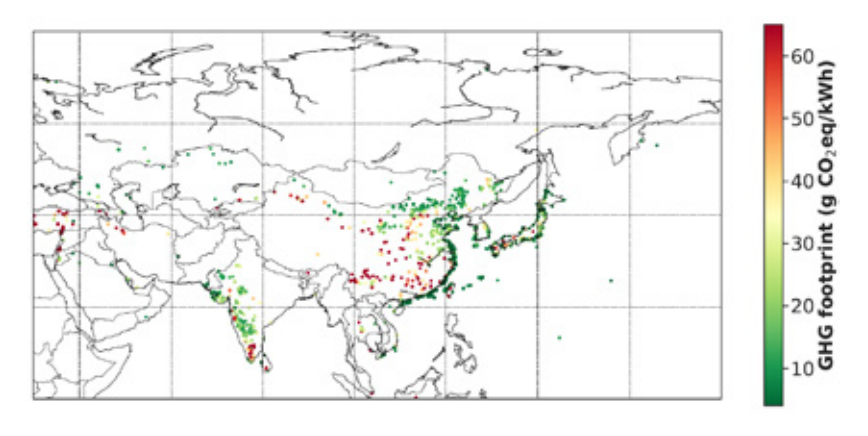


Figure A-6 GHG footprints of wind farms in Asia.

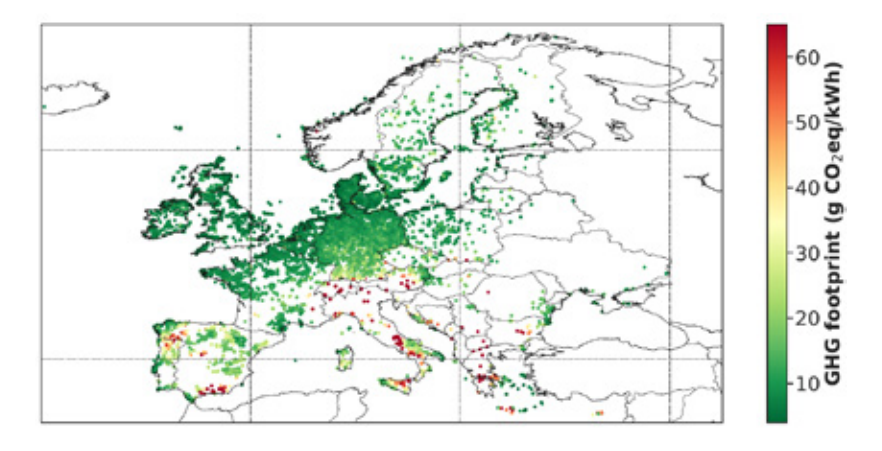


Figure A-7 GHG footprints of wind farms in Europe.

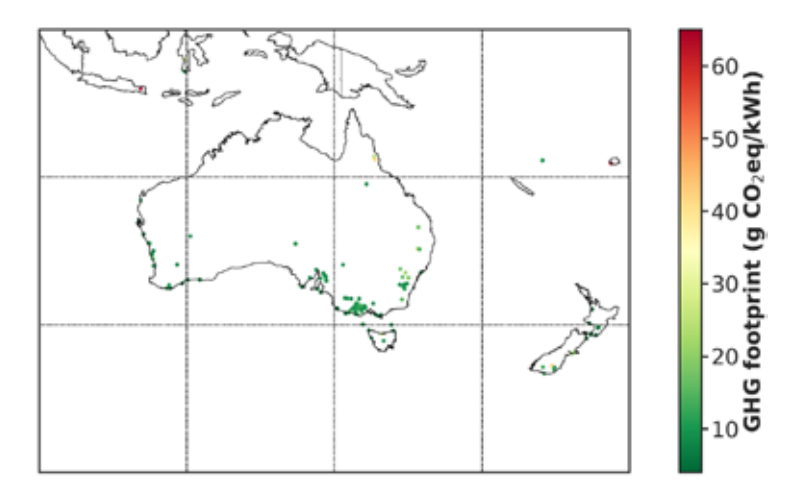


Figure A-8 GHG footprints of wind farms in Oceania.

The effect of gap filling on the GHG footprint of the wind farms included here is shown in Figure A-9.

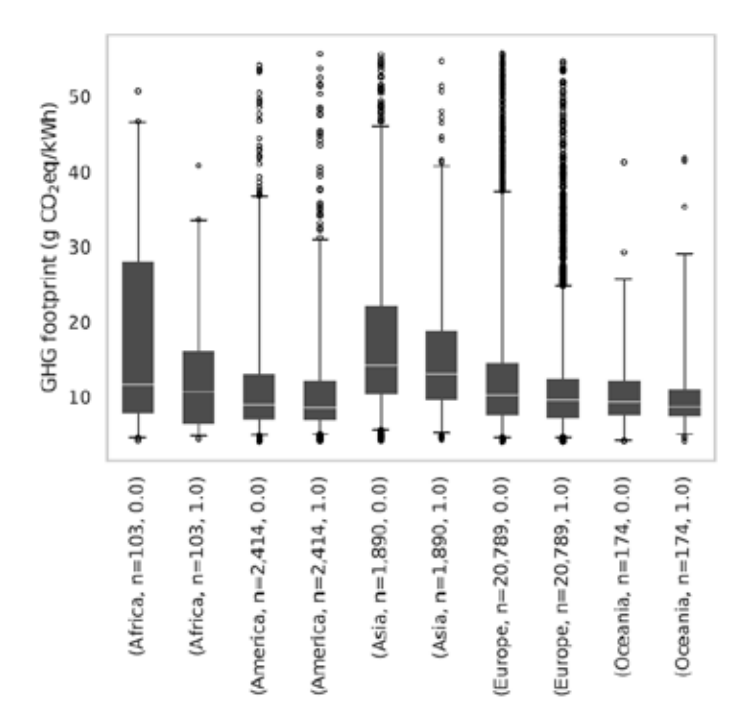


Figure A-9 Effect of gap filling on GHG footprint ranges per continent. 0: at least one wind farm characteristic had to be informed by gap filling. 1: all wind farm characteristics available in the data set.

A.7 Capacity factor of the global wind farm fleet

The capacity factor of a technology can be calculated by dividing the amount of electricity produced during a given time by the amount of electricity that could theoretically have been produced during that same time. Figure A-10 provides an overview of how the capacity factors of the wind farms included in this study distribute compared to the carbon footprint. Higher footprints are related to lower capacity factors, which can also be seen when comparing Figure A-11, which shows how capacity factors distribute globally, to the maps in section A.6.

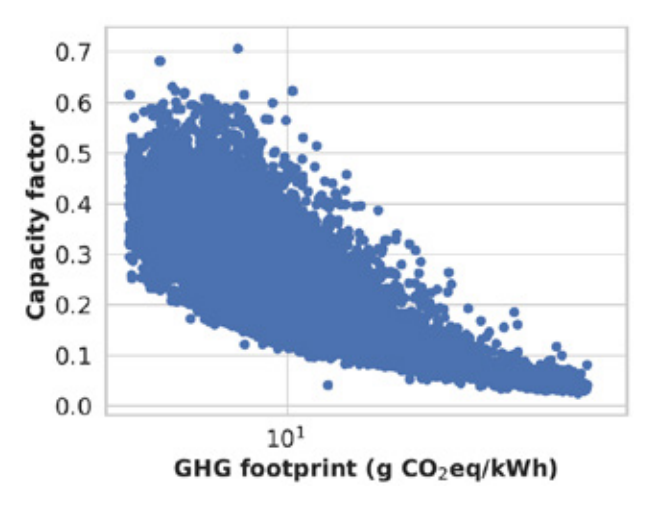


Figure A-10 Scatter plot of the GHG footprint versus the capacity factor of the global wind farm fleet.

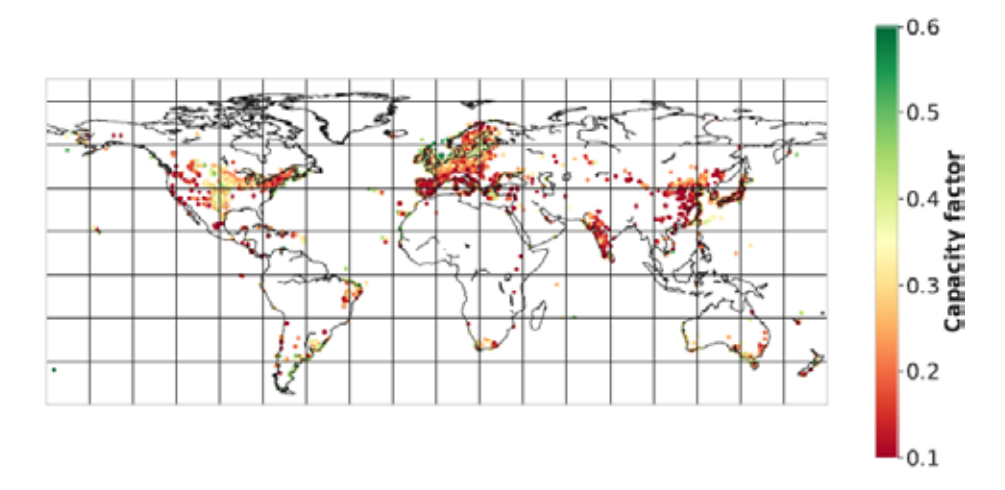


Figure A-11 Distribution of the capacity factor of the global wind farm fleet.

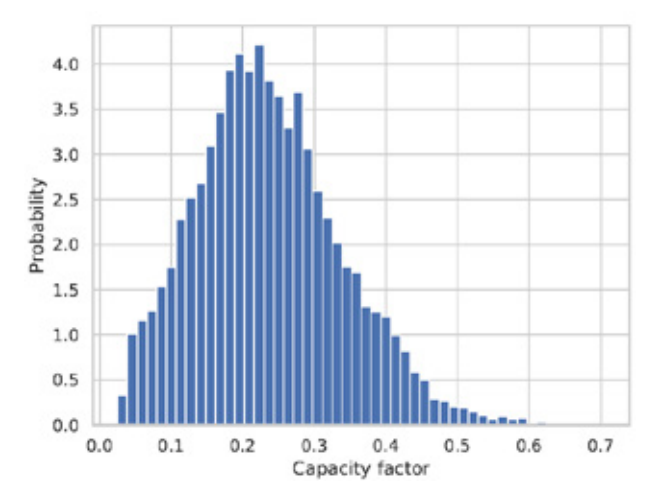


Figure A-12 Histogram of the capacity factor of the global wind farm fleet.

A.8 Literature review

Table A-3 summarizes the GHG footprints found in literature.

Table A-3 GHG footprints found in literature.

Reference	Information	GHG footprint (g CO ₂ eq/kWh)
[256]	49.5 MW, China	4.429
[257]	Three turbines in China	3.9
[258]	Onshore 1MW, TX, US	7.13
	Onshore 2MW, TX, US	6.86
	Onshore 2.3MW, TX, US	5.63
	Shallow water offshore 2MW, TX, US	9.11
	Shallow water offshore 2.3MW, TX, US	6.23
	Deep water offshore 2.3MW, TX, US	7.58
	Deep water offshore 5MW, TX, US	6.98
[259]	Offshore wind farm Tuno Knob	16.5
	Offshore wind farm Fjaldene	9.7
[52]	100 kW wind turbine set $(n = 542)$	45.3
	500 kW wind turbine set (n = 230)	19.1
	1MW wind turbine set $(n = 370)$	21.6
	2MW wind turbine set (n = 154)	17.3
	2MW offshore wind turbine set (n = 104)	11.7
[260]	Greek wind farm	4.1
[261]	Alpha ventus wind farm	32

Table A-3 Continued

Reference	Information	GHG footprint (g CO ₂ eq/kWh
[262]	Havsu I offshore wind farm	35.1
[263]	38 Vestas wind turbines in Joran	9.11
[264]	14 onshore wind turbines in Brazil	7.1
[265]	330kW turbine 50m hub in Pınarbaşı-Kayseri	40.36
	330kW turbine 80m hub in Pınarbaşı-Kayseri	36.46
	330kW turbine 100m hub in Pınarbaşı-Kayseri	33.96
	500kW turbine 50m hub in Pınarbaşı-Kayseri	38.96
	500kW turbine 80m hub in Pınarbaşı-Kayseri	32.01
	500kW turbine 100m hub in Pınarbaşı-Kayseri	29.97
	810kW turbine 50m hub in Pınarbaşı-Kayseri	26.57
	810kW turbine 80m hub in Pınarbaşı-Kayseri	21.66
	810kW turbine 100m hub in Pınarbaşı-Kayseri	20.41
	2050kW turbine 50m hub in Pınarbaşı-Kayseri	19.54
	2050kW turbine 80m hub in Pınarbaşı-Kayseri	16.63
	2050kW turbine 100m hub in Pınarbaşı-Kayseri	16.27
	3020kW turbine 50m hub in Pınarbaşı-Kayseri	28.61
	3020kW turbine 80m hub in Pınarbaşı-Kayseri	23.77
	3020kW turbine 100m hub in Pınarbaşı-Kayseri	22.29
[266]	Best case	29.5
	Future case	20.3
[267]	Dernah wind farm in Libya	10.42
[268]	49.5MW wind farm in China	28.6
[248]	186x1.65MW onshore wind farm in China	8.21
	100x3.00MW offshore wind farm in China	5.98
	100x3.00MW onshore wind farm in China	4.97
[269]	Donghai Bridge offshore wind farm in China	25.5
[46]	24x1.25MW wind farm in China	7.2
[270]	Saihan wind farm China	8.65
[271]	20x5kW turbines in Alberta, CA	17.8
	5x20kW turbines in Alberta, CA	25.1
	100kW turbines in Alberta, CA	42.7
[272]	11x660kW turbines in Italy	14.8
[118]	Vestas V112 wind farm	7.0
[273]	150mW wind farm in Inner Mongolia, China	7.2
[274]	5MW offshore wind farm in Germany	22.0
[275]	4.5MW wind turbine	16.0

Table A-3 Continued

Reference	Information	GHG footprint (g CO ₂ eq/kWh)
	250W wind turbine	46
[276]	Onshore V90-3.0MW turbine	4.6
	Onshore V90-3.0MW turbine	5.2
[277]	40x5MW offshore wind farm	11.5
[44]	Onshore turbine	7.0
	Offshore turbine	11.0
[278]	Vestas 2MW GridStreamer	7.7
[279]	180MW offshore wind farm	24.0
[280]	5MW offshore wind farm	16.8
	3MW onshore coastal wind farm	13.2
	2.5MW onshore inland wind farm	23.4
[47]	2.0MW geared wind turbine	7.59
	1.8MW gearless wind turbine	7.89
[281]		3.6
[49]	Buffalo Ridge wind farm, US	14
	Lake Benton wind farm, US	18
	Glenmore wind farm, US	34
[282]	5MW floating offshore turbine Umaine Spar	25.3
	5MW floating offshore turbine MIT TLB	18.0
	5MW floating offshore turbine SWAY	20.9
	5MW floating offshore turbine Umaine Semi-S	31.4
	5MW floating offshore turbine Umaine TLP	19.2
	5MW bottom-fixed offshore turbine OC4 Jacket	18.9
[283]	1.5MW onshore wind farm	11.8
[284]	Onshore Vestas V112-3.45MW turbine	5.3
[111]	Onshore Vestas V110-2.0MW turbine	7.2
[285]	Onshore Vestas V112-3.3MW turbine	5.8
[172]	Onshore Gamesa G128-5.0MW turbine	9.65
[173]	Onshore Gamesa G132-5.0MW turbine	8.58
[53]	Onshore, 1MW	17.6
	Onshore 1-3MW	15.5
	Onshore >3MW	14.1
	Offshore 1-3MW	13.6
[286]	Onshore 1MW	11.9
	Onshore 1-3MW	12.5
	Onshore >3MW	19.7

Table A-3 Continued

Reference	Information	GHG footprin (g CO₂eq/kWh
	Offshore 1-3MW	15.6
[103]	Mean, harmonized	15
	Minimum, harmonized	3.0
	Maximum, harmonized	45
[287]	3MW onshore turbine	7.25
	3MW onshore turbine	12.43
[288]	850kW wind turbine	10.28
	3MW wind turbine	9.30
[289]	5MW wind turbine, LT = 30 yrs, CF = 43%	2.8
	5MW wind turbine, LT = 30 yrs, CF = 20%	7.4
	5MW wind turbine, LT = 20 yrs, CF = 43%	4.2
	5MW wind turbine, LT = 20 yrs, CF = 20%	11.1
[290]	Onshore wind turbine	11
	Offshore wind turbine	13
[291]	44m hub, coastal, production & operation in GER	45
	44m hub, coastal, production in GER, operation BRA	15
	44m hub, coastal, production in GER & BRA, operation in BRA	8
	44m hub, coastal, production & operation in BRA	3
	44m hub, coastal, production & operation in BRA, recycled steel	2
	55m hub, coastal, production & operation in GER	48
	55m hub, coastal, production in GER, operation BRA	16
	55m hub, coastal, production in GER & BRA, operation in BRA	8
	55m hub, coastal, production & operation in BRA	3
	55m hub, coastal, production & operation in BRA, recycled steel	2
	55m hub, near coastal, production & operation in GER	61
	55m hub, near coastal, production in GER, operation BRA	20
	55m hub, near coastal, production in GER & BRA, operation in BRA	10
	55m hub, near coastal, production & operation in BRA	3
	55m hub, near coastal, production & operation in BRA, recycled steel	2
	55m hub, inland, production & operation in GER	81
	55m hub, inland, production in GER, operation BRA	27
	55m hub, inland, production in GER & BRA, operation in BRA	13
	55m hub, inland, production & operation in BRA	4
	55m hub, inland, production & operation in BRA, recycled steel	3
	65m hub, inland, production & operation in GER	77

Table A-3 Continued

Reference	Information	GHG footprint (g CO ₂ eq/kWh)
	65m hub, inland, production in GER, operation BRA	26
	65m hub, inland, production in GER & BRA, operation in BRA	12
	65m hub, inland, production & operation in BRA	4
	65m hub, inland, production & operation in BRA, recycled steel	3
[292]	Minimum	13
	Maximum	156
[293]	2MW turbine, base case	6.58
	2MW turbine, maximum case	9.29
	2MW turbine, minimum case	6.2
[294]	600kW wind turbine in Canada	13
[295]	600kW turbine wind farm	7.2
[296]	1.5MW onshore turbine	11
	2.5MW offshore turbine	9
[297]	Te Apiti wind farm	3.0
[298]	225kW wind turbine, renovation	7.2
	225kW wind turbine, relocation	11
	225kW wind turbine, recycling	11
[299]	300kW turbine	9.51
	170kW turbine	12.92
	400kW turbine	6.56
	100kW turbine	33.74
[300]	Coast, 0.15-1.5MW	9.2
	Inland, 0.15-1.5MW	27
	0.6MW, coast	7.9
	0.6MW, inland	24
[301]	25MW wind plant	15

A.9 Applicability domain

The applicability domain of the regression model used to calculate a wind turbine's lifetime GHG emissions as defined in [21] is defined by the minimum and maximum hub height and rotor diameter of the wind turbines used to build this model. The minimum hub height was 40 m, the maximum hub height 117 m. For the rotor diameter, the minimum value was 39 m and the maximum 126 m. Of all the turbines in the dataset used here, 78% fall within that range.

Appendix B Appendix for chapter 4

B.1 Facility-specific data and filling in missing data

We obtain facility-specific technological characteristics mainly from the proprietary Wiki-Solar dataset, available from http://wiki-solar.org. It contains data on utilityscale projects, ranging from a minimum capacity of 3.0 MWp ('p' for peak, indicating direct current output under standard testing conditions) to projects of 3 GWp. In this study we focus on photovoltaic (PV) plants (thus excluding concentrated solar power) and use the 9,992 with a known location out of 10,268 PV plants in the Wiki-Solar database (obtained in November 2019). In this section we describe what information is available from Wiki-Solar and how we fill in gaps.

Year. We use the age of a facility as a proxy for its efficiency, combined with panel type. For the 990 facilities where the year is not provided, we apply the median year per status of the 9,002 facilities where year is provided (2015 for operating facilities - status A, 2018 for facilities near completion - status B and 2020 for planned facilities - status C).

We then use efficiency values from Chen et al. [179], determined using their Figure 3 and a WebPlotDigitizer https://apps.automeris.io/wpd/. Efficiencies increase approximately linearly for the timeframe they consider (2006-2018). The majority of facilities in our dataset are within this timeframe too – only 7 predate 2006. For planned facilities (2019 or later) we extrapolate the linear increase of efficiencies over time. For amorphous silicon (a-Si), Chen et al. [179] does not provide values, so we use the 2009-2012 averaged values from Bhandari et al. [56] and the average growth rates of CdTe and CI(G)S. Table B-1 provides the parameters used to determine panel efficiencies.

We thus take into consideration that thin film panel efficiency improves faster than crystalline panel efficiency [179]. We note that applying a linear growth rate implies that our computations are valid for current facilities and those planned for the next couple of years, but our computations do not hold for future scenarios in which panel efficiencies may gradually approach their practical efficiency limits.

Table B-1 Parameters used to determine the panel efficiencies η [%] per type based on Chen et al. [179] and Bhandari et al. [56]. Efficiencies are determined as $\eta=a \cdot year + b$, values for 2016 are given as examples.

Panel type	Growth rate a [%]	Intercept b	η 2016
Mono-crystalline	0.4027	-794.87	16.97
Poly-crystalline	0.3509	-691.29	16.12
Cadmium telluride	0.8056	-1609.15	14.94
Copper indium (gallium) selenide	0.5062	-1005.89	14.61
Amorphous silicon	0.6559	-1311.80	10.49

Panel type. PV facility's impact I and power (electricity) output P furthermore depends on the type of PV, which is provided for 1,249 of the facilities in the Wiki-Solar database, i.e. 12.5% of the facilities. We extended this by using input from various sources. First, we used the US Energy Information Administration's database EIA-860 [184], matching utility-scale PV facilities from their 2018 data to those in Wiki-Solar using a proximity of maximum 0.1° latitude and longitude as well as a visual check for facility names and capacities. This yielded 858 facilities in the US with added information on panel type. Second, we obtained facility-specific panel types from the Global Energy Observatory [185], resulting in added information for 53 facilities globally. Third, we used the module supplier, provided in the Wiki-Solar database, as an indicator for type of panel. This yielded panel types for 771 facilities.

After these efforts to fill the gaps in panel types, we know for 1,348 out of 9,992 facilities which of the five most common types of panels is used (mono- and poly-crystalline silicon, amorphous silicon, cadmium telluride or copper indium (gallium) diselenide). For an additional 1,443 facilities, we know that crystalline panels are used, and for 17 facilities we know that thin film panels are used. For these facilities, we compute the footprint for each type, i.e. for the 1,443 crystalline facilities we compute both a footprint for mono- and poly-crystalline panels. For the thin film facilities, we compute footprints for amorphous silicon, cadmium telluride and copper indium (gallium) diselenide. For the remaining 7,148 facilities with unknown panel type, we compute footprints for all five types. This allows us to test the sensitivity of the footprint to panel type, such as in main Figure 4-4. In main Figure 4-3 showing the spatial distribution of EF_{GHG}, an overall footprint for facilities where type is unknown is computed based on a weighted average using the relative production of each type in 2016 for current facilities (status A and B) and 2019 for planned facilities (status C), see Table B-2. 2019 is the latest year for which type-specific market shares are available, which is assumed representative for planned facilities (for which the median year is 2020). We opted for the simpler computations of using 2016 and 2019 market shares instead of market shares of each year, as for most years in the dataset the market shares are very similar [183]. Only in recent years (2018, 2019) a shift to more mono-Si and less poly-Si becomes apparent. Thus, for instance for current locations where we know panels are of crystalline type, the weighted footprint is computed as

$$GHG_{weighted} = \frac{22.7}{22.7 + 71.2} \cdot EF_{GHG-monoSi} + \frac{71.2}{22.7 + 71.2} \cdot EF_{GHG-polySl}$$
(B-1)

Both mono-Si and poly-Si footprints are computed using the same facility-specific capacity, location and year of construction. The same approach is used for facilities with thin film or unknown panel type.

2016	2019
22.7	64.7
71.2	29.6
3.9	4.3
1.6	1.4
0.6	0.2
	22.7 71.2 3.9

Within the Wiki-Solar database we can distinguish between current facilities and those under development (planned), see Figure 4-2 in the main text. Current facilities include operating facilities as well as those near completion (status A and B in the Wiki-Solar dataset, as of end of 2019). Of the 7,982 current facilities, 5,221 (65.4%) have no information on panel type. For facilities in development (2,010 out of the total 9,992), there are relatively more plants with high capacity (>100 MW, Figure 4-2), and also relatively more facilities with no information on panel type (1,889 out of 2,010 - 94.0%).

Capacity. A facility's capacity is given in watt-peak (p, direct current) and/or in alternating current (ac, power that goes into the grid after e.g. inverter losses). In our computation of impacts, we use MWp when computing the surface panel area of a facility (see section 4.2.1 in the main paper). For 2,495 out of 9,992 facilities, MWp is unknown, and we compute it from MWac using a performance ratio of 0.8 (PR = MWac/MWp). This is the median value for the 2,049 plants for which both MWac and MWp are provided, as well as the IEA recommended value [182]. Fraunhofer ISE [183] indicates that a performance ratio of 80-90% is common for newer PV plants, up from ~70% before 2000. In our database all plants became operational in or after 2000, with a median in 2015/2016. A performance ratio of 80% is therefore a representative and even slightly conservative value for our computations.

For our computation of electricity output, we use MWac, in order to have kWh delivered to the grid as our functional unit. MWac is unknown for 5,451 and is computed from MWp and a PR of 0.8, as described above.

In some cases where both MWac and MWp are given, these were deemed too dissimilar if the PR was below 0.5 or above 1.0. For these cases (41), the MWp is set to MWac/0.8.

The global summed PV capacity of the 9,992 facilities used is 294 GWac, or 368 GWp. Figure 4-2 in the main paper shows the distribution of the plants in the database. Operating and near-operating facilities (7,120 and 862 facilities respectively) make up 215 GWp, and planned facilities make up 152 GWp. IRENA reports that in 2019, solar PV capacity reached 580 GWp [175]. Assuming 60% of this is utility-scale (https://www.iea.org/topics/renewables/solar/, the remainder consisting of residential, commercial and off-grid capacity) implies 348 GWp of utility-scale capacity. Counting all facilities built up to and including 2019 in the Wiki-Solar database results in 8,381 facilities with a total capacity of 233 GWp, or 67% of the IRENA-reported 2019 utility-scale capacity. Note however that numbers on capacity as well as distribution amongst utility, residential and commercial capacity can vary greatly per year and per source.

B.2 Impact I: GHG emissions

We calculate life cycle GHG emissions per facility using its surface area. Surface area is computed using equation (4-3), capacity and a year- and panel type-specific efficiency (see Main Figure 4-1, section B.1 - Facility-specific data and filling in missing data). We then compute impacts for the panels and BOS separately.

Panel impacts. Impacts per m² of panel depend on the panel type and production location. The latter is taken into account by using market shares by origin countries per continent [178] (proprietary) and production country-specific impacts I. No facility-specific information on production location was available or traceable, so instead we include variations in production countries by using the continent-specific market shares of origin (producing) countries. The data from Absolute Reports [178] provides supply for the years 2015 - 2020 for Asia Pacific, Europe, Africa and Middle East, North America, and South America. Here we use 2016 for current facilities and 2019 for current facilities, the same years used for the panel type market shares (see section B.1). Other years show very similar market shares (i.e. using 2015 and 2020 instead gives very similar results); there are only shifts in import from China, which is higher for 2019 in Europe compared to 2016 but lower for North America. Note that for North America we included values from the US Energy Information

Administration, which provides values for Chinese imports, which are not specified by Absolute Reports [178] (likely included in the category 'other' – they do specify Chinese imports for other continents). See EIA websites for 2016¹ and 2019².

The market shares we found are not type-specific, so we assume that they are valid for all panel types. Only for CdTe we use different market shares, based on the assumption that the CdTe market is dominated by one manufacturer (FirstSolar), who (currently) has production locations in Malaysia, the US and Vietnam (see their website https://www.firstsolar.com/en-Emea/About-Us/Locations). We did not find impact values for production of CdTe in Vietnam in literature and therefore assume 50% US and 50% Malaysian production for CdTe.

We combined the continent-specific market shares per producing country with type-specific impacts I_{panel} per producing country. As performing a full LCIA per panel type and per producing country was beyond the scope of this study, we obtained values from literature. There is no single source of impacts for all panel types and all producing countries. One of the most complete sources is de Wild-Scholten [190], who provide impacts for all panel type for both European and Chinese production. Values for production in the US and Malaysia are obtained from Leccisi et al. [60], and Kim et al. [189] provides values for Korea. For panel types and producing countries where we could not find the impacts, we used values from Ecolnvent 3.5, representing a weighted average for all PV-producing countries in the world ('GLO', see Table B-2 for market shares). These values where obtained through SimaPro 9.0.0.35. Specifically, we use allocation, cut-off by classification. We selected the ReCiPe2016 method [302] to translate life cycle emissions from the LCI into the midpoint impact category global warming (GHG emissions in kg CO₂eq.). We opted for 'GLO' instead of 'RoW' (rest of world) as both give almost the same impacts for each panel type, thus giving the same footprints.

We note that there is a wide range of values for I available from literature, see Table B-8 to Table B-11, reflecting different data sources, LCIA methods, production processes etc. Replacing the values we used (Table B-3) with values from other literature sources would change the exact values reported in our results, but not the main conclusions, as all studies report similar patterns (i.e. high impacts from production in China, low impacts from EU, intermediate values for the US). We furthermore acknowledge that by using impacts I from different sources there may be inherent differences in system boundaries, impact assessments etc.

https://www.eia.gov/todayinenergy/detail.php?id=34952

https://www.eia.gov/renewable/annual/solar_photo/pdf/pv_table7.pdf

Table B-3 Impacts in kg $\rm CO_2$ -eq/m² per producing country, per type, for panels (excl. BOS). Sources: dWS: de Wild-Scholten [190], Lec: Leccisi et al. [60], K14: Kim et al. [189], GLO (EcoInvent 3.5 'GLO'). GLO is used for production in countries other than China, EU, US, or KO, and for production of CI(G)S and a-Si in the US and KO, for which we did not find impacts.

	mono-Si	poly-Si	CdTe	CI(G)S	a-Si
China dws	415.88	214.32		102.61	81.90
EU dws	180.56	106.74		74.18	57.89
US ^{Lec}	263	153	51		
MY Lec			46		
KO K14	163.5	104.33			
GLO	277.1	209.5		131.2	77.5

Table B-4 Market shares in PV production used in 'GLO' by Ecolnvent, representative for 2018, based on electricity used in laminate production. CdTe production in North America is in the US alone. ROW represents rest of world. Market shares in 2016, the year used to weight footprints across panel types of current facilities, are very similar [183].

Panel type	Asia	Europe	Germany	North America	ROW
a-Si	46.1%	17.3%		21.5%	15%
CdTe			41%	59.0%	
CI(G)S	30.3%		36.1%	14.2%	19.4%
poly-Si	35.7%	36.0%		16.7%	11.6%
mono-Si	35.7%	36.0%		16.7%	11.6%

Combining the market shares by origin countries per continent [178] and impacts per producing country (Table B-3) we thus obtain continent- and type-specific panel impacts for current and planned facilities, see Table B-5. The market shares by origin countries were used as weights, just as the market shares of panel types (as described in Appendix B section B.1). For many continents and panel types there is little difference in impacts for current and planned facilities. A drop (increase) in impacts typically reflects less (more) import from China, where impacts per m² are higher (Table B-3). At the same time impacts for CI(G)S show a change in the opposite direction, as the Ecolnvent 'GLO' impacts are higher than those reported for China by de Wild-Scholten [190]. Note that for CdTe we used the same impact value for all locations (reflecting 50% US and 50% Malaysian production as described above). Also note that changes in impacts for current and planned facilities reflect changes in import and panel efficiency. We do not consider improvements in material and energy utilization in the production process, which likely result in lower impacts and footprints for newer facilities, e.g. [196].

Table B-5 Continent- and type-specific impacts in kg CO₂-eq/m² for panels (excl. BOS), based on market shares by origin countries per continent [178] and impacts per producing country (Table B-3). 2016 market shares are used for current facilities, 2019 for planned facilities (Table B-2).

	North Ame	ımerica	South America	merica	Europe	be	Africa & M	Africa & Middle East	Pacific Asia	: Asia
	2016	2019	2016	2019	2016	2019	2016	2019	2016	2019
mono-Si	299.0	276.5	367.8	362.8	319.7	365.5	350.7	350.0	379.7	379.6
poly-Si	196.3	196.4	212.6	212.5	188.4	199.9	212.1	212.0	208.3	209.0
CdTe					48.5	.5				
CI(G)S	124.5	129.4	112.5	113.5	118.8	111.0	116.0	116.2	109.0	109.2
a-Si	78.5	77.8	80.4	80.2	79.4	9.08	79.8	79.8	80.9	80.9

BOS. The GHG emissions of the balance of systems includes mounting hardware as well as inverters and cabling. Mounting hardware is considered per m², where the area of BOS required is assumed equal to the panel area (equation (4-3)). Specifically, we use GHG emissions per m² of mounting system provided by EcoInvent 3.5 for a 570 kWp poly-Si open-ground facility, independently of PV panel type. For inverters and cabling (i.e. electrical installation), EcoInvent provides GHG emissions for the entire 570 kWp facility, which includes 3.126 500 kW inverters (assuming a 15-year lifetime) and an electric installation consisting of cabling, an electric meter and a fuse box. We scale these GHG emissions for electrical installation to the capacity of each facility. These impacts for BOS, I_{ROS} represent a weighted average for all PVproducing countries in the world (`GLO', Table B-4). Table B-6 shows the values we used in our impact computations. For an easier comparison to panel and mounting system emissions, the emissions for electric installation are provided per m², which is type-specific because surface area depends on type-specific panel efficiency n · n depends on year too; Table B-6 represents 2016 values. Overall, crystalline panels have higher GHG emissions per m² for electric installations, because they require more inverters and cabling per m² due to higher efficiencies.

We note that the Ecolnvent results we use do not account for the end-of-life stage, so no cost for removal or benefits from recycling are considered.

Table B-6 GHG emissions per m² used in kg CO₂-eq, from EcoInvent 3. For electric installation, emissions per unit capacity have been translated to m² for easier comparison using equation (4-3) and 2016 efficiencies (Table B-1). GHG emissions per m² of panel are given in Table B-3.

	kg CO₂-eq
1 m ² mounting system	74
1 m² mono-Si electric installation	15.1
1 m² poly-Si electric installation	14.4
1 m ² CdTe electric installation	13.3
1 m ² CI(G)S electric installation	13.0
1 m ² a-Si electric installation	9.3
	1 m ² mono-Si electric installation 1 m ² poly-Si electric installation 1 m ² CdTe electric installation 1 m ² CI(G)S electric installation

B.3 Power computation

To compute the electricity output per PV plant we use equations from Jerez et al. [180], as briefly described in section 4.2.1 in the main text. Here we show the full equations and coefficients used.

$$Power(t) = PVpot(t) \cdot MWac$$
 (B-2)

PVpot is computed as a function of temperature ratio T_p, surface downward solar radiation rsds (W^{m2}) and rsds_{stc}, surface downward solar radiation under standard testing conditions at 1,000 Wm⁻²:

$$PVpot(t) = T_R(t) \frac{rsds(t)}{rsds_{STC}}$$
(B-3)

where the performance ratio $T_{\rm g}$ is a function of cell temperature:

$$T_R(t) = 1 + \gamma [T_{cell}(t) - T_{STC}]$$
 (B-4)

where T_{STC} = 25 °C and γ is a (negative) PV type-specific temperature coefficient, set to -0.0050 for mono-Si in Jerez et al. [180] and scaled to values reported in Crook et al. [303] for other types (see Table B-7).

 T_{coll} depends on the surrounding temperature T, incoming solar radiation rsds and wind speed vws (m/s) as follows:

$$T_{cell}(t) = c_1 + c_2 \cdot T + c_3 \cdot rsds(t) + c_4 \cdot vws(t)$$
 (B-5)

with $c_1 - c_2$ type-specific coefficients (see Table B-7), following Chenni et al. [304], TamizhMani et al. [305]. ERA5 wind speed at 10 m is rescaled to 2 m wind speed using the 1/7 logarithmic profile. Combining equations (B-4) and (B-5) shows that the performance of a PV plant increases (decreases) with lower (higher) T_{cell} with T_{cell} increasing with temperature and radiation, and decreasing with wind.

Equations (B-2) to (B-5) are applied to each of the 9,992 PV plants from the Wiki-Solar database using the hourly ERA5 climate reanalysis data for the grid cell in which the PV plant is located. The power production is then summed over 1988-2017, in order to ultimately express the lifetime environmental footprint per kWh. A 30-year lifetime is assumed to be representative of modern PV [182], but a different lifetime would of course affect the lifetime power output and GHG footprint. A 30-year lifetime is also used in comparable studies Pérez-López et al. [74], Louwen et al. [72]

and in the majority of literature (see Table B-8 to Table B-11). Using climate data over the period 1988-2017 is deemed to result in a power output representative of current climate, as a 30-year period is long enough to average out over climatic extremes and oscillations. Here we thus assume that the computed power output is representative for the facilities in our dataset which are all dating later than 2000. We tested that power output is not sensitive to the exact years chosen; for 1,460 locations we compared average power output for 2008-2017 to that of 1988-2017 and found that the difference is less than 1% for 88% of the locations, and all differences are less than 3%.

We furthermore apply a loss ratio (or panel degradation) of 0.7%/yr, amounting to a loss of power of 10.1% over the 30-year lifetime [182, 74]. The final lifetime power output is thus:

$$Power_{lifetime} = f_{loss} \cdot \sum_{1988}^{2017} Power(t)$$
 (B-6)

with $f_{loss} = 0.899$.

Table B-7 PV type specific parameters used in our computations. γ is the temperature coefficient used in equation (B-4), based on computations for mono-Si types in Jerez et al. [180]. For other types, γ is scaled to the values given in Crook et al. [303]. c_1 - c_4 are the coefficients used to compute cell temperature in equation (B-5), from TamizhMani et al. [305].

mono-Si -0.0050 3.9 0.942 0.028 -1.505 poly-Si -0.0044 5.1 0.926 0.030 -1.666	sm ⁻¹]
poly-Si -0.0044 5.1 0.926 0.030 -1.666	9
	5
a-Si -0.0022 4.1 0.943 0.026 -1.450)
CI(G)S -0.0039 4.0 0.960 0.029 -1.507	7
CdTe -0.0028 4.8 0.953 0.031 -1.667	7

B.4 The ERA5 climate reanalysis dataset

We use the most recent and highest-resolution global (re-analysis) dataset representing current climate at 0.25°x0.25° (roughly 30x30 km at equator) [144]. Hourly resolution allows us to include the daily cycle of radiation as well as temporal variation in cell efficiency due to cell temperature (including air temperature, radiation and wind, see section B.3 - Power computation). Hourly data gives improved estimates of PV power generation compared to lower-resolution data [187, 188], due to the non-linear interaction between air temperature and radiation.

Urraca et al. [306] find that surface irradiance from ERA5 is less biased than earlier reanalysis datasets (MERRA2, ERA-Interim), and gives results that are comparable to satellite-derived products. The benefit of ERA5 over satellite-derived products (covering the entire globe and excluding gaps in timeseries) makes it a valid alternative when satellite observations are lacking or incomplete. ERA5 is, however, considered inadequate in regions with high irradiance variability (coastal areas and mountains).

B.5 Regression model

When building the regression model, we chose an ordinary least squares approach because it gives an explicit equation which allows for easy interpretation. We build this model on the 1,348 facilities for which panel type is known.

The predictors, given in the top of Figure 4-1 in the main text, are year (used to represent facility age and determine panel efficiency), panel type (used to determine panel efficiency as well as in power output computation), capacity (used to determine panel area and in power output computation) and climate variables. We also include the interaction between panel type and construction year, because these together determine efficiency n used in the life cycle GHG emissions (Eg. (B-4), Appendix B section B.1). Note that we cannot currently take production location into account in this regression, as facility-specific production location is unknown (instead we used continent-specific weighted averages of production countries based on market shares). If production country would be known for each facility, this can be added to the regression model as a categorical variable (like panel type) and would likely reduce the uncertainty in facility-specific the GHG footprint.

For the climate variables, we use location-specific 30-year means of annually summed irradiation and mean day-time temperature and wind speed. We furthermore computed a coefficient of variation to account for inter-yearly variation in the climate variables, based on monthly and yearly summed irradiation and monthly and yearly mean temperature and wind, for example for temperature (°C):

$$T_{CV} = \frac{\overline{T_{mon,max} - T_{mon,min}}}{T_{ann,mean}} \tag{B-7}$$

where the bar indicates the 30-year mean.

For capacity, we used MWac, which gave the same conclusions from the regression model as using MWp. MWac is log-transformed because its distribution is rightskewed. We also log-transformed the response variable (EF_{GHG}) , because not doing so resulted in skewed model residuals.

Before building the regression model, we checked for multicollinearity. The correlation matrix is shown in Figure B-1, showing that correlations (R) are at or below 0.8. Furthermore, we checked variance inflation factors using the R package corvif [307], and found that all factors are below 5. Therefore, we conclude there is no multicollinearity in the predictors.

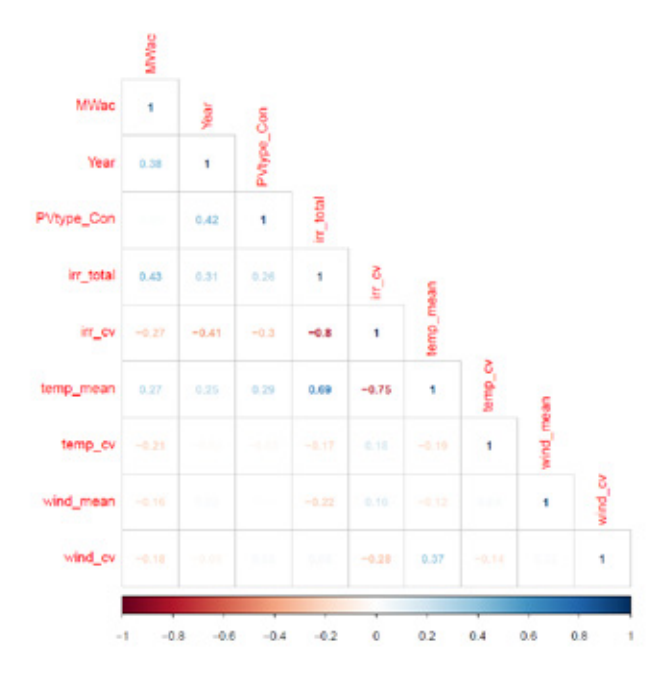


Figure B-1 Correlation plot for predictors and response variables in our footprint computation. PVtype_Con is a continuous representation of the 5 panel types (1-5), used for plotting purposes (a categorical variable such as PV type cannot be included in a correlation matrix).

We used the R package glmulti, considering main effects and one interaction (panel type - construction year) to find the best model based on AIC (Akaike's Information Criterion), which results in equation (4-5). This model has an AIC of -6167 and an $\rm R^2$ of 0.9868. It is built upon the predictors year (age), PV type, mean irradiation, mean temperature, mean wind, variation in irradiation ($\rm I_{cv}$) and the interaction between age and PV type. Predictors capacity and CV of temperature and wind are excluded, as including them leads to a higher AIC. This indicates that these are not important predictors of $\rm EF_{GHG}$. Capacity is a predictor of both impact I (higher capacity indicating higher surface area and thus higher lifetime GHG emissions) and

power output P, but our results indicate that this averages out for EF_{GHC}. Variation in wind and temperature can be important for temporally detailed location-specific power (electricity) output P [187, 308] but the regression model indicates it is of no importance for the lifetime power output used in EF_{GHG}.

Note that β_{type} in equation (4-5) has a fixed value per type, relative to a-Si. If the model is forced to use a different panel type as reference (using `contrasts' in R), the values of β_{type} and the intercept β_0 change but the other coefficients and the R^2 , as well as our conclusions, remain the same.

The best model results in an R² of 0.9868, see Figure B-2. The median residual (computed minus predicted) is -2.6 g CO₂-eq/kWh, the 2.5th and 97.5th percentiles are at -13.1 and 3.4 g CO₃-eq/kWh respectively, hence the regression slightly overestimates the footprints from the full computation.

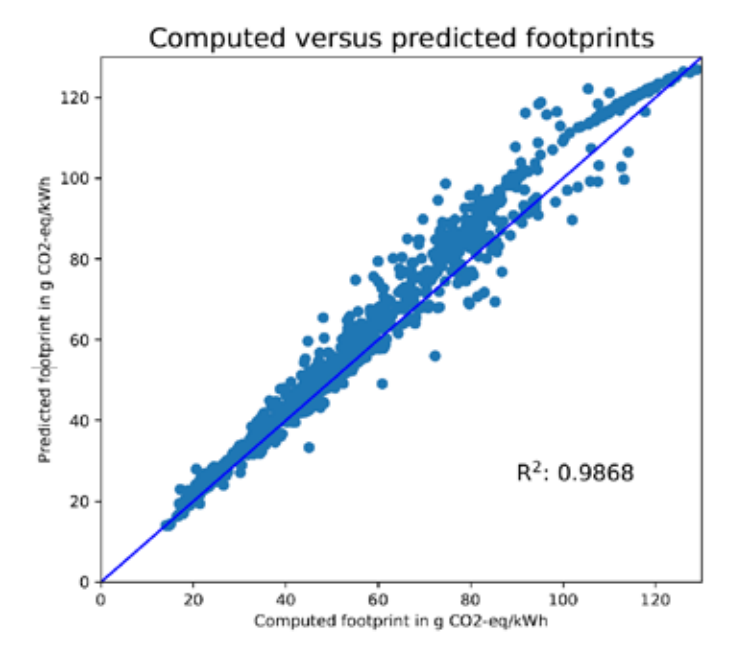


Figure B-2 Computed versus predicted (equation (4-5)) GHG footprints, based on 1,348 PV facilities. The 1:1 line is given in blue.

To formally test the importance of each predictor, we re-built the model of equation (4-5), randomizing each predictor in turn (leaving all other predictors unrandomized). The change in R² is indicative of the predictor's importance, a larger drop in R² indicating a higher importance. Figure 4-5 shows the results, indicating

that randomizing PV type causes the largest change in R^2 , followed by mean irradiation and year. We checked that not log-transforming the response variable EF_{GHG} leads to the same conclusions relating to predictor importance.

The shorter regression model (equation (4-6)), for easy use to any interested user, has an R^2 of 0.9862 and residuals of -1.4 [-11.6 - 5.1] g CO_2 -eq/kWh.

B.6 Comparison to literature

From literature, we selected studies that reported EF_{GHG} and/or impact I for any of the five panel types considered here (mono-Si, poly-Si, CdTe, Cl(G)S or a-Si) and which were fairly recent (dating from 2012 or later). Some studies summarize or harmonize earlier work on EF_{GHG} (such as Hsu et al. [54], Ludin et al. [71]) while others compute EF_{GHG} themselves. From the overview provided by Ludin et al. [71], we used their ranges based on studies from 2000 onwards, and selected ground-mounted systems. The range of values from Ludin et al. [71] reported here is therefore smaller than in their study, especially for crystalline panels, where some very high footprints were found for rooftop systems. We note that Nugent and Sovacool [65] provide a similar useful overview of PV footprints, which we do not report separately here as all values from ground-mounted systems are also reported in other studies shown in Figure 4-6 [71, 61, 69].

A range of system boundaries, life cycle inventories, impact assessment methods, etc. is used in previous studies, complicating comparisons across studies [67]. For the values reported in Figure 4-6 as well as those reporting impact I, we summarise the system boundaries in Table B-8 through Table B-11. System boundaries not given in the tables are for instance type of installation. All values given in Figure 4-6 are for ground-mounted systems. Only values from Hsu et al. [54] represent a mix of rooftop and ground-mounted systems. Results shown in Figure 4-6 are for the PV system (panels + BOS). To the values reported by Wetzel and Borchers [66], Yao et al. [191], Yue et al. [192], who include only panels, we added 6.5 g CO₂-eq/kWh for BOS as recommended by Wetzel and Borchers [66].

Table B-8 to Table B-11 include country of production and impact I for panel and BOS, where available. Impacts are either given in kg $\mathrm{CO_2}$ -eq/m² or kg $\mathrm{CO_2}$ -eq/Wp; the latter is converted to impacts per m² using efficiencies used by the study and equation (4-3). The tables thus show there is a range of reported values for both impact I and, subsequently, $\mathrm{EF_{GHG}}$ even within one country of production. For Hertwich et al. [59], values are derived from ReCiPe 1.08 and EcoInvent 2.2, and for PV values are presented for OECD North America. We therefore report production in the US for their study.

Lastly, we checked whether our method of computing electricity output is a reason for higher footprints. We include the effects of temperature and wind (see sections 4.2.1) and allow for the negative impact of panel temperature on electricity output. Other studies typically use a simpler approach (Power = I \cdot η · PR · A · LT) ignoring such temperature effects. If we re-compute electricity output P as well as EF_{GHG} using this simpler approach (also including the loss factor, hence Power = I · η · PR · A · LT · f_{loss}) we indeed find higher electricity power output and lower footprints compared to our original computations. However, the differences are small: instead of 56.7 [31.9-92.6] g CO_2 -eq/kWh we find 54.1 [30.0-92.6] g CO_2 -eq/kWh with the simpler computation of electricity output. We note that differences are larger at lower latitudes (where temperatures are higher) but are overall too small to explain the higher footprints in our study compared to others. Differences in irradiation, panel type, age or country of production thus seem to introduce larger variability in GHG footprints than the exact method of computing electricity output.

in years, η (panel efficiency) in %. PR stands for performance ratio (MWac/MWp). Impact I is given in kg CO₂-eq/m² for panels and BOS (mounting structure and average, MY: Malaysia, US: United States, CN: China). Ef_{erts} is given in g CO₂-eq/kWh for the entire system (panels + BOS). Ber: Bergesen et al. [68], Her: Hertwich et electrical components) separately, if provided by the study. If impacts were given per Wp, we computed impacts per m² using efficiencies used by the study and equation (4-3). n is the number of studies or facilities. Prod (production) is the country of production/manufacturing (EU: Europe, FR: France, GLO: weighted global al. [59], Ito: It et al. [73], Kim: Kim et al. [61], Lec: Leccisi et al. [60], Lud: Ludin et al. [71], Mil: Miller et al. [64], dWS: de Wild-Scholten [190], Bos: this study (for Bosmans **Table B-8** System boundaries used in studies for CdTe (including those whose footprints are shown in Figure 4-6). Irr (irradiation) is given in kWh/m²/yr, LT (lifetime) et al.). For our results (Bos) the values represent the median across all facilities of this type, with ranges [5-95th percentiles] in brackets.

Lir 1,800 30 1,737-2,344 30 1,700-2,400 30 1,000-2,300 30 1,700 2,060 30 1,700 1,700 30 1,700 30	11.6 11.6 13.2 10.9 15.6 10.9 11.9	0.84 0.84 0.8 0.75 0.77	Panel 60 60 46 51 51 61.6 61.6	180s 73 50	a 2 1 2 2 2 2 2 2 2 2 2 2 2 2 2 2 2 2 2	US US US RA MY US CN GLO EU CN	EF GHG 20 20 16 27 - 32 14 - 20 11 27 15 - 32 16 20 16	Notes TRACI 1.0, ReCiPe 1.08, Ecolnvent 2.2 ReCiPe 1.08, Ecolnvent 2.2 20° tilt, range: high-low irr Harmonized, range: high-low irr Range: high irr, MY production – low irr, US production Literature review CN electricity for upstream processes CN & GLO electricity for BOS Ecolnvent 2.2
30 [1,084-2,205]	13.3 [9.9- 18.2]	0.8 [0.74- 0.84]		87.3	416	OT5	26.1 [17.1- 57.0]	See Table B-5 for I panel Ecolnvent 3.5 GLO for BOS

in kWh/m²/yr, LT (lifetime) in years, η (panel efficiency) in %. PR stands for performance ratio (MWac/MWp). Impact I is given in kg CO₂-eq/m² for panels and BOS (mounting structure and electrical components) separately, if provided by the study. If impacts were given per Wp, we computed impacts per m² using efficiencies Her: Hertwich et al. [59], Ito: It et al. [73], Kim: Kim et al. [61], Lec: Leccisi et al. [60], Lud: Ludin et al. [71], Mil: Miller et al. [64], dWS: de Wild-Scholten [190], Bos: this Table B-9 System boundaries used in studies for CI(G)S and a-Si thin film panels (including those whose footprints are shown in Figure 4-6). Irr (irradiation) is given used by the study and equation (4-3). n is the number of studies or facilities. Prod (production) is the country of production/manufacturing (EU: Europe, FR: France, GLO: weighted global average, JP: Japan, US: United States, CN: China). EF_{erc} is given in g CO₂-eq/kWh for the entire system (panels + BOS). Ber: Bergesen et al. [68], study (for Bosmans et al.). For our results (Bos) the values represent the median across all facilities of this type, with ranges [5-95" percentiles] in brackets.

			`	-					,	
Ref	CI(G)S	5	r	PR	panel	l _{Bos}	u	Prod	EF _{GHG}	Notes
	ır									
Ber	1,800	30	12.0	0.8				SN	22	TRACI 1.0, ReCiPe 1.08, Ecolnvent 2.2
Her		30	12.0					NS	19.5	From ReCiPe 1.08, Ecolnvent 2.2
lto	1,737-2,344	30	13.0	0.83	116	92	2	FR	39 – 45	20° tilt, range: high-low irr
Kim	1,700-2,400	30	11.5	8.0			_		26 – 37	Harmonized, range: high-low irr
Lec	1,000-2,300	30	14.0	8.0	95	50	_	Ъ	19 – 43	Range: high-low irr
PnJ	1,700 2,017	20	10.0	0.78			2		33 – 57	Literature review
dWS	1,700	30	11.7	0.77	74.2		7	CN CN	21 28	Ecolnvent 2.2
Bos	1,648 [1,065-2,200] <u>a-Si</u>	30	14.1 [12.4-15.8]	0.8 [0.70-0.88]		87.0	73	OTD	44.7 [32.7 – 67.7]	See Table B-5 for I panel Ecolnvent 3.5 GLO for BOS
Kim	1,700-2,400	30	6.3	8.0			-		20 – 29	Harmonized, range: high-low irr
PnJ	1,700 2,017	20	5.5 7.0	0.97			м		27 – 57	Literature review
dWS	1,700	30	7.0	0.77	57.9 81.9		7	EU	35 45	Ecolnvent 2.2
Bos	2,015 [1,196-2,282]	30	7.9 [6.6-9.8]	0.8 [0.80-0.89]		83.3	73	OTS	49.4 [31.1 – 83.8]	See Table B-5 for l _{pinel} Ecolnvent 3.5 GLO for BOS

is given in kWh/m²/yr, LT (lifetime) in years, η (panel efficiency) in %. PR stands for performance ratio (MWac/MWp). Impact I is given in kg CO₂-eq/m² for panels and BOS (mounting structure and electrical components) separately, if provided by the study. If impacts were given per Wp, we computed impacts per m² using Prod (production) is the country of production/manufacturing (CN: China, EU: Europe, FR: France, GE: Germany, GLO: weighted global average, KO: Korea, US: United States). EF_{GHG} is given in g CO₂-eq/kWh for the entire system (panels + BOS). Hou: Hou et al. [63], Hsu: Hsu et al. [54], Ito: Ito et al. [73], K14: Kim et al. [189], Lec: Leccisi Table B-10 System boundaries used in studies for mono-crystalline panels (mono-5i) (including those whose footprints are shown in Figure 4-6). Irr (irradiation) efficiencies used by the study and equation (4-3). For Wetzel and Borchers [66] we used efficiencies of 2014 Table B-1). n is the number of studies or facilities used. et al. [60], Ludi. Ludin et al. [71], Mil: Miller et al. [64], Nia: Nian [62], Wet: Wetzel and Borchers [66], dWS: de Wild-Scholten [190], Yue: Yue et al. [192], Bos: this study (for Bosmans et al.). For our results (Bos) the values represent the median across all facilities of this type, with ranges [5-95th percentiles] in brackets.

Ī

ı

Ref	mono-Si Irr	5	<u>-</u>	PR	panel	l _{Bos}	ء	Prod	EF GHG	Notes
Hou	Hou 1,600	25	17				-	UN	65	Data from literature, visits, surveys
Hsu	Hsu 1,700	30	14.0	0.75, 0.8			13		40	Harmonized
lto	lto 1,737-2,344	30	15.9	0.81	194	70	2	FR	40 – 48	20° tilt, range: high-low irr
Lec	Lec 1,000-2,300	30	17.0	0.8	207 263 287	20	0	EU CN	27 - 82	Range: high irr, EU production – Iow irr, CN production
K14	1,310	30	15.96	8.0	163.5		-	ð	42	Primary data: Korean manufacturers
Pnq	1,200-1,800	25	14.0	0.7			9		36 – 87	Literature review
Mil	1,071-2,295	30	17				10	CN	45 – 91	CN electricity for upstream processes CN & GLO electricity for BOS
Nia	900-2,400	30	22.9	0.8					22 – 112	Range: various manufacturing sites for PV and BOS, and irradiation.
Wet	1,000-1,700	30		0.75	159		_∞	GE	31 – 69	Range: min-max irr and LT, min-max degradation
dWS	1,700	30	14.8	0.75	180.6 415.9		7	EN CN	38 81	Ecolnvent 2.2
Yue	1,700	30	14.0	0.75	199.8 386.7		7	EU	44 79	CLCD v0.8, Ecolnvent 2.2
Bos	1,612 [1,064-2,071]	30	14.6 [13.3-17.4]	0.8 [0.8-0.87]		89.1	450	GLO	82.2 [58.7 – 122.3]	See Table B-5 for I _{parel} Ecolnvent 3.5 GLO for BOS

Table B-11 System boundaries used in studies for poly-crystalline panels (poly-Si) (including those whose footprints are shown in Figure 4-6). See caption of Table B-10 for details. For Wetzel and Borchers [66] we used efficiencies of 2014 (Table B-1). Bey: Beylot et al. [69], Gra: Grant et al. [195], Her: Hertwich et al. [59], Yan: Yang et al. [309].

Ref	poly-Si Irr	5	נ	PR	_ panel	l _{Bos}	ء	Prod	F	Notes
Bey	1,700	30	14.0	0.855					38 – 53	30° tilt, range: various support types in BOS
Gra	1,314-2,810	30	16	0.8	519 255 201		м	CN En CS		Ecolnvent 2019, TRACI, Yao et al. [191]
Her		25	16					NS	57	From ReCiPe 1.08, EcoInvent 2.2
Hou	1,600	25	17				_	S	09	Data from literature, visits, surveys
Hsu	1,700	30	13.2	0.75, 0.8			13		47	Harmonized
lto	1,737-2,344	30	15.0	0.81	155	70	2	Æ	37 – 45	20° tilt, range: high-low irr
K14	1,310	30	14.9	8.0	104.3		_	9	32	Primary data: Korean manufacturers
Lec	1,000-2,300	30	16.0	0.8	132 153 165	20	6	US NS	20 – 56	Range: high irr, EU production – Iow irr, CN production
Pnd	1,200-2,017	25 30	13.9	0.67			0		32 - 89	Literature review
Mil	1,071-2,295	30	16				10	CN GLO	34 – 68	CN electricity for upstream processes CN & GLO electricity for BOS
Nia	900-2,400	30	18.5	0.8					25 – 65	Range: various manufacturing sites for PV and BOS, and irradiation
Wet	1,000	20		0.75	121		∞	æ	25 – 55	Range: min-max irr and LT, max-min degradation
dWS	1,700	30	14.1	0.75	106.7 214.3		2	CN	27 49	Ecolnvent 2.2

Table B-1	Table B-11 Continued									
Ref	poly-Si Irr	5	E .	PR	panel	Bos	۵	Prod	F GHG	Notes
Yao	1,700	30	12.4	0.8			2	N	213 110	Average practice Advanced practice
Yan					448 343 339		м	S		All production in China 52% of silicon imported 52% of Si and other materials imported
Yue	1,700	30	13.2	0.75	160.4 349.6		2	S E	38 76	CLCD v0.8, Ecolnvent 2.2
Bos	1,842 [1,111-2,220]	30	15.4 0.8 [14.4-17.4] [0.74-0.89]	0.8 [0.74-0.89]		88.4	402	OT9	52.1 [35.9 – 80.1]	52.1 See Table B-5 for I panel [35.9 – 80.1] Ecolnvent 3.5 GLO for BOS

Appendix C Appendix for chapter 5

C.1 Abbreviations used in the main article and the Appendix

Table C-1 Abbreviations used in the main article and the Appendix.

Abbreviation	Explanation
α	Trophic state adjustment factor
A _{res}	Reservoir area
ВІС	Bayesian Information Criterion
Во	Boreal climate zone
Chl-a	Chlorophyll-a
ст	Cool temperate climate zone
EF _{CH4,age≤20,j}	$\mathrm{CH_4}$ emission factor of reservoirs younger than 20 years in climate zone j
EF _{CH4,age>20,j}	CH_4 emission factor of reservoirs older than 20 years in climate zone j
EF _{CO2,age≤20,j}	CO ₂ emission factor of reservoirs younger than 20 years in climate zone j
EIA	US Energy Information Administration
F CH4,age≤20,j	Reservoir CH ₄ emissions in the first 20 years of operation in climate zone j
CH4,age>20,j	Reservoir CH_4 emissions after the first 20 years of operation in climate zone j
CH4,downstream	Downstream CH ₄ emissions
CH4,res	Reservoir CH ₄ emissions
CO2	Reservoir CO ₂ emissions
FP _{av}	Average GHG footprint
FP _{GHG}	GHG footprint
GDP	Gross domestic product
GHG	Greenhouse gas
GHG _{av}	Average greenhouse gas emissions
GHG _{tot}	Total greenhouse gas emissions
GWP _{CH4}	Greenhouse gas warming potential of CH_4
h	Dam height
c	Construction impact (kg CO ₂ eq/kWh)
0	Operational impact (kg CO ₂ eq)
D	Identification
PCC	Intergovernmental Panel of Climate Change
	Aggregated climate zone
kWh	Kilowatt hours
L	Large hydropower
LCA	Life cycle assessment
М	Medium hydropower

Table C-1 Continued

Abbreviation	Explanation
ММ	Man-made storage area
MW	Megawatt
MWh	Megawatt hours
n	The number of items in a set
n _{test}	Number of items in test set
n _{train}	Number of items in train set
NID	National Inventory of Dams
NL	Natural storage area
P	Power output
PV	Photovoltaic
q _{av}	Average yearly streamflow
\mathbf{q}_{cv}	Yearly streamflow seasonality
\mathbf{q}_{max}	Maximum yearly streamflow
\mathbf{q}_{\min}	Minimum yearly streamflow
R ² _{test}	R ² of test set
R ² train	R ² of training set
R_d	Fraction of downstream emissions
res	Reservoir plant
RMSE _{test}	Root mean square error of the test set
RMSE _{train}	Root mean square error of the training set
ror	Run-of-river plant
S	Small hydropower
T d/m	Temperate dry/montane climate zone
T m/w	Temperate moist/wet climate zone
WT d	Warm temperate dry climate zone
WT m	Warm temperate montane climate zone

C.2.1 Operating-phase emissions

Storage areas that have just recently been constructed (less than 20 years ago) emit both CO_2 and CH_4 . Storage areas that are older than 20 years are considered to emit only CH_4 in these later years [221]. Annual CO_2 emissions for the first 20 years of a storage area's life are calculated as follows:

$$F_{CO_2} = A_{res} \cdot EF_{CO_2,age \le 20,j}$$
 (C-1)

Annual CH₄ emissions from storage areas during their first 20 years can be calculated according to:

$$F_{CH_4,age\leq20,j} = F_{CH_4,res} + F_{CH_4,downstream}$$

$$F_{CH_4,res} = \alpha \cdot (EF_{CH_4,age\leq20,j} \cdot A_{res})$$

$$F_{CH_4,downstream} = \alpha \cdot (EF_{CH_4,age\leq20,j} \cdot A_{res}) \cdot R_d$$

$$F_{CH_4,age\leq20,j} = (\alpha \cdot (EF_{CH_4,age\leq20,j} \cdot A_{res})) \cdot (1 + R_d)$$
(C-2)

Annual CH₄ emissions from storage areas after their first 20 years are then calculated using:

$$F_{CH_4,age>20,j} = F_{CH_4,res} + F_{CH_4,downstream}$$

$$F_{CH_4,res} = \alpha \cdot (EF_{CH_4,age>20,j} \cdot A_{res})$$

$$F_{CH_4,downstream} = \alpha \cdot (EF_{CH_4,age>20,j} \cdot A_{res}) \cdot R_d$$

$$F_{CH_4,age>20,j} = (\alpha \cdot (EF_{CH_4,age>20,j} \cdot A_{res})) \cdot (1 + R_d)$$
(C-3)

These equations can be combined to give equation (C-4). It is important to note that because we assume a 100-year lifetime of the hydropower facility and equation (C-1) and (C-2) only apply to storage areas younger than 20 years and equation (C-3) only applies to storage areas older than 20 years, they are multiplied by 0.2 and 0.8, respectively, to represent emissions over the entire 100-year storage area lifetime.

$$\begin{split} GHG &= \left(F_{CH_4,age \leq 20,j} \cdot 0.2 + F_{CH_4,age \geq 20,j} \cdot 0.8\right) + F_{CO_2} \cdot 0.2 \\ &= \left(\left(\left(\alpha \cdot EF_{CH_4,age \leq 20,j} \cdot A_{res}\right) \cdot (1+R_d)\right) \cdot 0.2 + \left(\left(\alpha \cdot \left(EF_{CH_4,age \geq 20,j} \cdot A_{res}\right)\right) \cdot (1+R_d)\right) \\ &\quad \cdot 0.8\right) \cdot GWP_{CH_4} + A_{res} \cdot EF_{CO_2,age \leq 20,j} \cdot 0.2 \\ &= A_{res} \cdot \left(\left(EF_{CH_4,age \leq 20,j} \cdot 0.2 + EF_{CH_4,age \geq 20,j} \cdot 0.8\right) \cdot \alpha \cdot GWP_{CH_4} \cdot (1+R_d) + EF_{CO_2,age \leq 20,j} \cdot 0.2\right) \end{split}$$

(C-4)

The emission factors used for the calculations are aggregated in Table C-2. Trophic state adjustment factors α are listed in Table C-3.

Table C-2 Emission factors for different climate zones as used in equations (C-1) to (C-4) [221].

Aggregated climate zone	j	CH ₄ (≤20y, kg CH ₄ /ha/yr)	CH₄ (>20y, kg CH ₄ /ha/yr)	CO₂ (≤20y, t CO ₂ /ha/yr)
Boreal	1	13.6	27.7	0.94
Cool temperate	2	54.0	84.7	1.02
Warm temperate/dry	3	150.9	195.6	1.70
Warm temperate/moist	4	80.3	127.5	1.46
Tropical dry/montane	5	283.7	392.3	2.95
Tropical moist/wet	6	141.1	251.6	2.77

Table C-3 Trophic state adjustment factors based on the chlorophyll concentration (Chl-a, in g/L) and related trophic class, adapted from [221].

Trophic class	Chl-a	Average trophic state
	(g/L)	adjustment factor
Oligotrophic	0 – 2.6	0.7
Mesotrophic	2.6 – 20	3
Eutrophic	20 – 56	10
Hypereutrophic	56 - >155	25

C.2.2 Construction-phase emissions

Construction phase emissions in this study are based on the classification from Kadiyala et al. [219], who have grouped hydropower facilities according to type (res: reservoir; ror: run-of-river) and capacity (S – less than 0.1 MW; M – 0.1 to 30 MW; L – more than 30 MW). GHG emissions in g CO_3 eq/kW are shown in Table C-4.

Table C-4 Classification table of hydropower facilities adapted from Kadiyala et al. [219].

Dam type	Number of facilities in the dataset in [219]	GHG emissions (g CO ₂ /kW)
res-M	24	21.05 (±6.25)
res-L	8	40.63 (±80.57)
ror-S	3	47.82 (±34.53)
ror-M	133	27.18 (±10.38)
ror-L	3	3.45 (±1.43)

When information on the capacity was not available, we used weighted averages of the GHG emission factors based on the facilities for which information was available as follows:

Reservoir facility of unknown capacity:

$$EF_{res,unknown} = \frac{EF_{res,L} \cdot frac_{res,L} + EF_{res,M} \cdot frac_{res,M}}{2}$$
(C-5)

Run-of-river facility of unknown capacity:

$$EF_{ror,unknown} = \frac{EF_{ror,L} \cdot frac_{ror,L} + EF_{ror,M} \cdot frac_{ror,M} + EF_{ror,S} \cdot frac_{ror,S}}{3}$$
(C-6)

Unknown mode of operation with medium capacity:

$$EF_{unknown,M} = \frac{EF_{res,M} \cdot frac_{res,M} + EF_{ror,M} \cdot frac_{ror,M}}{2}$$
(C-7)

Unknown mode of operation with large capacity:

$$EF_{unkown,S} = EF_{ror,S}$$
 (C-8)

Unknown mode of operation of unknown capacity:

$$EF_{unknown} = \frac{EF_{res,unknown} \cdot frac_{res} + EF_{ror,unknown} \cdot frac_{ror}}{2}$$
(C-9)

C.3 Data preparation

Different databases have been combined in this study, namely the National Inventory of Dams (NID) [214], HydroLAKES [223] and the EIA [163]. The main database is the NID. Information from the other databases has been added to the NID as needed. Climate zone information has been added to the NID using OIGS. An IPCC climate zones map has been overlayed with the hydropower facilities' database and matched by location. HydroLAKES has been added to the NID using an algorithm that matches the two databases based on reported latitudes and longitudes of the pour points in HydroLAKES and the hydropower facility location in NID using an implementation of the Haversine formula:

$$d = 12742 \cdot arcsin\left(\left(0.5 \cdot \frac{cos((lat_2 - lat_1) \cdot p)}{2} + cos(lat_1 \cdot p) \cdot cos(lat_2 \cdot p)\right) \cdot \frac{1 - cos((long_2 - long_1) \cdot p)}{2}\right)^{\frac{1}{2}}$$
(C-10)

C.4 Imputation of electricity generation data

C.4.1 Defining streamflow seasonality

Since the database FLO1K [217] provides maximum, minimum and average streamflow values for each year at each 30 arcmin grid-cell, we calculated the yearly streamflow seasonality q_{cv} as

$$q_{cv} = \frac{q_{max} - q_{min}}{q_{av}} \tag{C-11}$$

where q_{av} is the average yearly streamflow and q_{max} and q_{min} are the maximum and minimum yearly streamflow.

C.4.2 Sampling of flow data

Prior to sampling streamflow data from FLO1K to obtain average, maximum and minimum yearly streamflow values at the hydropower facility locations, we snapped the facilities to the hydrological network of FLO1K. This was done to avoid sampling from the wrong locations due to the discrepancy between the reported geo-coordinates in the NID dataset and the location of the actual river according to the arcseconds river network of FLO1K [217]. We used the upstream catchment area reported in the NID database to snap the locations to the river network. We used the FLO1K sampler tool provided at https://github.com/vbarbarossa/flo1k_sampler.

C.4.3 Model development

Key information of the model development process is given in the following figures and tables. The model selection ranking for the power output calculation is given in Table C-5, with the best model printed in bold. Figure C-1 and Figure C-2 show the distributions of the predictor and response variables respectively before and after transformation. Figure C-3 depicts the correlation matrix of the variables after transformation. Finally, Table C-6 and Table C-7 show the ten-fold cross-validation across all observations and across hydropower facilities, respectively.

Table C-5 Model selection ranking for the power output calculation. The best models for each set of predictors (≥3) are summarized. The final model used for the conditional R?; I: intercept; GDP: average GDP of the administrative unit connected to the hydropower plant; h: dam height; A....; total surface area of the reservoir; qa.. imputation, which represents the least complex model among the first 10 BIC points, is highlighted in bold. No: number of predictors; R² and R²: the marginal and yearly average streamflow; q_{cv}; yearly streamflow seasonality.

q _w :h	0.05	0.05	0.05	0.05	0.04	0.05	0.05	0.06	0.05	1											
A _{res} :h	,	,		,		,	0.04	0.03	0.03	,											
GDP	,	,		,	-0.02	1	1	1	1	ı											
ď	,	,		-0.01		-0.01	-0.01	-0.01	-0.01	,	GDP:q _{cv}				,		-0.01	0.00	0.00	0.00	,
ďav	0.39	0.39	0.39	0.38	0.38	0.37	0.38	0.38	0.37	0.40	GDP:q _{av}	0.03	0.03		0.03	0.03		0.03	0.03	0.03	
Ares	,	,		1		0.03	1	0.02	,	1	q _{cv} :q _{av}	-0.02	-0.02	-0.02	-0.02	-0.02	-0.02	-0.02	-0.02	-0.02	,
ح	0.55	0.55	0.55	0.55	0.55	0.53	0.54	0.54	0.55	0.55	GDP:A _{res}		1		1			-0.01		0.01	-0.01
_	-0.03	-0.03	-0.03	-0.03	-0.04	-0.03	-0.05	-0.05	-0.05	-0.01	q _{cv} :A _{res}		,		,			,	,	0.01	,
R,	0.95	0.95	0.95	0.95	0.95	0.95	0.95	0.95	0.95	0.95	q _{av} :A _{res}				0.01	0.01	0.01	0.01	,	0.02	
R ²	0.61	0.62	0.62	0.61	0.62	0.62	0.62	0.62	0.62	09:0	GDP:h		-0.04		,	-0.04	-0.04	,	-0.03	-0.04	
BIC	-1318	-1315	-1313	-1306	-1300	-1284	-1283	-1276	-1271	-1256	d:^b				1				0.00		,
No	5	9	4	7	∞	6	10	11	12	3	No	2	9	4	7	∞	6	10	11	12	33

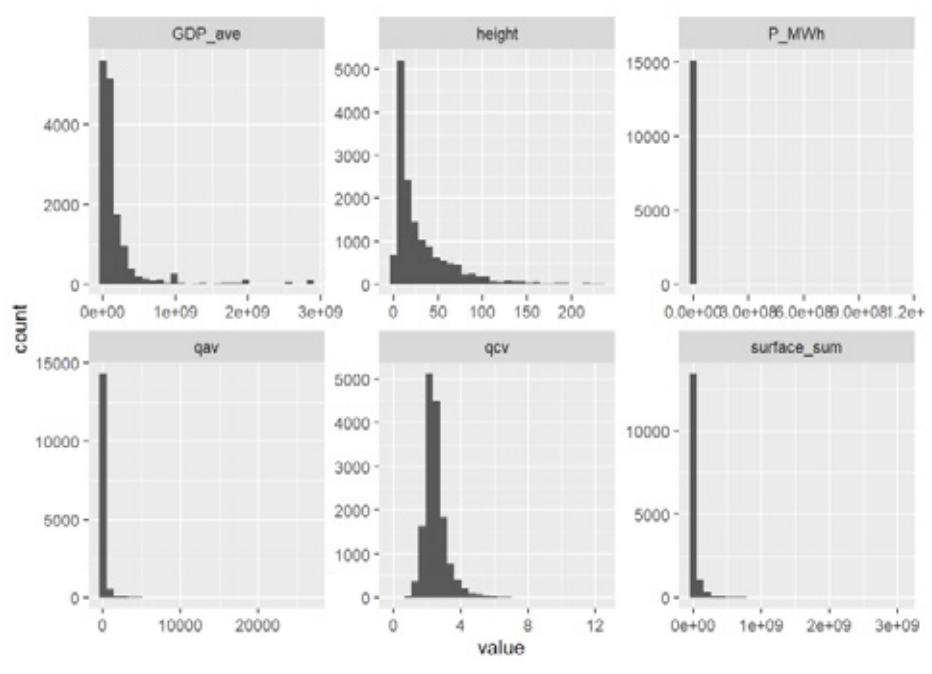


Figure C-1 Histogram of predictor and response variables used in the linear mixed effect model. GDP_{ave} : average GDP of the administrative unit connected to the hydropower plant; height: dam height; P_{MWh} : yearly electricity generated in MWh; q_{av} : yearly average streamflow; q_{cv} : yearly streamflow seasonality; surface s_{uum} : total surface area of the reservoir.

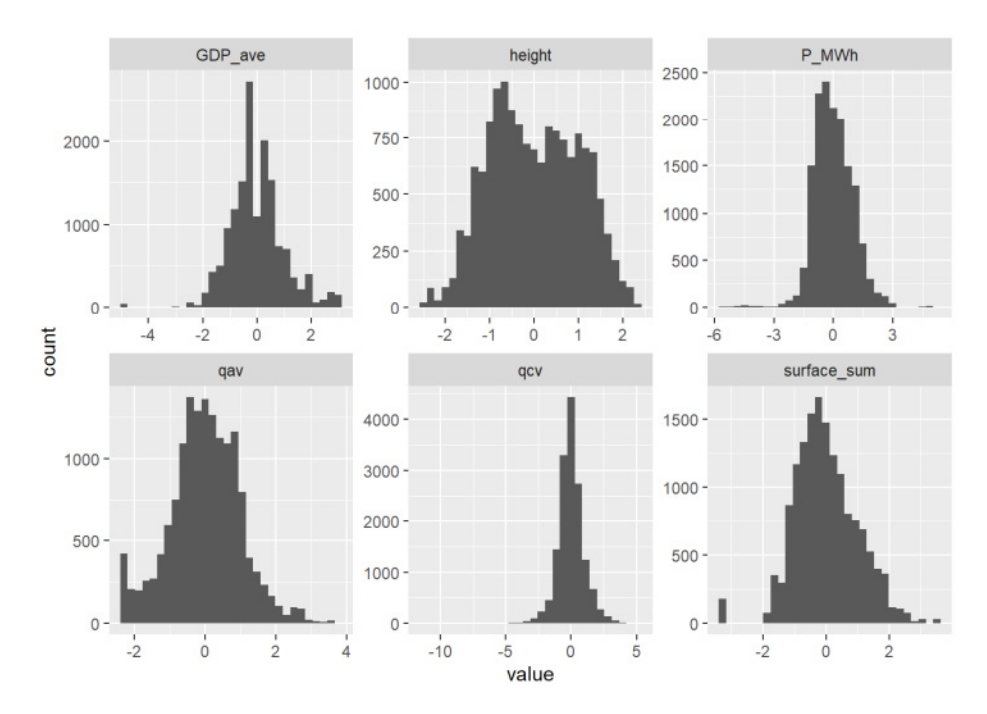


Figure C-2 Histogram of transformed predictor and response variables used in the linear mixed effect model. P_{MWh} was log-transformed, while the other variables were transformed according to a Yeo-Johnson transformation. All variables were standardized to mean 0 and standard deviation 1. GDP_{avg} : average GDP of the administrative unit connected to the hydropower plant; height: dam height; P_{MWh} : yearly electricity generation in MWh; q_{av} : yearly average streamflow; q_{cv} : yearly streamflow seasonality; surface s_{sum} : total surface area of the reservoir.

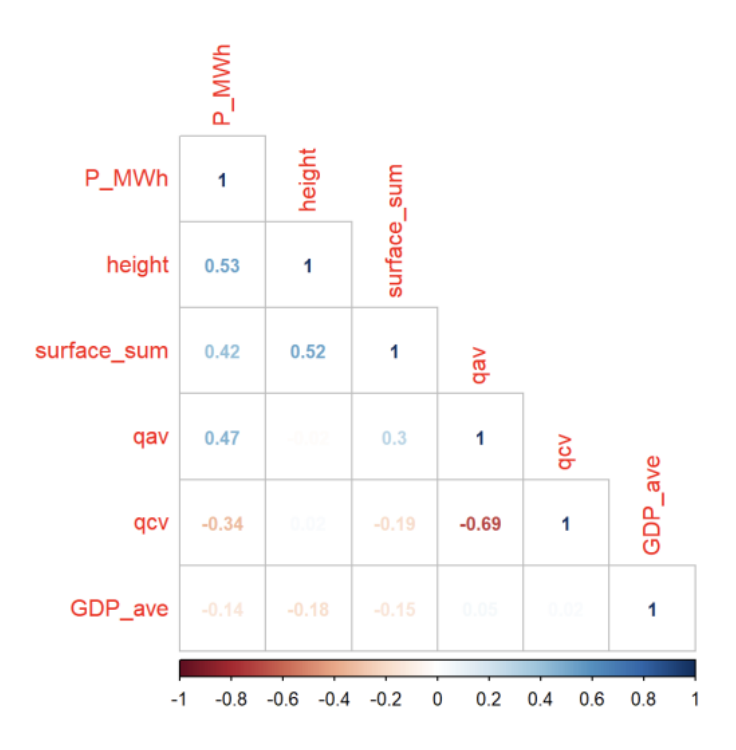


Figure C-3 Correlation matrix of the transformed model variables. Correlation is expressed as Pearson's r. GDP_{ave} : average GDP of the administrative unit connected to the hydropower plant; height: dam height; P_{MWh} : yearly electricity generated in MWh; q_{av} : yearly average streamflow; q_{cv} : yearly streamflow seasonality; surface q_{cv} : total surface area of the reservoir.

Table C-6 Ten-fold cross-validation across all observations. For each fold, 10% of the total observations (i.e. hydropower facilities \cdot year) are in the test set. Number of observations (n), coefficient of determination (R²) and Root Mean Square Error (RMSE) are reported for train and test sets.

n _{train}	n _{test}	R ² train	R ² test	RMSE _{train}	RMSE _{test}
12865	1430	0.95	0.95	0.19	0.20
12866	1429	0.95	0.95	0.19	0.20
12866	1429	0.95	0.94	0.19	0.22
12864	1431	0.95	0.94	0.19	0.22
12866	1429	0.95	0.94	0.19	0.22
12865	1430	0.95	0.95	0.19	0.21
12865	1430	0.95	0.95	0.19	0.20
12866	1429	0.95	0.95	0.19	0.21
12866	1429	0.95	0.95	0.19	0.20
12866	1429	0.95	0.95	0.19	0.21

Table C-7 Ten-fold cross-validation across hydropower facilities. For each fold, 10% of the power plants are in the test set. Number of observations (n), coefficient of determination (R2) and Root Mean Square Error (RMSE) are reported for train and test sets.

n _{train}	n _{test}	R ² train	R ² test	RMSE _{train}	RMSE _{test}
12899	1396	0.95	0.62	0.19	0.53
12971	1324	0.95	0.73	0.19	0.47
12625	1670	0.95	0.65	0.19	0.53
13044	1251	0.95	0.74	0.20	0.44
12809	1486	0.95	0.75	0.19	0.49
12404	1891	0.95	0.68	0.19	0.49
12974	1321	0.95	0.72	0.19	0.53
12921	1374	0.95	0.64	0.19	0.51
12999	1296	0.95	0.64	0.19	0.54
13009	1286	0.95	0.69	0.19	0.51

C.5 Results

Table C-8 shows the underlying data for Figure 5-4 and Figure 5-5. The GHG footprints of hydropower facilities classified as having a man-made storage area are shown in Figure C-4. Those facilities being classified as having a natural storage area are shown in Figure C-5. Finally, yearly electricity generation is shown in Figure C-6.

Table C-8 The medians, 5th percentile, 95th percentile and number of hydropower facilities in each category depicted in Figure 5-4, Figure 5-5, Figure C-4 and Figure C-5.

Climate zone	Number of dams	Type of storage area	Median (kg CO ₃ eq/kWh)	5 th percentile (kg CO ₃ eq/kWh)	95 th percentile (kg CO ₃ eq/kWh)
Boreal	5	Natural	1.4·10 ⁻²	5.6·10 ⁻³	4.1·10 ⁻²
	4	Man-made	1.1·10 ⁻²	6.0·10 ⁻³	2.7·10-2
Cool temperate	935	Natural	2.6·10 ⁻²	5.6·10 ⁻³	5.9·10 ⁻²
	342	Man-made	5.5·10 ⁻²	7.5·10 ⁻³	2.6
Tropical dry/	9	Natural	8.4·10 ⁻²	4.2·10-2	1.2
montane	17	Man-made	3.8	8.4·10 ⁻¹	27.4
Tropical	15	Natural	6.6·10 ⁻³	5.7·10 ⁻³	7.3·10 ⁻²
moist/wet	15	Man-made	1.3·10 ⁻¹	7.4·10 ⁻³	11.4
Warm	34	Natural	2.7·10 ⁻²	4.8·10 ⁻³	1.5·10 ⁻¹
temperate dry	55	Man-made	2.9·10 ⁻¹	2.1.10-2	4.6
Warm temperate	182	Natural	2.8·10 ⁻²	4.2·10-2	5.7·10 ⁻²
moist	199	Man-made	1.1.10-1	6.1.10-3	1.6
All climate zones	1,180	Natural	2.6·10 ⁻²	5.6·10 ⁻³	6.5·10 ⁻²
	632	Man-made	7.9·10 ⁻²	6.4·10 ⁻³	4.3

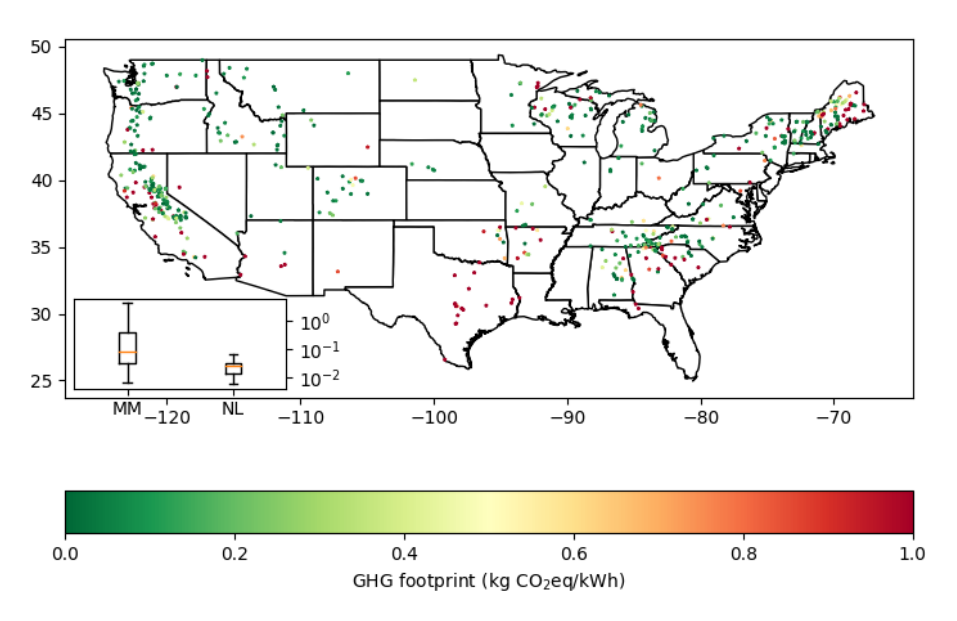


Figure C-4 GHG footprint (kg CO_2 eq/kWh) of facilities classified as having a man-made storage area in the US. For reference, the boxplot shows the distribution of GHG footprints of man-made storage areas (MM) and natural ones (NL). The orange line represents the median, the boxes the 25-75th percentile and the whiskers the 5-95th percentiles.

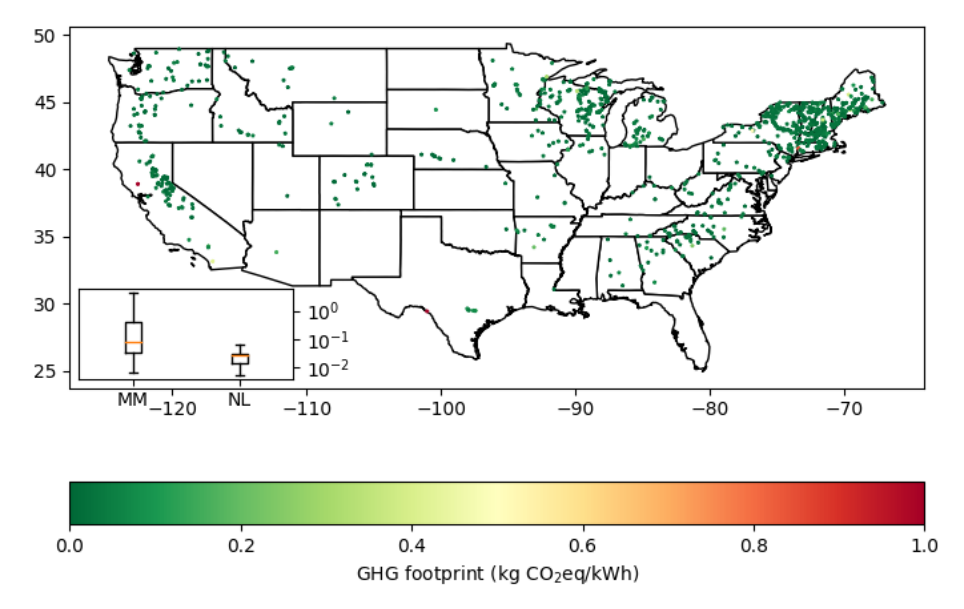


Figure C-5 GHG footprint (kg CO_2 eq/kWh) of hydropower facilities in the US classified as having a natural storage area. For reference, the boxplot shows the distribution of GHG footprints of man-made storage areas (MM) and natural ones (NL). The orange line represents the median, the boxes the 25-75th percentile and the whiskers the 5-95th percentiles.

Comparison of electricity generation

We compared the average yearly electricity generation calculated by Turner et al. [243] with the average yearly electricity generation calculated in our study. The results are shown in Figure C-6. We see a very good fit with the exception of two extreme outliers. Data has been matched by hydropower facility name and state, because no other overlapping information was available in the two databases, which could explain the outliers as they may be two different facilities with the same name in the same state. Another possible explanation is that facilities have been combined differently between the two databases.

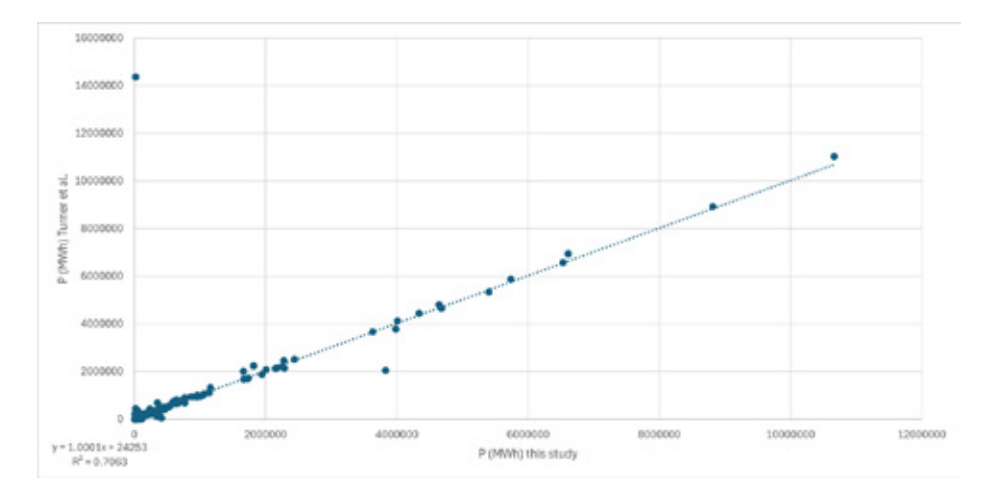


Figure C-6 Comparison of average yearly electricity production in Turner et al. [243] and this study.



End matter

Summary

Fossil fuels have been the world's primary power source since the industrial revolution. The large-scale use of these fossil fuels has led to a tremendous increase of greenhouse gasses (GHGs) in the atmosphere, and in turn has become a key driver of climate change. In order to reduce climate change, cleaner alternative energy sources have been developed. For electricity production, this includes different types of wind, solar and hydropower.

Many studies quantified the GHG footprints of wind, solar and hydropower. However, integrating spatial, temporal and technical variation into one assessment has not been done at larger spatial scales. Such an assessment adds value because it enables policy makers and developers to easily assess differences in GHG performance between either different technologies in the same location or the same technology in multiple locations. Furthermore, the comparison to other (non-)renewable electricity sources offers the possibility to determine how much can be gained in terms of GHG emission mitigation at each location. This thesis aims to provide a basis for such an assessment by developing models that allow for easy calculation of the GHG footprints of the most important non-biomass renewable electricity sources at facility level, using a key set of technological and meteorological variables.

Chapter 2 describes the space, time and size dependencies of the greenhouse gas payback times of wind turbines in Northwestern Europe. The net greenhouse gas benefits of wind turbines compared to their fossil energy counterparts depend on location-specific wind climatology and the turbines' technological characteristics. Assessing the environmental impact of individual wind parks requires a universal but location-dependent method. Here, the greenhouse gas pay-back time for 4,161 wind turbine locations in northwestern Europe was determined as a function of (i) turbine size and (ii) spatial and temporal variability in wind speed. A highresolution wind atlas (hourly wind speed data between 1979 and 2013 on a 2.5 by 2.5 km grid) was combined with a regression model predicting the wind turbines' life cycle greenhouse gas emissions from turbine size. The greenhouse gas payback time of wind turbines in northwestern Europe varied between 1.8 and 22.5 months. averaging 5.3 months. The spatiotemporal variability in wind climatology has a particularly large influence on the payback time, while the variability in turbine size is of lesser importance. Applying lower-resolution wind speed data (daily on a 30 by 30 km grid) approximated the high-resolution results well.

Chapter 3 then covers the variability in GHG footprints of the global wind farm fleet. While it is known that technological characteristics largely determine the greenhouse gas (GHG) emissions during the construction of a wind farm and meteorological circumstances the actual electricity production, a thorough analysis to quantify the GHG footprint variability (in g CO₂eg/kWh electricity produced) between wind farms is still lacking at the global scale. Here, we quantified the GHG footprint of 26,821 wind farms located across the globe, combining turbinespecific technological parameters, life cycle inventory data, and location- and temporal-specific meteorological information. These wind farms represent 79% of the 651 GW global wind capacity installed up until 2019. Our results indicate a median GHG footprint for global wind electricity of 10 g CO_seg/kWh, ranging from 4 to 56 g CO₂eg/kWh (2.5th and 97.5th percentiles). Differences in the GHG footprint of wind farms are mainly explained by spatial variability in wind speed, followed by whether the wind farm is located onshore or offshore, the turbine diameter, and the number of turbines in a wind farm. I also provided a metamodel based on these four predictors for users to be able to easily obtain a first indication of GHG footprints of new wind farms.

In Chapter 4, the GHG footprints of utility-scale PV facilities on a global scale are covered. Technological characteristics and meteorological conditions are major determinants of the greenhouse gas (GHG) footprints of photovoltaic facilities. By accounting for technological and meteorological differences, we quantified the GHG footprints of 9,992 utility-scale photovoltaic facilities worldwide. We obtained a median greenhouse gas footprint of 58.7 g CO₂eq/kWh, with a 3-fold spread (28.2-94.6 g CO₃eg/kWh, 2.5th and 97.5th percentiles). Differences in panel type appeared to be the most important determinant of variability in the GHG footprint, followed by irradiation and a facility's age. We also provided a metamodel based on these three predictors for users to determine the facility-specific greenhouse gas footprint. The total cumulative electricity produced by the utility-scale photovoltaic fleet computed in our study is 457 TWh/yr, 99.6% of which is produced at footprints below 100 g CO₂eq/kWh.

Chapter 5 describes the variability of GHG footprints of hydropower in the United States of America (US). Hydropower is the largest source of renewable energy in the US. While it is generally considered to be a low-carbon electricity source, technological and regional differences can lead to large variations in hydropower's GHG footprints. Here, I quantified greenhouse gas footprints of 1,812 individual hydropower facilities in the US, accounting for facility-specific differences in electricity production as well as differences in life cycle GHG emissions during the

construction and operation of the hydropower facility. I found that the GHG footprint of hydropower facilities in the US range from $5.6\cdot10^{-3}$ to $1.1~\rm kg~CO_2eq/kWh~[5-95^{th}~percentile]$, with a median of $2.8\cdot10^{-2}~\rm kg~CO_2eq/kWh$. My results show that the GHG footprint of hydropower with natural storage areas is systematically lower compared to man-made storage areas. Variation in GHG footprints of hydropower from man-made storage areas can be large and is mainly caused by differences in size, trophic state and climate zone.

Finally, **chapter 6** reflected on the lessons learned. Starting from in-depth analyses, metamodels for wind and solar power were developed to predict GHG footprints at the facility-level with a minimum of information. Using in-depth analysis first helped to understand the limitations of simplifications and approximations made in the metamodels. The metamodels allow for an easier comparison of GHG footprints for specific technologies at distinct locations, which is important because it offers the possibility to determine how much can be gained in terms of GHG emission mitigations when comparing different (non-)renewable electricity sources. It also offers the potential to develop a tool that supports decision makers which electricity generation technology is best suited at a certain location to minimize environmental impacts and trade-offs.

Samenvatting

Fossiele brandstoffen zijn sinds de industriële revolutie de belangrijkste energiebron ter wereld. Het grootschalige gebruik van deze fossiele brandstoffen heeft geleid tot een enorme toename van broeikasgassen (BKG's) in de atmosfeer, wat op zijn beurt een belangrijke aanjager van klimaatverandering is geworden. Om die klimaatverandering tegen te gaan, zijn schonere alternatieve energiebronnen ontwikkeld. Voor de productie van elektriciteit gaat het om verschillende soorten wind- en zonneenergie en waterkracht.

Er zijn al veel studies uitgevoerd die de klimaatvoetafdruk van wind-, zonne- en waterkrachtbronnen hebben berekend. Het integreren van ruimtelijke, temporele en technische variatie in één beoordeling is echter niet gedaan op grotere ruimtelijke schaal. Een dergelijke beoordeling voegt waarde toe omdat het beleidsmakers en ontwikkelaars in staat stelt om eenvoudig verschillen in broeikasgasuitstoot te beoordelen tussen verschillende technologieën op dezelfde locatie of dezelfde technologie op verschillende locaties. Bovendien biedt de vergelijking met andere (niet-)hernieuwbare elektriciteitsbronnen de mogelijkheid om te bepalen hoeveel reductie aan broeikasgasuitstoot op elke locatie kan worden gerealiseerd. Dit proefschrift heeft tot doel een basis te bieden voor een dergelijke beoordeling door modellen te ontwikkelen die het mogelijk maken om eenvoudig de klimaatvoetafdruk van de belangrijkste hernieuwbare energiebronnen op iedere locatie te berekenen.

Hoofdstuk 2 beschrijft de ruimtelijke, temporele en technologische variatie in de terugverdientijden van broeikasgassen van windturbines in Noordwest-Europa. De netto broeikasgasvoordelen van windturbines in vergelijking met hun fossiele tegenhangers zijn afhankelijk van de locatiespecifieke windklimatologie en de technologische kenmerken van de turbines. Het beoordelen van de milieuimpact van individuele windparken vereist een universele, maar tegelijkertijd locatieafhankelijke methode. In dit hoofstuk is de terugverdientijd van broeikasgassen voor 4 161 windturbinelocaties in Noordwest-Europa bepaald als functie van (i) turbinegrootte en (ii) ruimtelijke en temporele variabiliteit in windsnelheid. Een windatlas met hoge resolutie (gegevens over de windsnelheid per uur tussen 1979 en 2013 op een raster van 2,5 bij 2,5 km) is gecombineerd met een regressiemodel dat de broeikasgasemissies van productie van de windturbines voorspelt op basis van de grootte van de turbines. De terugverdientijd van windturbines in Noordwest-Europa varieerde tussen de 1,8 en 22,5 maanden en is gemiddeld 5,3 maanden. De spatiotemporele variabiliteit in de windklimatologie heeft een bijzonder grote invloed op de terugverdientijd, terwijl de variabiliteit in turbinegrootte van minder belang is. Het toepassen van windsnelheidsgegevens met een lagere resolutie (dagelijks op een raster van 30 bij 30 km) benaderde de resultaten met hoge nauwkeurigheid.

Hoofdstuk 3 behandelt vervolgens de variabiliteit in klimaatvoetafdruk van windparken wereldwijd. Hoewel al bekend is dat technologische kenmerken grotendeels bepalend zijn voor de uitstoot van broeikasgassen tijdens de bouw van een windpark en meteorologische omstandigheden voor de werkelijke elektriciteitsproductie, ontbreekt een grondige analyse om de variabiliteit van de klimaatvoetafdruk (in g CO₂eg/kWh geproduceerde elektriciteit) tussen windparken te kwantificeren. Ik heb de klimaatvoetafdruk van 26 821 windparken over de hele wereld gekwantificeerd, waarbij ik turbinespecifieke techno-logische parameters, een inventarisatie van informatie over het materiaalgebruik gedurende de levenscyclus en locatie- en temporele specifieke meteorologische informatie combineerde. Deze windparken vertegenwoordigen 79% van de 651 GW wereldwijde windcapaciteit die in 2019 operationeel was. De resultaten laten een mediane klimaatvoetafdruk voor wereldwijde windelektriciteit van 10 g CO₂eq/kWh zien, variërend van 4 tot 56 g CO₃eq/kWh (2,5e en 97,5e percentiel). Verschillen in de klimaatvoetafdruk van windparken worden voornamelijk verklaard door ruimtelijke variabiliteit in windsnelheid, gevolgd door of het windpark op land of op zee ligt, de turbinediameter en het aantal turbines in een windpark, lk heb ook een metamodel ontwikkeld waarmee op basis van deze vier predictoren de klimaatvoetafdruk van nieuwe windparken kan worden berekend.

In **hoofdstuk 4** worden de klimaatvoetafdrukken van zonneparken wereldwijd behandeld. Technologische kenmerken en meteorologische omstandigheden zijn belangrijke bepalende factoren voor de klimaatvoetafdruk van zonneparken. Door rekening te houden met technologische en meteorologische verschillen, heb ik de klimaatvoetafdruk van 9 992 zonneparken wereldwijd gekwantificeerd. De mediane klimaatvoetafdruk van deze zonneparken is 58,7 g CO₂eq/kWh, met een 3-voudige spreiding (28,2-94,6 g CO₂eq/kWh, 2,5° en 97,5° percentiel). Verschillen in paneeltype bleken de belangrijkste bepalende factor te zijn voor de variabiliteit in de klimaatvoetafdruk, gevolgd door zonne-instraling en de leeftijd van een zonnepark. Ik heb ook een metamodel op basis van deze drie predictoren beschikbaar gesteld voor gebruikers om de klimaatvoetafdruk per zonnepark te bepalen. De totale cumulatieve elektriciteit die wereldwijd door de zonneparken, die zijn meegenomen in deze studie, wordt geproduceerd, bedraagt 457 TWh/jaar, waarvan 99,6% wordt geproduceerd met een voetafdruk van minder dan 100 g CO₂eq/kWh.

Hoofdstuk 5 beschrijft de variabiliteit van de klimaatvoetafdruk van waterkracht in de Verenigde Staten van Amerika (VS). Waterkracht is de grootste bron van hernieuwbare energie in de VS. Hoewel het over het algemeen wordt beschouwd als een koolstofarme elektriciteitsbron, kunnen technologische en regionale verschillen leiden tot grote variaties in de klimaatvoetafdruk van waterkracht. Hier heb ik de klimaatvoetafdruk van 1 812 individuele waterkrachtcentrales in de VS gekwantificeerd, waarbij ik rekening heb gehouden met locatiespecifieke verschillen in elektriciteitsproductie en verschillen in broeikasgasemissies gedurende de levenscyclus van de waterkrachtcentrale (de bouw en het gebruik). De klimaatvoetafdruk van waterkrachtcentrales in de VS varieert van 5,6·10⁻³ to 1,1 kg CO₂eg/kWh [5-95e percentiel], met een mediaan van 2,8·10⁻² kg CO₂eg/kWh. Miin resultaten tonen aan dat de klimaatvoetafdruk van waterkrachtcentrales zonder door de mens gemaakte reservoirs lager is in vergelijking met door de mens gemaakte reservoirs. De variatie in de klimaatvoetafdruk van waterkracht uit door de mens ge-maakte reservoirs kan groot zijn en wordt voornamelijk veroorzaakt door verschillen in grootte, nutrient-status en klimaatzone.

In hoofdstuk 6 reflecteer ik op de geleerde lessen. Op basis van gedetaillerde analyses werden metamodellen voor wind en zonneenergie ontwikkeld om de klimaatvoetafdruk op faciliteitsniveau te voorspellen met een minimum aan informatie. De eerst uitgevoerde gedetaillerde analyses hielpen bij het begrijpen van de beperkingen van de vereenvoudigingen en benaderingen in de metamodellen. De ontwikkelde metamodellen maken het mogelijk om de klimaatvoetafdruk gemakkelijker te vergelijken voor specifieke technologieën op verschillende locaties, wat belangrijk is omdat het de mogelijkheid biedt om te bepalen hoeveel broeikasgasreductie kan worden behaald bij het vergelijken van verschillende (niet-)hernieuwbare elektriciteitsbronnen. Daarnaast vormt dit een basis om een instrument te ontwikkelen dat besluitvormers ondersteunt bij de keuze voor elektriciteitsopwekking op een bepaalde locatie op basis van milieueffecten.

Research Data Management

This thesis research has been carried out under the RDM policy of the Radboud Institute for Biological and Environmental Sciences, version 9-Jan-2025 accessed at www.ru.nl/ribes.

The data used in this thesis can be accessed from the following links:

Chapter 1: No data has been produced.

Chapter 2: The wind farm-specific technological characteristics and locations from The WindPower.net are proprietary and can be obtained from https:// www.thewindpower.net/. The wind data used can be obtained for free from the KNMI (http://www.knmiprojects.nl/projects/knw-atlas).

Chapter 3: Underlying data for the figures is available at the journal: https:// onlinelibrary.wiley.com/action/downloadSupplement?doi=10.1111%2Fjiec.13325& file=iiec13325-sup-0002-SuppMatS2.xlsx.

The wind farm-specific technological characteristics and locations from The WindPower.net are proprietary and can be obtained from https://www.thewindpower. net/. The climate data used in this study can be obtained from the Copernicus Climate Change Service (https://cds.climate.copernicus.eu/cdsapp#!/home) for free.

Chapter 4: The facility-specific technological characteristics and locations from Wiki-Solar are proprietary and can be obtained from https://wiki-solar.org. The continent-specific market shares by origin countries are also proprietary, and can be obtained through https://www.marketreportsworld.com/TOC/12344406#TOC. We used Chapter 8 (Global Solar Photovoltaic (PV) Market Analysis, by Geography) (http://www.marketreportsworld.com/TOC/12344406#TOC). The climate data used in this study can be obtained from the Copernicus Climate Change Service (https:// cds.climate.copernicus.eu/cdsapp#!/home) for free. We used ERA5's hourly single level data.

Chapter 5: Data will be made openly available upon publication. Now key supporting information is added as Appendix C in this thesis.

Chapter 6: No data has been produced.

Acknowledgements

Embarking on this PhD journey has been both a challenging and rewarding experience, and it would not have been possible without the support and guidance of many people. First and foremost, my gratitude goes out to my supervisors, Mark and Joyce, without whom I would not have been able to complete this journey. Your expertise, knowledge, patience and insightful feedback have helped shape this thesis and have been invaluable

I am also thankful to my colleagues at the Department of Environmental Science who have made this experience so much more complete. I am grateful to everyone who contributed, directly or indirectly, to this research. Your generosity and kindness have helped me reach this milestone, and I am sincerely appreciative of your part in this journey.

To my family and friends, special thanks for your unwavering support and belief in me. Manuel, thanks for helping me with the thousands of coding questions I bothered you with. Johannes, I am grateful that you were there for me in the long last months until this thesis was finally sent out to the printer. All my former colleagues at Manege De Veerkracht: Thanks for keeping me sane during this endeavour. Everyone from the Ameland crew: Thanks for listening to all my drama. All DNV colleagues: Thanks for repeatedly asking me how things were going with this thesis and thus keeping me going.

Curriculum vitae

I was born on September 15th, 1989, in Minden, Germany, and grew up in the nearby village of Lahde. I graduated in 2009, after which I moved to Nijmegen to start studying at the Radboud University. In 2015, I received my master's degree in biology. After finishing my Master's, I started working as an environmental consultant at DNV for about 1.5 years. I then went back to Radboud University and started working at the Department of Environmental Science in November 2017, on the PhD project that ultimately led to this thesis. After 4.5 years at the department, I again took a position as a consultant at DNV in 2022, where I am still working today. In the meantime, I finalized this PhD thesis.

Publications

Louise Christine Dammeier, Jessica M. Loriaux, Zoran J.N. Steinmann, Daan A. Smits, Ine L. Wijnant, Bart van den Hurk, Mark A.J. Huijbregts, "Space, Time and Size Dependencies of Greenhouse Gas Payback Times of Wind Turbines in Northwestern Europe", Environmental Science & Technology, vol. 53, no. 15, 9289-9297, 2019. https://doi.org/10.1021/acs.est.9b01030

David E.H.J. Gernaat, Harmen-Sytze de Boer, Louise Christine Dammeier, Detlef P. van Vuuren, "The role of residential rooftop photovoltaic in longterm energy and climate scenarios", Applied Energy, vol. 279, 115705, 2020. https://doi.org/10.1016/j.apenergy.2020.115705

Joyce H.C. Bosmans, Louise C. Dammeier, Mark A.J. Huijbregts, "Greenhouse gas footprints of utility-scale photovoltaic facilities at the global scale", Environmental Research Letters, vol. 16, no. 9, 094056, 2021. https://doi.org/10.1088/1748-9326/ac1df9

Louise Christine Dammeier, Joyce H.C. Bosmans, Mark A.J. Huijbregts, "Variability in greenhouse gas footprints of the global wind farm fleet", Journal of Industrial Ecology, vol 27, no. 1, 272-282, 2022. https://doi.org/10.1111/jiec.13325

Joyce H.C. Bosmans, Louise Christine Dammeier, Mark A.J. Huijbregts, "Corrigendum: Greenhouse gas footprints of utility-scale photovoltaic facilities at the global scale (2021 Environ. Res. Lett. 16094056)", Environmental Research Letters, vol. 18, no. 5, 059501, 2023. https://doi.org/10.1088/1748-9326/accc48

